Technische Universität München

Nuclear Magnetic Resonance Characterization of Aggregating Biological Systems and Membrane Proteins

Diana Carolina Rodriguez Camargo

Vollständiger Abdruck der von der Fakultät für Chemie der Technischen Universität München zur Erlangung des akademischen Grades eines

Doktors der Naturwissenschaften (Dr. rer. nat.)

genehmigten Dissertation.

Vorsitzender: Univ.-Prof. Dr. Michael Sattler

Prüfer der Dissertation:

Univ.-Prof. Dr. Bernd Reif

Univ.-Prof. Dr. Aphrodite Kapurniotu

Die Dissertation wurde am 14.08.2015 bei der Technischen Universität München eingereicht und durch die Fakultät für Chemie am 30.10.2015 angenommen.

Dedicated to my family

La vida no es fácil, para ninguno de nosotros. Pero... ¡qué importa! Hay que perseverar y sobre todo, tener confianza en uno mismo. Hay que sentirse dotado para realizar alguna cosa y que esa cosa hay que alcanzarla, cueste lo que cueste.

- Marie Curie

Acknowledgments

First I would like to express my appreciation for all the support which the members of my Thesis Committee provided me with throughout the years of my doctoral studies, the support that helped me develop my professional as well as personal skills. Special thanks go to Prof. Dr. Bernd Reif for giving me the fantastic opportunity of working with this fascinating project in his group. Thank you for providing me with working conditions and funding after so many problems in my Doktorarbeit life ☺. Thank you for sharing your expertise and knowledge, for cheering me up and telling me off. Thank you for motivating me to continue and letting me test my crazy ideas, for improving my funny language and being a great example for me to follow. Thanks for listening and discussing all the scientific ideas and problems with me. Thanks for helping me develop my biggest dream of becoming a scientist.

I would also like to thank PD. Dr. Sonja Dames for introducing me to the bio-molecular NMR work and for letting me work on this interesting project which provided me with tools and knowledge for developing myself as a scientist.

I am deeply grateful for the institutions that provided me with financial support during my Doctoral studies: DFG, Helmholtz Zentrum München, TUM, HELENA, TUM Graduate School.

My thanks go to my colleagues and friends: Christoph Hartlmüller, Kostas Tripsianes, Riddhiman Sarkar, Divita Garg, Elke Prade, Andras Franko, Vanessa Morris, Gerd (Gustav ;)) that help me a lot to develop my project. Thank you for all the discussions and time invested in the development of this project.

And most importantly I would like to thank my family who shared with me the difficulty of being away from each other for so long. Thank you for making so many sacrifices for me and being there for me every moment. I want to express my profound gratitude to my mother Nuris, my father Jaimito and especially to my brother Andres Rodriguez for helping me so much in my life and in my work. He was and is my best colleague and friend ever. I am so proud and happy to have worked together with my brother! That was

the best time of my life. The long nights in the lab and the bicycle rides home at the late night! I thank God for my family - without their support all of these wonderful things wouldn´t have been possible.

Also I thank the rest of my family in Colombia and my lovely life partner Simon Pöllmann, and his lovely family, who in recent months has become my support and unconditional help☺. Thanks to him I have had the strength to fight and pursue the one of the most difficult period in my life and in Doctorarbeit the end!

I would also like to thank my Au Pair family, the family Marx. This beautiful family gave me the opportunity to come to Germany and helped me very much in my life. My German family made me feel welcomed and loved in the new country. Thank you for making me *feliz* ☺.

I also want to say “Thank you very much guys!” to all the people that I call my friends, “Mis Amigos”, for making my Doctoral studies an enjoyable experience. Thank you very much guys for everything: Beers, coffees, parties, dinners, wines, jokes, trips, cheers, gossips, tears, smiles, and all the uncountable experiences that brought joy to my being. Thanks to all the people that left so much time ago and also to the people that walked with me this long way and shared with me the same feelings and experiences. I would especially like to thank Divita Garg, for introducing me to the crazy world of the bio part of the chemistry and for enriching me as a person. Thanks go to my dear Elke (mi companera de viaje y aventura) for helping me so much and being my friend for such a long time. Mathias Wittwer, for the funny moments and drinks days to forget the frustration, Natalia Sarmiento (la amable chicha del tren), Angela Peter (mi primera amiga y compañera en mi vida en Alemania), Gerald Peter, Alex and Masha, my English teacher, Hamed and Alex my old friends.

And of course - Thanks a lot to my more recent friends like Valentin Bauer, Riddihiman Sarkar, Ashis Kawale, Leo, Carolina, Comal, Pravin my dear Maristella De Cicco (mi companera de fiestas ☺), Sandra Scanu, Gininna Scanu, Martin Viertel, Benjamin Boudeax, Vanessa Morris, Chistoph Hartmüller and the whole bunch! You guys make happy every day of my life here. Thanks a lot for the crazy and funny parties “Fiestas” and barbeques.

Publications

- Rodriguez Camargo, D. C. et al. The FKBP-rapamycin binding domain of human TOR undergoes strong conformational changes in the presence of membrane mimetics with and without the regulator phosphatidic acid. Biochemistry 51, 4909-4921 (2012).

- Rodriguez Camargo, D. C. et al. Change of the redox environment in a β-cell triggers conformational changes at the N-terminus of hIAPP and influences its aggregation in Type II Diabetes. Paper in preparation for submission (2015).

- Rodriguez Camargo, D. C. et al. Cloning, expression and purification of the human Islet Amyloid Polypeptide (hIAPP) from Escherichia coli. Protein expression and purification 106, 49-56 (2015).

Table of contents

Acknowledgments 1

Publications 3

1. Abstract 5

2. Introduction 7

2.1 Nuclear Magnetic Resonance 7

2.2 Diabetes Mellitus 11

2.3 Islet Amyloid polypeptide (IAPP) 15

2.4 Ser/Thr kinase target of rapamycin (TOR) protein 16

3. Methods 17

3.1 NMR sample preparation 17

3.2 Circular Dichroism (CD) 17

3.3 Thioflavin T Fluorescence assay 18

3.4 Transmission Electron Microscopy (TEM) 18

4. Description of the first hIAPP publication 19

5. Description of the second hIAPP manuscript 28

6. Description of the third publication of FRB domain from TOR protein 39

7. References 54

1. Abstract

This dissertation presents results that contribute to the understanding of the atomic and molecular characterization of biomolecules like polypeptides and proteins by NMR. The NMR results are complemented with other biophysical techniques such as circular dichroism spectroscopy (CD), thioflavin T (ThT) assays or electron microscopy (EM). The work shows a complete characterization of the aggregation properties of the human hormone Islet Amyloid polypeptide hIAPP with respect to its oxidation state and for the first time its monomeric structure in solution. The aggregation of this hormone plays a fundamental role in the formation of Diabetes Mellitus type II. Furthermore, the interaction of the FKBP12-rapamycin binding (FRB) domain of TOR protein with different membrane systems is analyzed using NMR, enabling a better understanding of the localization of this protein and its function within the cell. This document contains an introductory part presenting a brief review of the most important aspects of NMR spectroscopy, an overview of the disease Diabetes Mellitus, followed by a description of the biological relevance of hIAPP and the protein TOR. The methodological part describes NMR sample preparation, circular dichroism, ThT assay and Electron Microscopy. The integrated analysis of the results obtained from these biophysical experiments enables the understanding of the mechanistic details of protein aggregation.

In the first publication, the development of a comprehensive protocol for the production of recombinant human IAPP hormone in Escherichia coli is presented. This process allows the production of the peptide as a C-terminally amidated monomer including a cystein disulphide bridge between residues 2 and 7 and no extra residues at the cleavage sites. All these characteristics are of fundamental importance for the biological relevance of any in vitro experiment. The system presented here is an appropriate tool to produce labeled protein for NMR and large amounts of unlabeled protein for any biophysical study. The relevance of this work is reflected in the many requests for the DNA-sequence of our clone from groups in different countries, establishing project collaborations and giving the possibility for complementary studies.

The second manuscript presents for the first time a structural analysis of the full-length hormone human IAPP by solution-state-NMR without addition of any denaturant, detergent, organic solvent or lipid. It is shown that the peptide has a α-helical structural propensity at the N-terminus stabilized by the disulfide bridge between cysteine residues 2 and 7. Furthermore, we demonstrate that disruption of the disulfide bridge results in reduced stability and induces aggregation of the peptide. We therefore propose that changes in the redox potential within pancreatic β-cells during diabetes type II development accelerate the aggregation of the peptide and result in apoptosis. This hypothesis is supported by published in-vivo studies, showing that diabetes mellitus alters the redox state in the cell, especially in the endoplasmic reticulum. These results are of fundamental importance as they establish a basis for the understanding of T2D pathogenesis and might enable the design of specific inhibitors that interfere with aggregation.

In the third publication, the FRB membrane domain of TOR the Ser/Thr kinase Target of Rapamycin is characterized with respect to its interaction with membranes. This protein plays an important role in controlling cellular growth and metabolism. Therefore, misregulation of TOR is correlated with the development of tumors, diabetes, obesity, depression and certain types of cancer. In this work, the analysis of the interaction between TOR and various mimetic membrane systems is presented. We found that the isolated domain preferentially binds to negatively charged lipids and has no preference for phosphatidic acid (PA)-containing membranes as it was proposed in some previous studies. The domain preserves the α-helical secondary structure content but the membrane environment induces a strong conformational change presumably by dispersion of the helices in the lipids. We have as well shown that the FRB domain binding surface responsible for interaction with lipids and the interface in the complex FKBP12-rapamycin are overlapping. Rapamycin is an inhibitor of TOR and its binding site is the FRB domain. Upon formation of this complex the FRB is prevented from interaction with some membrane mimetic systems at lower lipid concentrations resulting in important consequences for the localizations of TOR in the cell.

2. Introduction

2.1 Nuclear Magnetic Resonance

Nuclear Magnetic Resonance (NMR) is a powerful analytical spectroscopy method allowing the experimentalist to obtain information on the structure at atomic resolution. NMR experiments yield information on the chemical environment of specific nuclei in NMR. The simplest nuclei to work with have a half-integer spin, i.e. ½, such as ^{15}N, ^{13}C and ^{1}H. The quantum mechanics suggests that a nucleus of spin I will have 2I + 1 possible orientations. A nucleus with spin of ½, for example ^{15}N, will have 2 possible orientations. If a magnetic field is applied to this nucleus, the energy levels split. The energy difference ΔE between the two states is called the nuclear Zeeman splitting (Figure 1).[1-4]

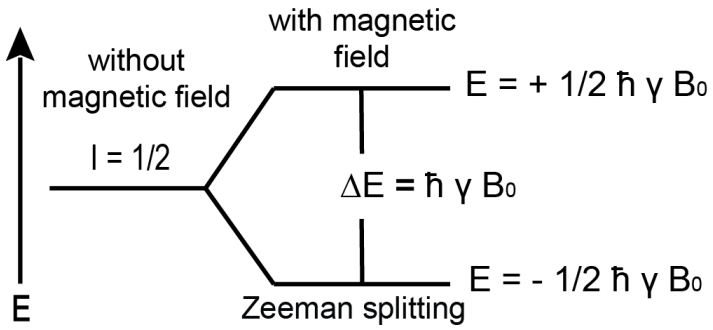

Figure 1: Zeeman splitting of nuclear-energy levels in a magnetic field. Where I is the spin of the nucleus, E is the energy, ħ is the Planck constant divided by 2π; γ is the gyromagnetic ratio and B_0 is the external magnetic field.

Each energy level is given a magnetic quantum number *m*. When this nucleus is in a magnetic field, the energy levels are populated according to the Boltzmann distribution. Lower energy levels will contain slightly more nuclei than higher levels. Application of a radiofrequency field excites these nuclei into the higher level. The frequency of the radiation necessary for this change is determined by ΔE. The handling of pulses of different shapes, frequencies and durations, specifically designed patterns or pulse sequences allows the spectroscopist to extract many different types of information from the molecule.[1-4]

The transition between these two energy levels results in a single line at the Lamor frequency of the spin, which is observed as a resonance in the spectrum. The oscillation of the signal is transformed by Fourier Transformation (FT) into a signal in the frequency domain. The signal is expressed as chemical shift δ in parts per million (ppm) (Figure 2). The ppm value is calculated as the ratio of the detected frequency from the sample and the absolute resonance frequency of a standard reference compound. [1-4]

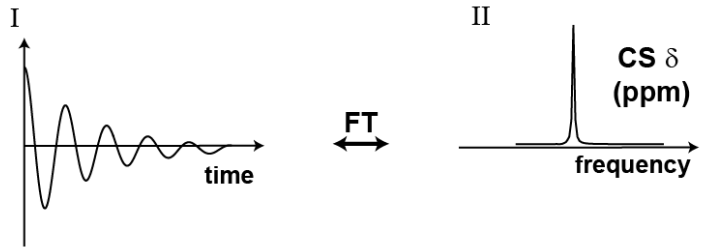

Figure 2: NMR signal. For analysis, the free induction decay (FID) (I) is Fourier transformed to yield a signal in the frecuency domain. The resonance frequency is given in ppm with respect to a reference.

The recovery of this spin into its lower energy state is called relaxation. The relaxation time is analyzed in terms of two isolated processes, each with its own time constant. The longitudinal (or spin-lattice) relaxation time T_1 is the decay constant for the readjustment of the *z* component of the nuclear spin magnetization and it is responsible for the loss of signal intensity. The other process, associated with the decay constant for the component of the total magnetization *M* perpendicular to B_0, designated M_{xy}, is called the transverse (or spin-spin) relaxation time T_2. It is responsible for the broadening of the signal. Both T_1 and T_2 depend on the rate of molecular motions as well as the gyromagnetic ratios of both, the resonating and their strongly interacting, next-neighbor nuclei not at resonance. [1-4]

In NMR of biomolecules typically more than one spin is coupled in the system. This spin combination produces also a spectrum of the two coupled spins consisting of two doublets. The splitting of the doublets is the scalar coupling J12 expressed in Hz. The shifts of the two spins are called $\delta 1$ and $\delta 2$, and give corresponding Lamor frequencies. The spin system can be specified as homonuclear or heteronuclear incidental to the type of the nuclei. This variety of systems together with sample

labeling allows the NMR spectroscopist to produce a substantial variation of NMR experiments. Although the fundamental concept of 2D-FT NMR was initially suggested by Jean Jeener, this idea was largely developed by Richard Ernst, including multi-dimensional FT NMR, who matured this technique into a powerful methodology for studying structure of biomolecules.[5-7] A typical example of a 2D experiment is a COSY spectrum, where the magnetization is transferred by scalar J-coupling between the HN to the Hα and vice versa which is part of the same scalar coupled spin system.[1-4]

In proteins, experiments are classified into two sets of interactions, characterized by the magnetization transfer between the nuclei. The first one is the through-bond interaction, forwarding the perfect strategy for the back bone resonance assignment in a biomolecule. This involves the use of 15N and 13C labelled nuclei and the measurement of a major number of NMR experiments like CBCANH[8] and CBCA(CO)NH[8] spectra for small proteins. In addition, complementary experiments like HNCA[9], NH(CO)CA[10], HNCO[9,11], and HN(CA)CO[12] spectra might be necessary. If the biomolecule is very large, containing more than 250 residues, a deuteration of the sample may be required. In this case experiments like CBCA(CO)NH spectra need to be used.[8] The through-space interaction can be probed employing the Nuclear Overhauser Effect to yield distances between atoms. Combination of these different types of experiments and various isotope-labeling techniques have recently opened the possibility to study biomolecules and obtain valuable information about the structure, interaction and dynamics of proteins, nuclei acids, and their complexes. However, the application of traditional NMR spectroscopy in solution, which currently is limited to a size of 50 kDa. Introduction of transverse relaxation-optimized spectroscopy (TROSY)[13], which reduces the effective relaxation of the measured signal during the pulse sequence and during data acquisition, can help. To apply the TROSY[13] technique, at least two different interfering relaxation mechanisms must contribute to relaxation. If the interference is additive, the effective relaxation is reduced. Consecutively, the line widths and sensitivity can be improved in NMR experiments to successfully study molecules up to 110 kDa[14]. A practical application of TROSY[13] is the determination of structures of membrane proteins[15], intermolecular

interaction and drug design[16], scalar couplings across hydrogen bonds[17] and measurement of residual dipolar couplings (RDCs)[18]. In solution-state NMR, the orientation dependence is averaged to zero. If a molecule in solution is deliberately aligned, residual dipolar couplings (RDCs) can be reintroduced with a size of a few Hz. If high-resolution spectra are obtained, the distance and orientation dependence of D is reintroduced and provides valuable structural information. For example, from the H-N dipolar couplings the projection angles θ and φ can be obtained. This alignment can be performed by dilution of the biomolecule into a liquid crystalline media, e.g. bicelles, stretched polystyrene (PS) gels, rod-shaped viruses including filamentous bacteriophage, DNA nanotubes, Otting media etc.[18,19] In solid state, this leads to large dipolar splitting and broad linewidths since dipolar couplings, e.g. H-N, are in the kHz range. This characteristic is the major difference between solid- and solution-state NMR. For this reason is in solid-state NMR spectroscopy the sample is rotated under a specific angle in the magnetic field, called the "magic angle" $\beta_{RL} = \arctan\sqrt{2} \approx 54.74°$. Raymond Andrew pioneered the development of high-resolution solid-state nuclear magnetic resonance and introduced MAS (magic angle spinning).[20-22] This technique allows to improve the spectral resolution by emulating a tumbling molecule, which removes the anisotropic broadening from the spectra. The extent, to which the anisotropic interaction are averaged, depends on the frequency of the rotation ω_r (Figure 3).

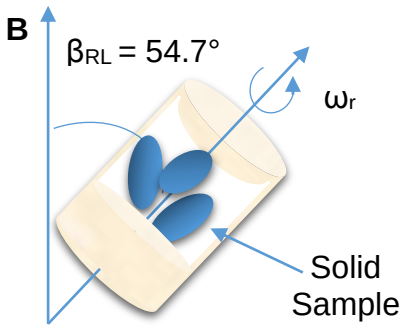

Figure 3: Representation of the principle of MAS solid-state NMR. The sample is rotate in the magnetic field (B_0) under an angle of 54.7° which is referred to as the magic angle, ω_r refers spinning frequency and β_{RL} is the angle between the static magnetic field (B_0) and the axis of rotation.

To increase sensitivity Pines *et al.* introduce cross-polarization[23]. After this, the cross polarization and magic angle spinning was combined (commonly named CP-MAS), which now is a standard tool in solid-state NMR. Other improvements for sensitivity and resolution in ^{13}C or ^{15}N detecting experiments are obtained by heteronuclear decoupling.[24] The simplest method implies the application of a strong unmodulated rf-field close to the Larmor frequency of the proton, leaving ^{13}C or ^{15}N spin unchanged. This method is called continuous wave or CW decoupling. More advanced methods include the two-pulse phase-modulation (TPPM) method[25], SPINAL-64[26] and similar schemes, frequently producing better decoupling than the CW method.[27-29]

In the last years solid-state NMR spectroscopy is applied extensively for studying biological systems[30]. It has become an important method which allows to better understand now the misfolding of peptides and protein amyloids, which is a common motif in many diseases like hIAPP (Diabetes mellitus type II)[31], β-Amyloid (Alzheimer's Disease)[32], α-synuclein (Parkinson' Disease)[33].[34] Furthermore, it is applied to membrane proteins[35], cytosceleton associated proteins[36], microtubules[37] and large soluble protein complexes[38]. These systems are difficult to access by X-ray crystallography or standard solution-state NMR methods. Elucidation of protein structure by solid-state NMR[39] is relies on secondary chemical shifts and spatial contacts between heteronuclei. In addition, paramagnetic contact shifts[40], specific proton-proton distances can be included in any structure calculation[39]. Solid-state NMR is a valuable tool to study local dynamics[41], kinetics[42], and thermodynamics[43].

2.2 Diabetes Mellitus

Diabetes mellitus is a chronic metabolic disorder with a variety of causes affecting the amount of insulin and thus the glucose uptake in the body, generating hyperglycemia in the body[44]. Diabetes increasingly affects millions of people worldwide[45]. The causes for the development of this disease are currently unclear. However, many studies propose a correlation between genetic predisposition and environmental factors. These two conditions trigger a complex network of biological

reactions affecting the cell and generating β-cell dysfunction that finally results in cell apoptosis[46-48]. Diabetes is divided into Type 1 and Type 2 diabetes. T1D is also referred as IDDM (Insulin-dependent diabetes), an autoimmune disease, in which the immune system of the body degrades the β-cells. Patients, which suffer from T1D, need to inject insulin on a daily base to overcome insulin insufficiency and restore glucose metabolism.

T2D is referred to as NIDDM (Non-insulin-dependent diabetes). The development of T2D is correlated with genetic and environmental factors. Risk factors are excess intake of food rich in sugar and fat, constant stress and little exercise. These increase the probability of developing diabetes[44]. The increase in obesity and as a consequence the risk to develop T2D is almost epidemic[44]. The probability to develop T2D is proportional to the BMI[49-51] (Figure 4). In addition to environmental factors, genetic susceptibility plays a significant role for the pathogenesis of the disease. Certain genes or combinations of genes increase the risk. For example, studies have demonstrated that modifications of the two non-coding single-nucleotide polymorphisms in transcription factor 7-like 2 (TCF7L2) gene increase susceptibility to develop T2D up to 80% compared to people not carrying this gen variant[52]. Further ethnicity plays an important role: The disease occurs more frequently in Africa, Asia, South- and Northamerica[53-56]. Risk genes for obesity are melanocortin-4 receptor, leptin, leptin receptor, prohormone convertase 1 (PC1) and pro-opiomelanocortin (POMC)[57]. The gene variations associated with insulin sensitivity are the P12A polymorphism in PPARγ[58,59], genes associated with β-cell dysfunction include hepatocyte nuclear factor-4α and 1α, E23K polymorphism in the islet ATP-sensitive potassium channel Kir6.2 (encoded by KCNJ11), mutations in the mitochondrial genome and the glucose transporter GLUT2 among others [53,57-61].

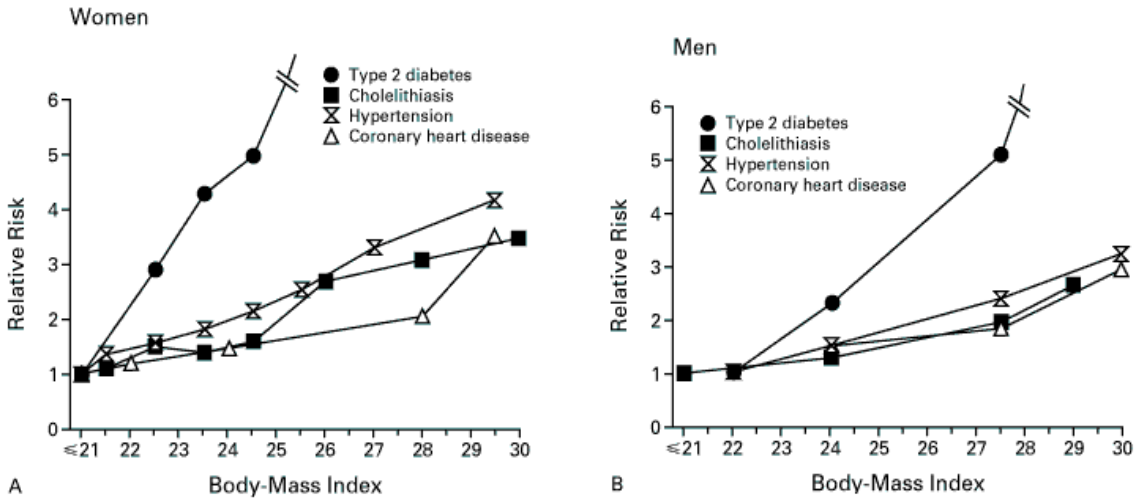

Figure 4: Correlation between the body weight and the prevalence of diabetes. Figure is taken from Willet et Al, (1999).

Five principal mechanisms contribute to the genesis of T2D (Figure 5). First, environmental factors like obesity yield an excess of free long-chain fatty acids in the blood generating lipotoxicity that can contribute to insulin resistance and β-cell dysfunction[62-68]. The second factor, glucotoxicity, changes insulin secretion and induces β-cell dysfunction. Over time, high blood glucose levels damage nerves and blood vessels and consecutively increase the susceptibility for secondary diseases like heart or kidney problems, resulting in blindness or amputation.[31,68-72] The third factor is oxidative stress, which is governed by a series of cell stressors, of which one is glucose. Metabolism of glucose induces the production of reactive oxygen species. As β-cells have very low levels of anti-oxidants, this factor is important for the development of insulin resistance and the damage of β-cells[73-76]. The fourth factor is stress of the endoplasmic reticulum (ER). As a consequence of insulin resistance, β-cells increase dramatically the insulin and IAPP production. The high production and flux of proteins through the ER results in an ER imbalance and malfunctioning of the ER.[77-81]

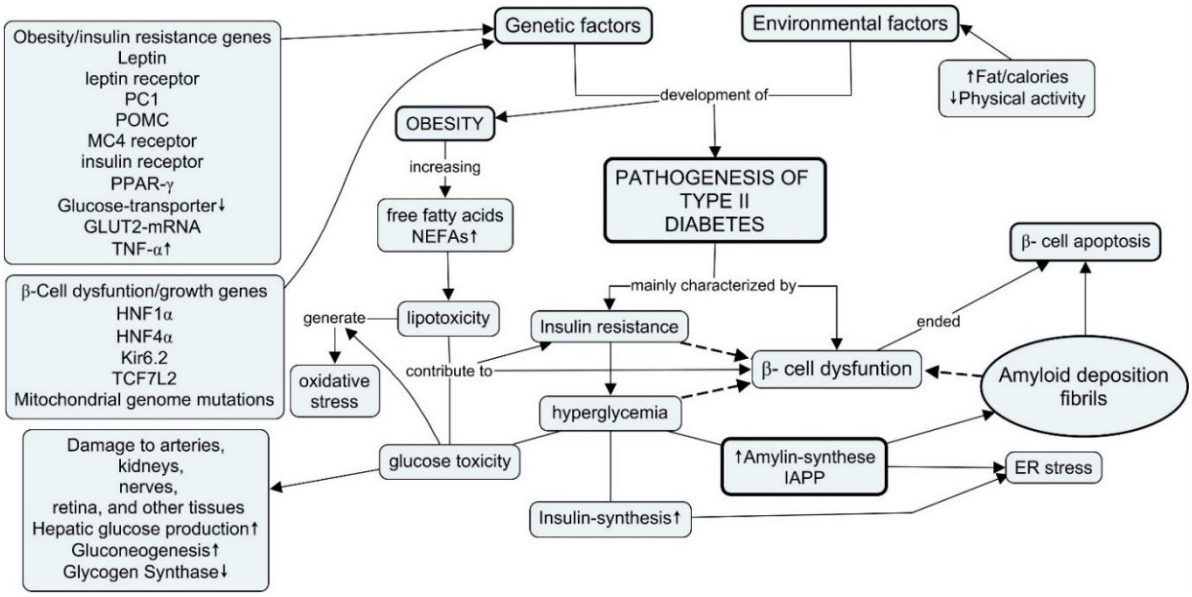

Figure 5: Flow chart summarizing the factors resulting in the development of the pathogenesis of type II Diabetes.

The fifth factor is amyloid deposition, commonly observed in T2D patients. For many years, these deposits were very difficult to identify and to characterize due to their insolubility. In 1987, *Cooper et al*. were able to identify the so called diabetes-associate-peptide (DAP), also known as human Islet PolyPeptide (hIAPP)[82]. Immunohistopathological studies clearly showed amyloidogenic deposits (Figure 6). Aggregates are found in the whole islets[83-87]. However. it remains unclear whether aggregation of human IAPP is a cause or a consequence of β-cells failure[88].

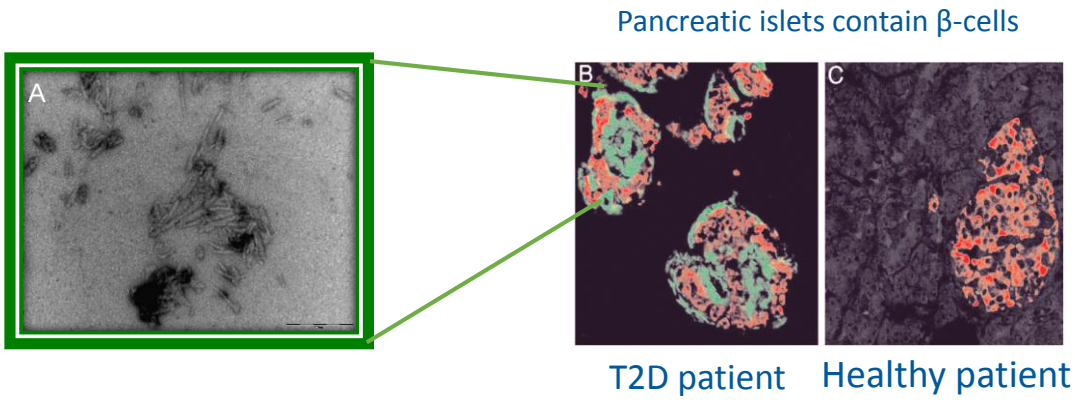

Figure 6: EM of a typical hIAPP fibril sample A). Immunohistochemical comparison between islet cells in T2D patient B) and healthy individual C). Aggregates of hIAPP are labeled in green and the insulin present in the islet cells in red. Figure adapted from Westermark et Al, (2008).

2.3 Islet Amyloid polypeptide (IAPP)

The Islet Amyloid polypeptide, also called amylin, is a hormone co-secreted with insulin. This peptide has a length of 37 residues and the following primary sequence: KCNTATCATQRLANFLVHSSNNFGAILSSTNVGSNTY. It was found in Type 2 diabetic patients as the principal component of deposits in the pancreas[82,83].

IAPP is a member of the calcitonin-like peptide family including calcitonin, calcitonin gene-related peptide (CGRP) and adrenomedulin. Human IAPP has 43-46% identity with the gene-related peptide (CGRP). Human IAPP activates prohormones, hormones and neurotransmitters in the cell[83,89,90].

IAPP is expressed as an 89 amino acid residue pre-protein containing two flanking peptides that are cleaved off by two endoproteases, the prohormone convertases PC2 and PC1/3. This process is pH-dependent and occurs in the late golgi and the secretory granules. This process yields the fully active, C-terminally amidated hormone containing a N-terminal disulphide bridge. These two features are of fundamental importance for the full biological function of the hIAPP[91-97]. IAPP is preferentially expressed in the ß-cells but also in δ-cells in rats and mice; furthermore in the gastrointestinal tract of different mammals and in the sensory neurons of the mice[98-101]. The expressed peptide is stored in the insulin secretory granules. These granules are a complex system, including many components such as insulin and pro-insulin, which control and inhibits the aggregation of IAPP by an unknown mechanism. In these granules, hIAPP remains soluble up to concentrations of 1-4 mM.[92] It is unclear, why hIAPP does not aggregate under these conditions, given the fact that the peptide precipitates rapidly in vitro at concentrations which is a 1000 times lower. One plausible reason might be the pH between 5 and 6 within the insulin secretory granules. This pH value is favorable for the dissolution of basic molecules like IAPP (PI: 8.9). [46,85,92,102-105]

2.4 Ser/Thr kinase target of rapamycin (TOR) protein

In all eukaryotes, the TOR protein or Ser/Thr Kinase target of rapamycin controls cell growth and survival as well as cytoskeletal reorganization processes[106]. Misregulation of the TOR pathway results in development of diseases such as diabetes, obesity, depression and certain types of cancer, because this protein integrates the input from pathways, including insulin, growth factors, cellular nutrients, oxygen, energy levels and amino acids[106,107].

TOR is a 2500 residue protein consisting five domains. TOR is divided into two distinct complexes: TORC1 and TORC2. TORC1 controls the accumulation of cell mass in response to nutrients and energy. Some metabolic processes controlled by TORC1 are protein and lipid synthesis, ribosome and mitochondrial biogenisis and autophagy[108]. TORC1 is highly sensitive to the specific inhibitor complex composed of the macrolide rapamycin and the cellular protein FKBP12-rapamycin which bind to its FRB domain[109]. The FRB domain is 100 amino acid long and mediates TORC1 interaction with the cellular membrane. TORC2 is insensitive to rapamycin and was reported to be an important regulator of the cytoskeleton by mediating phosphorylations via its serine/threonine protein kinase[108,110].

3. Methods

3.1 NMR sample preparation

Samples were prepared using solvents that contain at least 5% of deuterium instead of hydrogen. The deuterium signal is used for the NMR lock which yields a stabilization of the spectrometer. The sample must be soluble and the volume has to cover the complete coil. The resolution in the spectra depends on the solubility and size of the molecule in the sample, as big species in solution or high viscosity decrease the molecular tumbling and increase the spectral linewidth.

Isotopic enrichment is achieved by addition of isotopically labeled nutrients to the minimal bacterial medium. This process has been an integrated and powerful tool for the advancement of NMR applied to biological molecules. There are numerous labeling strategies in NMR, such as uniform isotopic labeling of one or more isotope types, and selective isotopic labeling in which different precursors or nutrients with specific labeling are added. This results in the incorporation of isotopes at specific sites in the sequence[111].

3.2 Circular Dichroism (CD)

Determination of the secondary structure and folding properties of proteins and peptides are complemented by physical tools examining the folding state and integrity of the samples containing the biomolecules. This technique uses only low amounts of the sample and can be performed within minutes. The circular dichroism CD can be defined as the unequal absorption of left and right distributed circularly polarized light. Every structure has a characteristic spectrum with a minimum visual detectable: alpha-helical conformation present a minimum negative at 222 nm and 208 nm and a positive band at 193 nm. Antiparallel beta sheets show a negative band a 218 nm and a positive band at 195 nm. Random coil conformations feature a very low ellipticity above 210 nm and negative bands near to 195 nm[112]. Normalization of measured data

is obtained by calculating the molar ellipticity. This normalization allows to compare the structures of different sample concentrations and different constructs.

3.3 Thioflavin T fluorescence assay

The thioflavin T fluorescence assay for amyloid fibrils is a useful method that helps to monitor the formation or aggregations and fibril formations. Thioflavin T is a compound obtained by the methylation of dehydrothiotoluidine with methanol in the presence of hydrochloric acid. This reaction results in the production of a benzothiazole salt. This works like a dye used to envisage and quantify the presence of misfolded proteins, oligomers and fibrils. The molecule binds to the structures with a high amount of beta-sheet, such as aggregates and amyloids proteins. The dye emit a higher fluorescence and a characteristic red shift of its emission spectrum. With the monitoring of the change in absorption per time is the fluorescence spectroscopy a powerful tool to determine the kinetic of the fibril formation. In general the ThT presents fluorescence in the spectral region with a maximum at 478-484 nm.[113]

3.4 Transmission Electron Microscopy (TEM)

This type of microscopy uses electrostatic and electromagnetic lenses to control the electron beam and focuses it to form an image. The electron beam is accelerated by an anode, typically at +100 keV (40 to 400 keV) with respect to the cathode. In EM it is necessary to stain the sample with a suspension of an electron-opaque solution such as uranyl acetate. This preparation is made on a suitably coated EM grid, on which the sample is blotted and dried. The corrected focus image can finally be recorded photographically at a high-resolution with help of a fiber optic light-guide to the sensor of a CCD (charge-coupled device) camera. The image detected by the CCD can be displayed on a monitor or a computer. In older models or microscopes the same result can be achieved by exposing a photographic film or plate directly to the electron beam.[114]

4. Description of the first hIAPP publication

Cloning, expression and purification of the human Islet Amyloid Polypeptide (hIAPP) from Escherichia coli

Protein Expr Purif 2015 Feb 6;106:49-56. Epub 2014 Nov 6.
Diana C Rodriguez Camargo, Konstantinos Tripsianes, Tobias G Kapp, Joaquim Mendes, Jasmin Schubert, Burghard Cordes, Bernd Reif.

The Production of recombinant human IAPP is complicated as it has a high tendency to aggregate even at low concentrations or temperatures. The limit of solubility at 4 °C is about 150 uM. The whole peptide is aggregated after three days. For its production in *E. Coli*, a long construct with different tags at the N and C-termini was necessary to avoid aggregation of the peptide during purification. The Intein-Chitin-Binding-Domain tag at the C–terminus effectuates intrinsic amidation at the last amino acid of the peptide. This amidation is fundamental for the biological activity of every hormone. In contrast to previously published systems, amidation is quantitative in the final product after purification. Additionally, the system allows the production of peptide without any methionine or other overhanging residues at the N-terminus. This was achieved by designing the solubility leader sequence with a terminal glutamic acid. Enzymatic processing is achieved with V8 Protease (GluC), which cleaves after a glutamic acid residue without introducing any extra residue. Finally, oxidized hIAPP was obtained by adding catalytic amounts of H_2O_2 to the peptide in aqueous buffer.

The purification is based on affinity and reverse phase chromatography. The protocol yields monomeric hIAPP in either unlabeled or isotopically labeled form. The final product contains all biologically relevant features for biophysical studies to investigate its structure and aggregation kinetics. The quality of the final product was confirmed by mass spectrometry, gel electrophoresis and solution-state NMR. The complete assignment was obtained by solution-state NMR.

Protein Expression and Purification 106 (2015) 49–56

Contents lists available at ScienceDirect

Protein Expression and Purification

journal homepage: www.elsevier.com/locate/yprep

Cloning, expression and purification of the human Islet Amyloid Polypeptide (hIAPP) from *Escherichia coli*

Diana C. Rodriguez Camargo [a,b], Konstantinos Tripsianes [c], Tobias G. Kapp [b], Joaquim Mendes [a], Jasmin Schubert [a], Burghard Cordes [b], Bernd Reif [a,b,*]

[a] Helmholtz Zentrum München (Deutsches Forschungszentrum für Gesundheit und Umwelt), Ingolstädter Landstr. 1, 85764 Neuherberg, Germany
[b] Munich Center for Integrated Protein Science (CIPS-M) at Department Chemie, Technische Universität München (TUM), Lichtenbergstr. 4, 85747 Garching, Germany
[c] Central European Institute of Technology (CEITEC), Masaryk University, Kamenice 5/A35/1S081, 62500 Brno, Czech Republic

ARTICLE INFO

Article history:
Received 24 June 2014
and in revised form 20 October 2014
Available online 6 November 2014

Keywords:
Amyloid
Diabetes
Recombinant protein
human Islet Amyloid Polypeptide (hIAPP)
Escherichia coli
Nuclear magnetic resonance (NMR)

ABSTRACT

Type II diabetes is characterized by deposition of the hormone human Islet Amyloid Polypeptide (hIAPP). Formation of hIAPP amyloid fibrils and aggregates is considered to be responsible for pancreatic β-cell losses. Therefore, insight into the structure of hIAPP in the solid-state and in solution is of fundamental importance in order to better understand the action of small molecules, which can potentially dissolve protein aggregates and modulate cell toxicity. So far, no procedure has been described that allows to obtain the native human IAPP peptide at high yields. We present here a cloning, expression and purification protocol that permits the production of 2.5 and 3 mg of native peptide per liter of minimal and LB medium, respectively. In the construct, hIAPP is fused to a chitin binding domain (CBD). The CBD is subsequently cleaved off making use of intein splicing reaction which yield amidation of the C-terminus. The N-terminus contains a solubilization domain which is cleaved by V8 protease, avoiding additional residues at the N-terminus. The correct formation of the disulfide bond is achieved by oxidation with H_2O_2.

Introduction

The human Islet Amyloid Polypeptide (hIAPP)[1], also known as amylin, is an active pancreatic islet hormone which is co-secreted with insulin in beta cells [1]. These two hormones, together with glucagon, control the glucose homeostasis in the body [2,3]. hIAPP regulates the glucose uptake by affecting the rate of gastric emptying or food intake [4]. At the same time, hIAPP also inhibits insulin release and the rate of blood glucose elimination [5]. hIAPP contains 37 amino acid residues, and is co-expressed with insulin into the endoplasmic reticulum (ER) of pancreatic β-cells. The pro-hormone consists of 89 amino acids containing a 22 amino acid signal peptide and two short flanking regions, which are cleaved off by a series of pro-hormone convertases (PCs) [6–11]. The aggregation mechanism of the mature hIAPP is so far not understood; however hIAPP self-aggregation is considered to be the primary cause of pancreatic cell loss in type II diabetes patients [12,13]. Self-aggregation of hIAPP can even become a problem in the treatment of diabetes type I patients after transplantation of healthy pancreatic islets [14,15]. Therefore, structural insights into the hIAPP aggregation mechanism are of fundamental importance to better understand the action of potential inhibitors that modulate cell toxicity. In the past, solution-state [16–19] and solid-state NMR experiments [20–23] were carried out to characterize different hIAPP fragments at atomic resolution. In order to carry out these NMR experiments, isotopically-enriched hIAPP is required. However, the high costs of the isotopically labeled reagents, together with the difficulty associated with the chemical synthesis of hIAPP prevented more detailed NMR studies [24]. Furthermore, amyloidogenic peptides that are prepared by solid-state synthesis can differ in their aggregation behavior, as well as in their toxicity on neuronal cell due to a potential racemization reaction at the Cα carbon atom [25]. For this reason, a method for the recombinant production of hIAPP in *Escherichia coli* is of vital importance. So far, the large scale biosynthesis of human hIAPP was hampered due to its high intrinsic aggregation propensity. In fact, hIAPP was recently reported to be one of the most amyloidogenic polypeptide

* Corresponding author at: Helmholtz Zentrum München (Deutsches Forschungszentrum für Gesundheit und Umwelt), Ingolstädter Landstr. 1, 85764 Neuherberg, Germany.
E-mail address: reif@tum.de (B. Reif).

[1] *Abbreviations used:* TFA, trifluoroacetic acid; CAC, chitin affinity chromatography; NMR, nuclear magnetic resonance; CBD, chitin binding domain; ER, endoplasmic reticulum; RP-HPLC, reverse-phase high pressure liquid chromatography; MS, mass spectrometry; hIAPP, human Islet Amyloid Polypeptide; HSQC, heteronuclear single quantum coherence; SDS–PAGE, polyacrylamide gel electrophoresis; DTT, dithiothreitol; IPTG, isopropyl β-D-1-thiogalactopyranoside; NEB, New England Biolab.

http://dx.doi.org/10.1016/j.pep.2014.10.012
1046-5928/

known to date [26]. Until now, only a few protocols have been described for the production of recombinant human IAPP. These protocols, however, yield non-native hIAPP. The resulting peptides contain either extra amino acids at the N-terminus [27], or are not amidated at the C-terminus [28–30]. Cyanogen bromide cleavage reactions [23] results often in overhanging residues and potential toxic residual chemicals in the preparation that might influence cellular assays [23]. In case, hIAPP is expressed into inclusion bodies, residual detergents such as urea might cause problems in subsequent biophysical studies [29]. We present here an expression and purification procedure that yields 2.5 mg of hIAPP per liter of minimal medium, and 3 mg of peptide in Luria broth (LB) that does not suffer from the above mentioned draw-backs. The final peptide is amidated at the C-terminus and contains a disulfide bridge between cysteines 2 and 7, which is essential for its biological function as a hormone [8,33–35]. The cystein bridge stabilizes the secondary structure of the hormone and plays potentially an important role in receptor binding. It is furthermore speculated that amidation of the C-terminus has an effect on the aggregation propensity of the IAPP peptide [17]. Similar effects have as well been reported for other amyloidogenic peptides [36].

In our preparation, no additional overhanging residues are appended at the N and C-termini. The protein is prepared in aqueous buffer. No toxic compounds such as cyanogen bromide is required, and the final product contains no residual organic solvents. The construct design follows a protocol suggested by Williamson and Miranker [31,37] who studied the rat IAPP peptide. In contrast to rat IAPP, which does not form amyloid fibrils, the human sequence is highly prone to aggregation, which complicates expression and purification. For this reason, the purification protocol had to be adapted. Mass spectroscopy, gel electrophoresis and solution NMR were employed to characterize the final monomeric peptide product.

Materials and methods

Cloning and construction of the recombinant plasmid

The plasmid termed pTXB1EEI was constructed using a 180 bp cDNA fragment containing the coding sequence for mature human IAPP (Fig. 1). As a template for cloning the hIAPP sequence, the vector pGEX-TK-MIAPP (kindly provided by Prof. Westermark, University of Uppsala, Sweden) has been employed. Primers for PCR were purchased from Eurofins MVG-operon. The vector for cloning pTXB1 was purchased from New England Biolab (NEB # N6707S). The insert was ligated using a NdeI (NEB # R0111L) restriction site at the 5′ end and a SpeI (NEB # R0133L) restriction site at the 3′ end of the IAPP sequence. The hIAPP sequence was fused to an INTEIN-Chitin-binding-domain affinity tag (INTEIN-CBD) which is subsequently cleaved off by making use of an Intein splicing reaction [38,39].

The N-terminus consists of a solubilization domain termed "leader" which contains a C-terminal glutamic acid residue. The glutamic acid is necessary to cleave off the leader sequence using V8 protease [40,41]. The hIAPP sequence contains no further glutamic acid residue. From the 5′ end of the insert, the first six nucleotides encode the NdeI restriction site, the following 57 nucleotides the leader sequence and the recognition site of the V8 protease, the next 111 nucleotides encode the 37 residues of the hIAPP sequence and the last 6 nucleotides the SpeI restriction site at the 3′ end. The insert for the fusion protein was synthesized by PCR using the reverse complement. After ligation of the insert into the plasmid with the respective enzymes, the plasmid was amplified into XL-1 Blue cells (NEB # C2992I). Plasmid cDNA was extracted by mini-prep using the standard protocol of the Wizard® Genomic DNA Purification Kit (Promega # A1120). The correctness of the clone was confirmed using DNA sequencing (GACT Biotech). The clone was designed using a strategy originally suggested by Miranker and co-workers. In contrast to the original plasmid which codes for the rat sequence [31], our construct was optimized for the human IAPP sequence. The first four amino acids of the insert in the leader sequence, corresponding to position −20 to −17 of the insert, were substituted from KIEE into KIQH (Fig. 1). This change significantly improves the unselective activity of the V8 protease so that the amount of protease necessary for the cleavage reaction can be largely reduced. Furthermore, the proline in position −1 was replaced with a glutamic acid to enhance protease activity. Finally, the threonine at position 3 of the intein fragment was exchanged for a cysteine, which yields a higher stability for the fusion protein during the expression process [42]. QuikChange® site-directed mutagenesis was performed using the PfuTurbo DNA polymerase standard protocol (Mutagenesis Kit, Agilent Technologies) and a temperature cycler. The final construct is represented in Fig. 1.

Expression of hIAPP fusion protein

The protocol for expression of hIAPP is based on the standard protocol for this vector (Impact™ Kit from NEB) with some modifications. For expression, *E. coli* cells (BL21-DE3, NEB # C2527I) were transformed first with the fusion protein plasmid. A single fresh colony was chosen to grow a 25 mL starter culture in LB or minimal medium (M9) overnight at 37 °C for every liter of final culture. All media were supplemented with 100 μg/mL ampicillin (ROTH # HP62.1). The next day, the starter culture was centrifuged (10 min, 4.000g at room temperature). Cells were transferred into 1 L of fresh minimal medium that contains 0.1% $^{15}NH_4Cl$ (Cortecnet # CN80P20) and 0.2% ^{13}C-glucose (Eurisotop # CLM-420). Others components of M9 were added as described by Marley et al. [43]. Typically, cells require 3.5 h to reach an OD_{600} of 0.6. For induction, isopropyl-beta-D-thiogalactopyranoside – IPTG (Sigma–Aldrich # I6758-10G) was added to a final concentration of 0.3 mM. The culture was grown overnight (16 °C and 180 RPM shaking). The cells were subsequently harvested at 6.000 g for 25 min. Approximately 4 g (wet weight) cells were obtained from 1 L of culture.

Cell lysis and affinity purification of the fusion protein

After centrifugation, the cell pellet was resuspended in 20 mL (for 1 L culture) ice-cold buffer A (20 mM HEPES, 0.1 mM EDTA, 2 M urea, 50 mM NaCl, pH 8). Cells were lysed by sonication on ice (sonication power ~35%, 15 s pulse, 45 s pause for 10 min; Bandelin Sonopuls HD 3200). The re-suspended cells were supplemented with a tablet of protease inhibitor (Roche # 06538282001). No lysozyme was added in this step to prevent degradation of the chitin column. The cell extract was then centrifuged at 24.000g for 1 h at 4 °C. The pellet was discarded and subsequent purification was carried out at 4 °C. The cell lysate was purified by affinity chromatography using a chitin-bead gravity flow resin (NEB # S6651L), employing a glass funnel from Scott Duran (Pore number 3, 125 mL capacity Sigma–Aldrich # Z232548-1EA). The chitin column (filled with 35 mL of chitin beads suspension) was equilibrated with three column volumes of buffer A. The lysate was loaded onto the almost dry chitin beads and incubated for 2 h while the suspension was gently mixed with a spatula for 10 s every 30 min. The loaded column was first washed with 15–20 column volumes of buffer A (~500 mL). The Intein cleavage reaction is initiated by addition of 50 mL of buffer B (= buffer A, supplemented with 100 mM DTT and 2 M ammonium bicarbonate, pH 8.5). After elution of approximately 25 mL, the column flow is

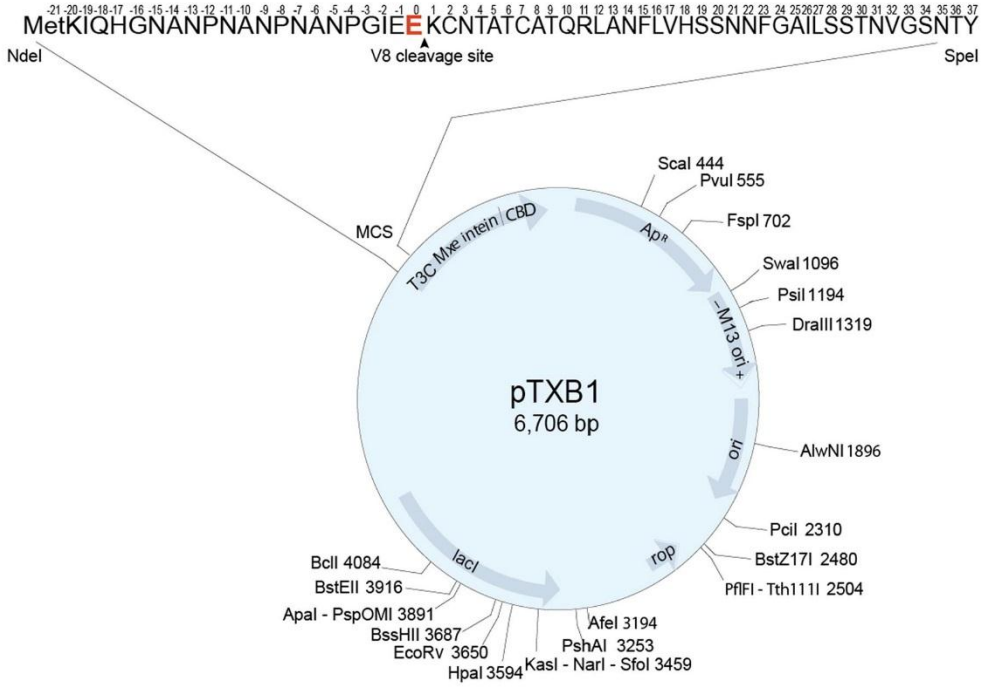

Fig. 1. The pTXB1EEI expression vector constructed for production of hIAPP.

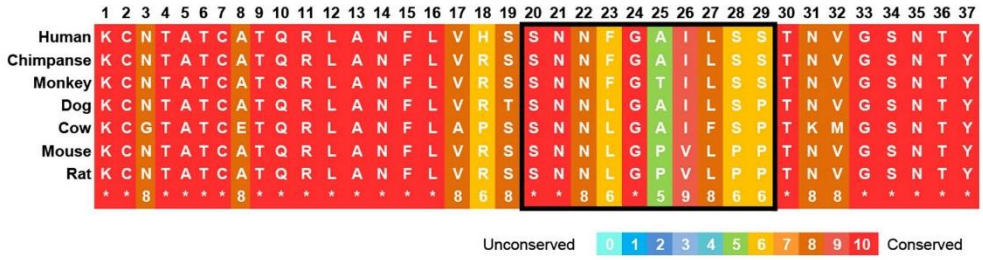

Fig. 2. Amino acid sequences of IAPP in different mammals (numbering according to the human sequence). The sequence of IAPP is highly conserved. The region containing residues 20–29 shows the lowest similarities and is highlighted with a black box. The dog, rat, mouse and cow IAPP sequences contain one or more proline residues that inhibit fibril formation.

stopped. The content of the column is then incubated for ca. 16 h. Ammonium bicarbonate in the buffer is required to yield amidation of the C-terminus [44]. The protein was subsequently eluted with a total volume of 100 mL of buffer A. The elution contains the fusion protein leader-hIAPP. In order to avoid aggregation of the protein, all steps must be carried out at 4 °C.

V8 protease cleavage

Subsequently, the buffer for the fusion protein leader-hIAPP was exchanged using dialysis (3500 Da MW cut-off membrane, Spectra/Por® 7 # 132112). The 100 mL sample was first dialyzed five times against 1 L of buffer A (20 mM HEPES, 0.1 mM EDTA, 2 M urea, 50 mM NaCl, pH 8) for 1 h to remove DTT and ammonium bicarbonate. To prepare for the V8 cleavage reaction, the 100 mL solution containing the fusion protein was concentrated using an Amicon filter (MWCO = 3 kDa, 4.000 g, 4 °C, Millipore # UFC900324) yielding a final volume of 15 mL with absorbance (280 nm) on the order of 0.6–0.8 (corresponding to a concentration of ~1 mg/mL). The 15 mL solution was filtered before mixing with the protease (cellulose acetate filter, 4.5 µm pore size, Thermo Scientific # 03-376-221) to avoid any possible initiation of aggregation. V8 protease (2 mg Roche # 10791156001) was freshly dissolved into 500 µL of pure distilled water and added to the 15 mL fusion protein sample. Generally, 1 h at 4 °C is sufficient to yield quantitative cleavage. Subsequently the V8 protease was separated from the leader fragment and hIAPP using an Amicon filter (MWCO = 10 kDa, 4.000 g, 4 °C, Millipore # UFC901008). The flow through containing hIAPP was concentrated further with an Amicon filter (MWCO = 3 kDa, 4.000 g, 4 °C) to yield a final volume of 5 mL.

RP-HPLC purification

Up to this point, all purification steps were carried out at 4 °C. The protein solution was kept on ice at all times. Immediately prior

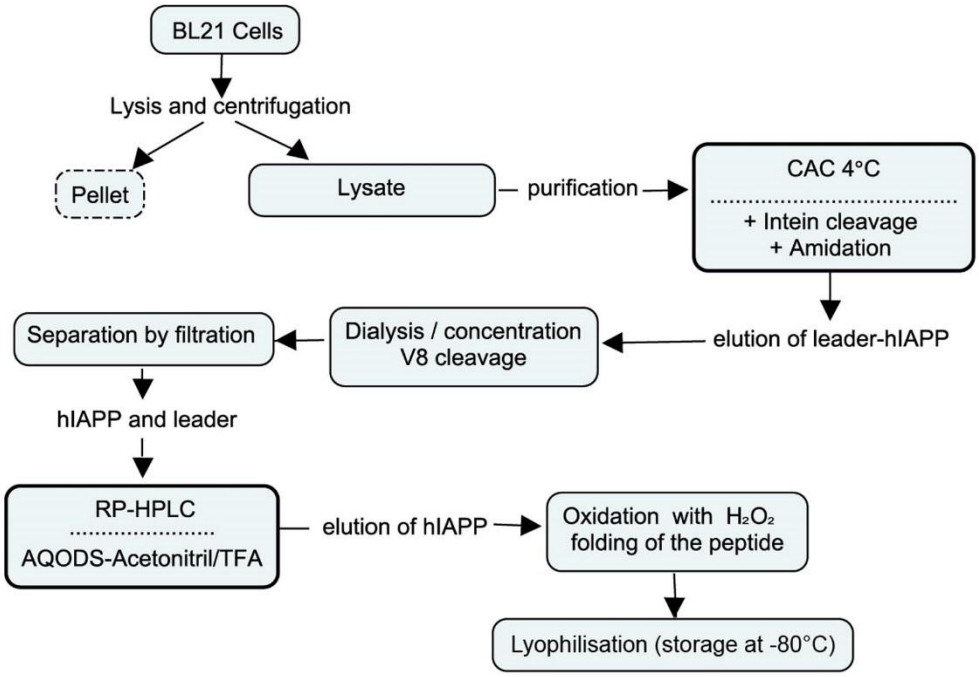

Fig. 3. Schematic representation of the purification protocol.

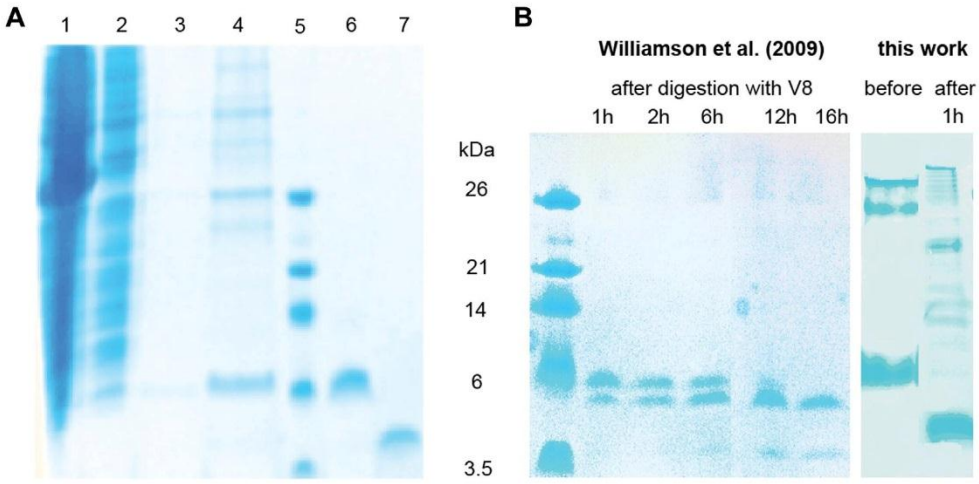

Fig. 4. hIAPP purification monitored by Tricine SDS–PAGE. (A) Lysate of induced BL21 cells containing leader-hIAPP-intein-CBD (1), flow-through of the chitin resin (2), wash after loading the chitin affinity column (3), eluate from the chitin affinity column (4), protein marker (5), concentrated fraction containing leader-hIAPP after RP-HPLC (6), fraction containing the purified hIAPP (~4 kDa) (7). (B) Comparison of the V8 protease digestion efficiency using the construct of Williamson et al. [37] (left), and the construct presented in this work (right). In the previous work, 50 mg of V8 are necessary to yield quantitative cleavage. The experiments are carried out using comparable concentrations of V8 (2 mg).

to injection onto the RP-HPLC column, the temperature of the protein solution is shifted to room temperature. The column (YMC-PackODS-AQ semi-preparative HPLC Column, 10 mm i.d., 12 nm, S-05 µm, 250 × 10.0 mm, YMC # AQ12S05-2510WT) was pre-equilibrated with solvent A (0.05% TFA in water). After sample injection, a gradient of solvent B (0.05% TFA in 100% acetonitrile) from 0% to 70% was applied, setting the flow rate to 6–9 mL/min. hIAPP is eluted as a single peak at 65–69% solvent B. The hIAPP containing fractions were collected and lyophilized.

Disulfide bond formation using H_2O_2

The lyophilized powder containing reduced hIAPP was dissolved in 3 mL acetic acid (30 mM, pH 5.3) and then mixed with

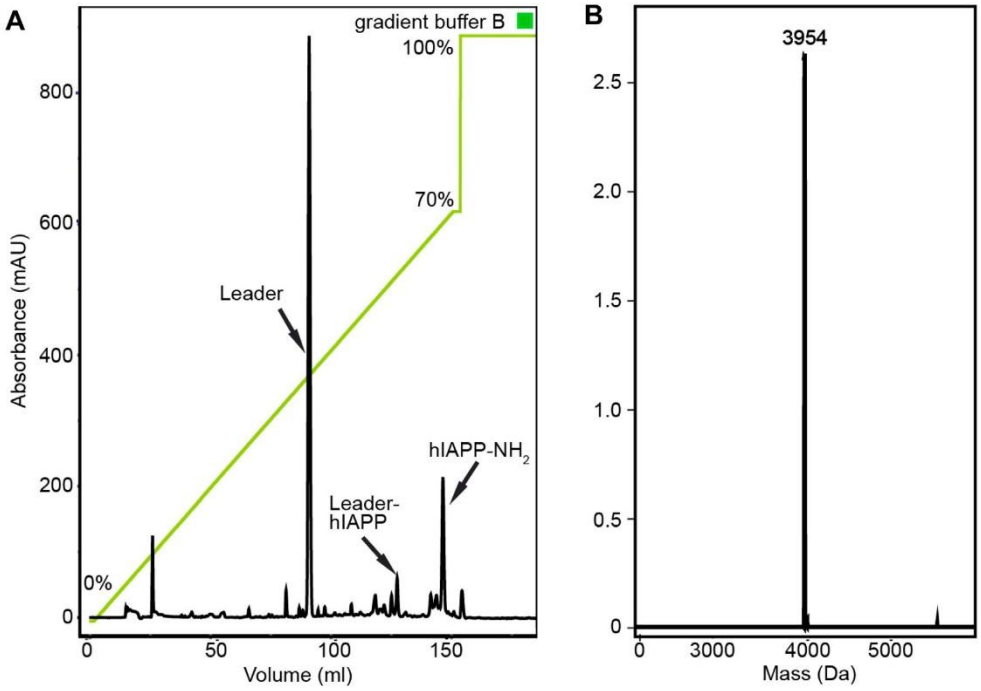

Fig. 5. (A) RP-HPLC chromatogram. Elution profile displaying impurities, the leader peptide, the non-cleaved leader-hIAPP peptide and the final hIAPP. Purified hIAPP elutes at 65–69% solvent B. Elution was monitored at 280 nm. All peptides were identified by MS. (B) Mass spectrum of purified hIAPP. The experimental mass of 3954 Da is close to the theoretical mass of 3953.4. The hIAPP-samples were collected during HPLC purification and directly used for the mass spectrometric analysis.

H_2O_2. The final concentration of hIAPP and H_2O_2 were ~0.15 mM and 2 mM, respectively. The reaction was carried out at 4 °C for only 4–6 h to prevent oxidative modification of the final peptide. Afterwards, the solution was lyophilized again and then stored at −80 °C. Oxidation of hIAPP was monitored by solution-state NMR (Fig. 6C).

Gel electrophoresis

Tricine–SDS–PAGE gel electrophoresis was performed using 16% Tris-tricine–SDS gels [45]. The gels were fixed for 10 min in 50% methanol and 20% acetic acid, and stained for 10 min with a 0.25% solution of the dye Coomassie (Serva), dissolved in 15% methanol and 10% acetic acid. Gels were subsequently washed with de-ionized water, and destained for 10 min with 10% acetic acid. The final gel was stored in water.

Mass spectrometry

hIAPP samples collected during HPLC purification were directly subjected to a mass spectrometric analysis. High resolution mass spectra (HR-MS) were recorded on a Thermo Finnigan LTQ-FT (ESI-ICR) spectrometer (Software: XCalibur 3.0.63) working in the range of 50–2000 m/z. Deconvolution of the spectra was performed using ProMass 2.8.

Nuclear magnetic resonance spectroscopy

The lyophilized hIAPP peptide was dissolved in a 30 mM solution of acetic acid (pH 5.3). The final NMR sample was supplemented with 10% D_2O. To prevent aggregation, the concentration of hIAPP was kept below 150 μM, and the sample was always kept at 4 °C. NMR experiments were recorded using a 500 MHz Bruker spectrometer equipped with a cryo-cooled triple resonance probe. The proton chemical shift was referenced with respect to the water resonance frequency (4.78 ppm at 4 °C). The ^{15}N shifts were referenced indirectly using the ratio of the ^{1}H and ^{15}N gyromagnetic ratios. The 2D-NOESY spectrum of the amidated hIAPP was recorded using a 700 MHz NMR spectrometer employing a mixing time of 150 ms. The ^{1}H, ^{15}N-HSQC and the NOESY were recorded at 5 °C.

Results

Human IAPP forms easily fibrils whereas the peptide encoding the rat sequence does not form fibrils *in vitro* at all. An alignment of the primary sequences of IAPP from different mammalian species is shown in Fig. 2. As a hormone, IAPP is very conserved in mammals [8]. However in the region comprising residues 20–29, the sequences show some important variations. For dog, rat, mouse and cow this region contains one or more proline residues. Prolines do not easily adopt β-sheet structure and therefore act as inhibitors for fibril formation.

Structural insights into the different human IAPP conformations are of fundamental importance in order to better understand the patho-physiological role of this hormone. NMR investigations to study the structure of hIAPP, its aggregation behavior and its interaction with small molecules require the production of a large amount of isotopically enriched peptide. The existing biochemical protocols only allow the production of non-native hIAPP: expression in inclusion bodies, no amidation at the C-terminus, extra amino acids at the N-terminus, use of toxic chemicals such as cyanogen bromide and residual urea or organic solvents like TFA (trifluoroacetic acid) or HFIP (hexafluoroisopropanol) [23,27–29,31,32].

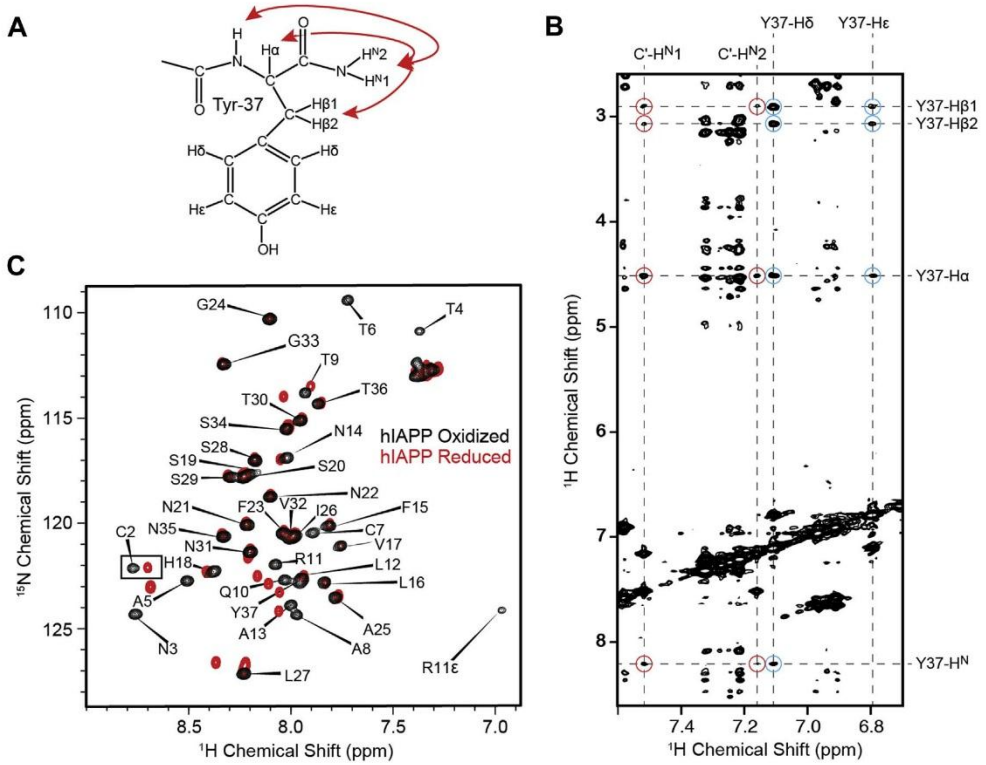

Fig. 6. (A) Structural representation of the amidated Tyr-37 in hIAPP. Expected and observed NOESY correlations are indicated with red arrows. (B) 2D-NOESY spectrum of amidated hIAPP, recorded using a 700 MHz NMR spectrometer employing a mixing time of 150 ms. The resonances of the C-terminal amide group are assigned based on NOE contacts to Tyr37-Hα and Tyr37-H^N (red circles). Intra-residual NOE cross peaks to the Tyr aromatic ring are highlighted (cyan circles). (C) NMR spectra of oxidized (black) and reduced (red) hIAPP. The largest chemical shift changes are observed for residues that are located in the vicinity of the two cysteins C2 and C7. Spectral changes induced by oxidation can be followed in real-time to optimize the reaction conditions for the oxidation process. After quantitative disulfide bond formation, no intensity at peak positions representing the reduced form of the peptide is observed.

Our construct was optimized for the human IAPP sequence and yields native hIAPP in a soluble form, amidated at the C-terminus with no extra residues at the N-terminus.

The hIAPP plasmid contains an intein-tag ligated to a chitin binding domain (CBD) affinity tag at the C-terminus. At the N-terminus, a solubility tag termed leader was included. After expression, the CBD is cleaved off making use of intein splicing reactions. This way, the C-terminus of the protein is amidated by adding ammonium bicarbonate in the cleavage-solution. Cleavage from the column is achieved by addition of thiol reagents such as dithiothreitol (DTT). This purification strategy utilizes the inducible self-cleavage activity of protein splicing elements (termed inteins) [39]. The intein splicing involves a nucleophilic reaction of the first cysteine of the intein to form a linear thioester intermediate, followed by a cleavage and reorganization from the intein with a terminal cyclic imide and the target amidated hIAPP. The high efficiency of C-terminal amidation using inteins has been described previously in the literature [44]. We furthermore confirmed the quantitative attachment of the amino group using NMR spectroscopy (Fig. 6A and B). After elution, the protein is dialyzed to prepare for the cleavage of the solubility leader tag by the V8 protease at the N-terminus. The N-terminal leader solubility tag terminates with a glutamic acid residue which can be cleaved using V8 protease. The hIAPP sequence contains no other glutamic acid residues. The V8 protease is active at pH 8.0 and also in presences of urea [41], a condition which favors hIAPP solubility. A graphical representation of the employed construct is shown Fig. 1. After V8 cleavage, the digestion products are separated by filtration with Amicon filters. The peptide is finally purified by RP-HPLC. Oxidation of the two cysteines in the sequence is achieved by addition of H_2O_2. The final product is lyophilized and stored at −80 °C. An outline of the purification procedure for hIAPP is presented in Fig. 3.

The plasmid containing the hIAPP sequence was transformed into BL21 competent cells. Cells were grown up to an OD_{600} of 0.6 before induction using 0.3 mM IPTG. Induced cells were incubated overnight at 16 °C reaching an OD_{600} of 1.8. Subsequently, the cells were harvested and centrifuged. Protein expression levels were followed by Tricine SDS PAGE. The gel shows a large protein band with an approximate mass of ~32 kDa (Fig. 4A, lane 1). By MS, this band was confirmed to be the fusion protein (data not shown).

Fig. 4, lane 2 shows the flow through of the chitin affinity column after loading it with the lysate. We find that more than 90% of the fusion protein binds to the resin. After loading, the resin is washed using 15–20 column volumes. The wash fractions were also monitored by SDS PAGE, however, due to the high degree of dilution no contaminations were visible on the gel (lane 3). After addition of DTT (incubation overnight), the intein-CBD tag is cleaved, and the 6-kDa leader-hIAPP fusion protein is obtained (lane 4). At this point, we yield approximately 15 mg fusion protein per 1 L of medium. The fusion protein is subsequently cleaved

using V8 protease. Cleavage efficiency is on the order of 90% (Fig. 4B). In comparison to Miranker's construct [31,37], the reaction time and the amount of protease required for cleavage could be significantly reduced. The efficiency of the cleavage reaction increases the final yield and significantly reduces the costs of hIAPP production. In particular, we could show that the amount of protease required can be reduced from 50 mg using the construct of Williamson et al. [37] to 2 mg using the presented strategy. In the construct employed by Miranker and co-worker, two glutamic acid residues occur in the first four amino acids of the leader sequence. These glutamic acid residues are recognize by the V8 protease yielding two bands on the gel (Fig. 4B). In addition, a proline residue was placed in front of the glutamic acid residue in the original construct. Prolines can potentially produce problems for the protease, because the protease cleavage site is more difficult to access. These two changes significantly improved the selective activity of the V8 protease, so that the amount of protease necessary for the cleavage reaction could be significantly reduced (by a factor 25). Simultaneously, the incubation time required for quantitative cleavage could be reduced from 24 h to 1 h. Time is an important factor as hIAPP is highly amyloidogenic and long reaction times compromise the quality of the peptide due to aggregation of hIAPP in the cleavage solution. The cleaved hIAPP is separated from the leader peptide, the non-cleaved fusion protein and the other impurities by RP-HPLC purification (Fig. 4A, lanes 6 and 7). The non-cleaved leader-hIAPP and the cleaved hIAPP are both represented with the same intensity on the gel, using a sufficiently large amount of leader-hIAPP. The final amount of non-cleaved leader-hIAPP is on the order of 0.25 mg per liter culture, which confirms the efficiency of the cleavage.

In the RP-HPLC, the peak containing hIAPP elutes as a single peak at a volume of approximately 140 mL, corresponding to a 65–69% solvent B (100% acetonitrile +0.05% TFA) (Fig. 5A). The collection of this fraction is performed manually to avoid contamination of the product with non-cleaved fusion protein. The purified hIAPP yields a single band on the gel corresponding to a molecular weight of ~4 kDa. The absence of other contaminating bands in the gel indicates a high purity of the sample. Mass spectrometry was performed to determine the exact mass of the purified peptide (Fig. 5B). The mass of the ^{15}N-labeled hIAPP sample was found to be 3954 Da, which closely corresponds to the theoretical mass (3903.4 + 50 for ^{15}N isotopic enrichment).

We finally performed solution-state NMR experiments with the purified hIAPP peptide. The peptide was dissolved in acetic acid (pH 5.3, 30 mM acetic acid). The ^{1}H, ^{15}N-HSQC yields a clean spectrum with 36 peaks corresponding to the 36 amino acids of the hIAPP sequence (Fig. 6C). Even at low contour levels, no additional peaks are observed indicating the high purity of the final product and the quantitative formation of the C2–C7 disulfide bridge in hIAPP. Oxidized and reduced hIAPP show distinct chemical shift patterns. NMR spectra recorded in real-time allow to optimize the reaction conditions for the oxidation process (Fig. 6C).

Discussion

The aim of this project was to establish an expression and purification protocol that allows production of high yields of the hormone hIAPP. The presented protocol allows a cost-efficient production of isotopically-enriched hIAPP, whereas the chemical synthesis of the uniformly-labeled peptide is prohibitively expensive. The *E. coli* fusion system allows to obtain amyloid peptides of high purity. Our construct yields hIAPP peptides with no additional residues at the N-terminus. Furthermore, amidation at the C-terminus is achieved by making use of an intein splicing reaction. Amidation and disulfide bond formation between cysteines 2 and 7 are essential for its biological function [8,33]. The purification is performed without addition of organic solvents such as HFIP, as traces of organic solvent can potentially interfere with the aggregation behavior of hIAPP. We note that purification of human IAPP is more complicated in comparison to purification of IAPP from other organisms such as rat. This is due to the high intrinsic amyloidogenicity of hIAPP. The strategy presented here has several advantages in comparison to previous reports such as C-terminal amidation. The method should be applicable to hIAPP mutants as well as to deletion constructs.

In conclusion, we demonstrated that it is possible to obtain pure human IAPP with yields of approximately 2.5 mg in minimal medium and 3 mg in LB medium from 1 L culture. We believe that the availability of this construct will stimulate further NMR spectroscopic investigations which will lead to a better understanding of protein misfolding.

Acknowledgments

This work was performed in the framework of SFB-1035/Project-B07 (German Research Foundation, DFG). We acknowledge support by the Helmholtz-Gemeinschaft, and the Deutsche Forschungsgemeinschaft (Grants Re1435). We are also grateful to the Center for Integrated Protein Science Munich (CIPS-M) for financial support. We want to thank the HELENA and the TUM graduate school, as well as Dr. Vanessa Morris, Ashish Kawale and Christoph Hartlmüller for stimulating discussions.

References

[1] A. Kanatsuka, H. Makino, H. Ohsawa, Y. Tokuyama, T. Yamaguchi, S. Yoshida, M. Adachi, Secretion of islet amyloid polypeptide in response to glucose, FEBS Lett. 259 (1) (1989) 199–201.
[2] B. Ludvik, A. Kautzky-Willer, R. Prager, K. Thomaseth, G. Pacini, Amylin: history and overview, Diabet. Med. 14 (S2) (1997) S9–S13.
[3] T. Sanke, T. Hanabusa, Y. Nakano, C. Oki, K. Okai, S. Nishimura, M. Kondo, K. Nanjo, Plasma islet amyloid polypeptide (amylin) levels and their responses to oral glucose in type 2 (non-insulin-dependent) diabetic patients, Diabetologia 34 (2) (1991) 129–132.
[4] H.J. Woerle, M. Albrecht, R. Linke, S. Zschau, C. Neumann, M. Nicolaus, J.E. Gerich, B. Göke, J. Schirra, Impaired hyperglycemia-induced delay in gastric emptying in patients with type 1 diabetes deficient for islet amyloid polypeptide, Diabetes Care 31 (12) (2008) 2325–2331.
[5] M.W. Cluck, C.Y. Chan, T.E. Adrian, The regulation of amylin and insulin gene expression and secretion, Pancreas 30 (1) (2005) 1–14.
[6] T. Sanke, G. Bell, C. Sample, A. Rubenstein, D. Steiner, An islet amyloid peptide is derived from an 89-amino acid precursor by proteolytic processing, J. Biol. Chem. 263 (33) (1988) 17243–17246.
[7] C. Betsholtz, V. Svensson, F. Rorsman, U. Engström, G.T. Westermark, E. Wilander, K. Johnson, P. Westermark, Islet amyloid polypeptide (IAPP): cDNA cloning and identification of an amyloidogenic region associated with the species-specific occurrence of age-related diabetes mellitus, Exp. Cell Res. 183 (2) (1989) 484–493.
[8] M. Nishi, S.J. Chan, S. Nagamatsu, G.I. Bell, D.F. Steiner, Conservation of the sequence of islet amyloid polypeptide in five mammals is consistent with its putative role as an islet hormone, Proc. Natl. Acad. Sci. 86 (15) (1989) 5738–5742.
[9] S. Mosselman, J. Höppener, C. Lips, H. Jansz, The complete islet amyloid polypeptide precursor is encoded by two exons, FEBS Lett. 247 (1) (1989) 154–158.
[10] L. Marzban, G. Trigo-Gonzalez, X. Zhu, C.J. Rhodes, P.A. Halban, D.F. Steiner, C.B. Verchere, Role of β-cell prohormone convertase (PC) 1/3 in processing of pro-islet amyloid polypeptide, Diabetes 53 (1) (2004) 141–148.
[11] J. Wang, J. Xu, J. Finnerty, M. Furuta, D.F. Steiner, C.B. Verchere, The prohormone convertase enzyme 2 (PC2) is essential for processing pro-islet amyloid polypeptide at the NH2-terminal cleavage site, Diabetes 50 (3) (2001) 534–539.
[12] F. Evers, C. Jeworrek, S. Tiemeyer, K. Weise, D. Sellin, M. Paulus, B. Struth, M. Tolan, R. Winter, Elucidating the mechanism of lipid membrane-induced IAPP fibrillogenesis and its inhibition by the red wine compound resveratrol: a synchrotron X-ray reflectivity study, J. Am. Chem. Soc. 131 (27) (2009) 9516–9521.
[13] G. Cooper, A. Willis, A. Clark, R. Turner, R. Sim, K. Reid, Purification and characterization of a peptide from amyloid-rich pancreases of type 2 diabetic patients, Proc. Natl. Acad. Sci. 84 (23) (1987) 8628–8632.
[14] A. Andersson, S. Bohman, L.A. Borg, J.F. Paulsson, S.W. Schultz, G.T. Westermark, P. Westermark, Amyloid deposition in transplanted human

pancreatic islets: a conceivable cause of their long-term failure, Exp. Diabetes Res. 2008 (2008) 562985.
[15] A.J. Shapiro, J.R. Lakey, E.A. Ryan, G.S. Korbutt, E. Toth, G.L. Warnock, N.M. Kneteman, R.V. Rajotte, Islet transplantation in seven patients with type 1 diabetes mellitus using a glucocorticoid-free immunosuppressive regimen, N. Engl. J. Med. 343 (4) (2000) 230–238.
[16] R. Mishra, M. Geyer, R. Winter, NMR spectroscopic investigation of early events in IAPP amyloid fibril formation, ChemBioChem 10 (11) (2009) 1769–1772.
[17] R.P. Nanga, J.R. Brender, S. Vivekanandan, A. Ramamoorthy, Structure and membrane orientation of IAPP in its natively amidated form at physiological pH in a membrane environment, Biochim. Biophys. Acta 1808 (10) (2011) 2337–2342.
[18] L. Wei, P. Jiang, W. Xu, H. Li, H. Zhang, L. Yan, M.B. Chan-Park, X.-W. Liu, K. Tang, Y. Mu, The molecular basis of distinct aggregation pathways of islet amyloid polypeptide, J. Biol. Chem. 286 (8) (2011) 6291–6300.
[19] J.R. Cort, Z. Liu, G.M. Lee, K.N. Huggins, S. Janes, K. Prickett, N.H. Andersen, Solution state structures of human pancreatic amylin and pramlintide, Protein Eng. Des. Sel. 22 (8) (2009) 497–513.
[20] E. Jack, M. Newsome, P.G. Stockley, S.E. Radford, D.A. Middleton, The organization of aromatic side groups in an amyloid fibril probed by solid-state 2H and 19F NMR spectroscopy, J. Am. Chem. Soc. 128 (25) (2006) 8098–8099.
[21] S. Luca, W.-M. Yau, R. Leapman, R. Tycko, Peptide conformation and supramolecular organization in amylin fibrils: constraints from solid-state NMR, Biochemistry 46 (47) (2007) 13505–13522.
[22] J.T. Nielsen, M. Bjerring, M.D. Jeppesen, R.O. Pedersen, J.M. Pedersen, K.L. Hein, T. Vosegaard, T. Skrydstrup, D.E. Otzen, N.C. Nielsen, Unique identification of supramolecular structures in amyloid fibrils by solid-state NMR spectroscopy, Angew. Chem. Int. Ed. Engl. 48 (12) (2009) 2118–2121.
[23] I. Kosicka, T. Kristensen, M. Bjerring, K. Thomsen, C. Scavenius, J.J. Enghild, N.C. Nielsen, Preparation of uniformly ^{13}C,^{15}N-labeled recombinant human amylin for solid-state NMR investigation, Protein Expr. Purif. 99 (2014) 119–130.
[24] M.R. Nilsson, L.L. Nguyen, D.P. Raleigh, Synthesis and purification of amyloidogenic peptides, Anal. Biochem. 288 (1) (2001) 76–82.
[25] V.H. Finder, I. Vodopivec, R.M. Nitsch, R. Glockshuber, The recombinant amyloid-β peptide Aβ1–42 aggregates faster and is more neurotoxic than synthetic Aβ1–42, J. Mol. Biol. 396 (1) (2010) 9–18.
[26] F. Meng, A. Abedini, A. Plesner, C.B. Verchere, D.P. Raleigh, The flavanol (−)-epigallocatechin 3-gallate inhibits amyloid formation by islet amyloid polypeptide, disaggregates amyloid fibrils, and protects cultured cells against IAPP-induced toxicity, Biochemistry 49 (37) (2010) 8127–8133.
[27] J.F. Paulsson, S.W. Schultz, M. Köhler, I. Leibiger, P.-O. Berggren, G.T. Westermark, Real-time monitoring of apoptosis by caspase-3-like protease induced FRET reduction triggered by amyloid aggregation, Exp. Diabetes Res. 2008 (2008).
[28] S.M. Patil, S. Xu, S.R. Sheftic, A.T. Alexandrescu, Dynamic alpha-helix structure of micelle-bound human amylin, J. Biol. Chem. 284 (18) (2009) 11982–11991.
[29] D.H. Lopes, C. Colin, T.L. Degaki, A.C. de Sousa, M.N. Vieira, A. Sebollela, A.M. Martinez, C. Bloch Jr., S.T. Ferreira, M.C. Sogayar, Amyloidogenicity and cytotoxicity of recombinant mature human islet amyloid polypeptide (rhIAPP), J. Biol. Chem. 279 (41) (2004) 42803–42810.
[30] E.A. Mireck, L. Gremer, S. Schiefer, F. Oesterhelt, M. Stoldt, D. Willbold, W. Hoyer, Engineered aggregation inhibitor fusion for production of highly amyloidogenic human islet amyloid polypeptide, J. Biotechnol. (2014).
[31] J.A. Williamson, A.D. Miranker, Direct detection of transient α-helical states in islet amyloid polypeptide, Protein Sci. 16 (1) (2007) 110–117.
[32] Y. Mazor, S. Gilead, I. Benhar, E. Gazit, Identification and characterization of a novel molecular-recognition and self-assembly domain within the islet amyloid polypeptide, J. Mol. Biol. 322 (5) (2002) 1013–1024.
[33] P. Westermark, A. Andersson, G.T. Westermark, Islet amyloid polypeptide, islet amyloid, and diabetes mellitus, Physiol. Rev. 91 (3) (2011) 795–826.
[34] A. Roberts, B. Leighton, J. Todd, D. Cockburn, P. Schofield, R. Sutton, S. Holt, Y. Boyd, A. Day, E. Foot, Molecular and functional characterization of amylin, a peptide associated with type 2 diabetes mellitus, Proc. Natl. Acad. Sci. 86 (24) (1989) 9662–9666.
[35] G.J.S. Cooper, A.J. Day, A.C. Willis, A.N. Roberts, K.B.M. Reid, B. Leighton, Amylin and the amylin gene: structure, function and relationship to islet amyloid and to diabetes mellitus, Biochim. Biophys. Acta – Mol. Cell Res. 1014 (3) (1989) 247–258.
[36] G. Forloni, E. Lucca, N. Angeretti, P. Della Torre, M. Salmona, Amidation of β-amyloid peptide strongly reduced the amyloidogenic activity without alteration of the neurotoxicity, J. Neurochem. 69 (5) (1997) 2048–2054.
[37] J.A. Williamson, J.P. Loria, A.D. Miranker, Helix stabilization precedes aqueous and bilayer-catalyzed fiber formation in islet amyloid polypeptide, J. Mol. Biol. 393 (2) (2009) 383–396.
[38] Y. Anraku, R. Mizutani, Y. Satow, Protein splicing: its discovery and structural insight into novel chemical mechanisms, IUBMB Life 57 (8) (2005) 563–574.
[39] S. Chong, F.B. Mersha, D.G. Comb, M.E. Scott, D. Landry, L.M. Vence, F.B. Perler, J. Benner, R.B. Kucera, C.A. Hirvonen, J.J. Pelletier, H. Paulus, M.-Q. Xu, Single-column purification of free recombinant proteins using a self-cleavable affinity tag derived from a protein splicing element, Gene 192 (2) (1997) 271–281.
[40] G.R. Drapeau, Y. Boily, J. Houmard, Purification and properties of an extracellular protease of *Staphylococcus aureus*, J. Biol. Chem. 247 (20) (1972) 6720–6726.
[41] J. Houmard, G.R. Drapeau, Staphylococcal protease: a proteolytic enzyme specific for glutamoyl bonds, Proc. Natl. Acad. Sci. 69 (12) (1972) 3506–3509.
[42] C. Cui, W. Zhao, J. Chen, J. Wang, Q. Li, Elimination of in vivo cleavage between target protein and intein in the intein-mediated protein purification systems, Protein Expr. Purif. 50 (1) (2006) 74–81.
[43] J. Marley, M. Lu, C. Bracken, A method for efficient isotopic labeling of recombinant proteins, J. Biomol. NMR 20 (1) (2001) 71–75.
[44] I.R. Cottingham, A. Millar, E. Emslie, A. Colman, A.E. Schnieke, C. McKee, A method for the amidation of recombinant peptides expressed as intein fusion proteins in *Escherichia coli*, Nat. Biotechnol. 19 (10) (2001) 974–977.
[45] H. Schägger, Tricine–SDS–PAGE, Nat. Protoc. 1 (1) (2006) 16–22.

5. Description of the second hIAPP manuscript

Change of the redox environment in a β-cell triggers conformational changes at the N-terminus of hIAPP and influences its aggregation in Type II Diabetes

Rodriguez Camargo, Diana C.[1,2]; Tripsianes, Konstantinos[3]; Hartlmueller, Christoph[2]; Goebl, Christoph[2]; Sarkar, Riddhiman[2]; Aichler, Michaela[1]; Mettenleiter, Gabriele[1]; Madl, Tobias[2]; Reif, Bernd[1,2].

Diabetes mellitus is a disease that affects a large amount of people in the world. Diabetes mellitus can be classified into two subtypes: T1D is characterized by a lack of insulin production and an autoimmune destruction of the β-cells. T2D is a non-insulin-dependent disease and is characterized by the development of insulin resistance in the body. The second characteristic of T2D diabetes is a β-cells failure. The loss of β-cells mass is attributed to the presence of an aggregate that consists of the hormone hIAPP that is normally co-secreted with insulin. In this paper we present the structural analysis of monomeric full-length hIAPP in aqueous buffer. The production of the isotopically labeled peptide was performed following our protocol published in 2014. 3D and 2D solution-state NMR experiments were performed to obtain assignments and distance restrains for structure calculations. We show that the peptide has a 50 % propensity for α-helical secondary structure at the N-terminus. This α-helix is stabilized by the disulphide bridge between residues 2 and 7. This disulphide bridge plays an important role in the stabilization of the structure of hIAPP and affects its aggregation properties. We show by NMR and fluorescence spectroscopy that the aggregation kinetics of the reduced and oxidized peptides are different. The reduced form of hIAPP is aggregating faster in comparison to the oxidized form of hIAPP. This behavior correlates with the hypothesis that changes in the redox environment in the cell are responsible for the acceleration of aggregation. Changes in the electro-chemical environment of the cell is produced by the disequilibrium of the concentration in the oxidizing and reducing agents, high concentration of metals, over production of reactive nitrogen species *RNS*, reactive oxygen species *ROS* in the cell and over expression and misfolding of proteins.

Yielding a shift of equilibrium from the oxidized to the reduced state of the molecule. These results indicate that a small concentration of reduced hIAPP has a dramatic impact on the aggregation properties of the (mostly) oxidized peptide and for this reason on the aggregation pathway of hIAPP. We used NMR to determine the redox potential of hIAPP. The hIAPP has a redox potential that is close to the redox value for an apoptotic cell, which observation also supports our hypothesis. In this paper we suggest a correlation between the redox state of a cell and the aggregation properties of hIAPP. Furthermore, we propose that the interference with the protein disulphide isomerase machinery in the ER due to redox change in the cell can have a fundamental impact on the progression of T2D.

Paper in preparation for submission in 2015

Change of the redox environment in a β-cell triggers conformational changes at the N-terminus of hIAPP and influences its aggregation in Type II Diabetes

Rodriguez Camargo Diana C.[1,2]; Tripsianes Konstantinos[3]; Göbl Christoph[1,2]; Hartlmüller Christoph[2]; Sarkar Riddhiman[2]; Aichler Michaela[1]; Mettenleiter Gabriele[1]; Madl Tobias[1,2,4,5]; Reif Bernd[1,2].

Abstract— **T2D is characterized by resistance of cells to insulin. This triggers the overproduction of regulatory hormones such as insulin and human islet amylin polypeptide (hIAPP). We present a characterization of the structure of hIAPP in solution. We found that the N terminus of hIAPP^{oxi} has a higher propensity to form an α-helical structure in comparation to hIAPP^{red}. At the same time, hIAPP^{red} shows an enhanced aggregation propensity compared to hIAPP^{oxi}. In T2D the resulting high flux of proteins through the endoplasmic reticulum generates ER stress and consequently leads to a shift of the ER to a more reducing environment. We suggest that a change in the redox environment of a diabetic pancreatic β-cell, coupled with an increase of available hIAPP, induces β-cell disruption by amyloid deposition.**

Terms— **Amyloid; diabetes; human islet amyloid polypeptide (hIAPP); redox environment; redox potential, nuclear magnetic resonance (NMR).** **E-mail to reif@tum.de**

I. Introduction

Type II diabetes or T2D is the most common form of diabetes. This is caused by a rich combination of genetic and environmental factors. This process ends principally in a characteristic insulin resistance and β-Cells failure[1,2]. These mechanisms are also linked to the tissue inflammation response[3]. The pathogenic mechanism in T2D has not been totally clarified by now. However, there are five principal factors identified that contribute to this: Insulin resistance of the cells, lipotoxicity, oxidative stress, Endoplasmic Reticulum stress and the Amyloid deposition in the islets[3,4]. In the islets of most patients with T2D these amyloid deposits are found. The plaques formed in the pancreas are composed by the 37 amino acids long polypeptide, called diabetes peptide or human Islet Amyloid Polypeptide (hIAPP). In other recent studies is also shown that soluble oligomers of this hormone are toxic for the cells, too[5,6].

The way this hormone can change its regulatory role to a pathophysiological role is unclear until now.

The structure of the hormone hIAPP in aqueous solvent was also not clear. It was reported for having a random coil structure[7]. However, some techniques like CD, MD simulations, some x-ray crystallography and NMR in different conditions were suggesting that the peptide forms at least a transient amphipathic helix in the N-terminal part[8-12].

For the first time, we present here the structure in solution of the monomer in biological conditions, similar to the insulin storage granules in the β-cells, where the peptide is stored together with insulin for posterior secretion. We used a 30 mM acetic acid buffer at pH 5.3. Similar to the acidic pH characteristic of these granules, which are typically between 5 and 6. It is proposed that the acidic pH is favorable for the dissolution of basic molecules like IAPP. How IAPP is soluble in the cell at concentrations between about 1-4 mM in these granules is a mystery, because in vitro IAPP aggregates with 1000 times lower that this concentration[12-14]. The knowledge of the structure of the monomer peptide allows the understanding of its pathologic role. It may also help to understand how possible inhibitors affect the monomer conformation to avoid the aggregation in the first step of the aggregation process.

In this paper it is shown that the full length c-terminal amidated monomer peptide presents an α-helix conformation at the N-terminus of the molecule. This helix ends in the amino acid histidine 18 (His18). This correlates with the observation published before, which suggests that the His18 is the principal key for the orientation of the molecule in the membrane[8]. It was also found that this α-helix is stabilized by the disulphide bridge between residue 2 and 7. This attribute makes hIAPP a redox sensitive molecule which changes its function, if the redox environment is modified. For this reason here it is proposed that the redox state of the cell plays an important role in the

Affiliations:
[1] Helmholtz Zentrum München (Deutsches Forschungszentrum für Gesundheit und Umwelt),Ingolstädter Landstr. 1, 85764 Neuherberg, Germany
[2] Munich Center for Integrated Protein Science (CIPS-M) at Department Chemie, Technische Universität München (TUM)
[3] Central European Institute of Technology (CEITEC), Masaryk University, Kamenice 5, 62500 Brno, Czech Republic
[4] Institute of Molecular Biology & Biochemistry, Center of Molecular Medicine, Medical University of Graz, Austria
[5] Omics Center Graz, BioTechMed Graz, 8010 Graz, Austria

Paper in preparation for submission in 2015

aggregation mechanism of the peptide and in consequence in the development of T2D. The complete mechanism of the aggregation process is unknown until now. However, we presume that the aggregation is influenced by conditions of concentration, pH and oxidative or reductants agents, which control the amount of open and close disulphide bridge in the cell, like Glutathione couple[7-10,12-16]. Because the redox buffering in the cell is principally controlled by the couple of Glutathione[17], the redox potential of the hIAPP in vitro was measured by the titration of the oxidized monomer utilizing varying ratios of oxidized and reduced glutathione[18]. With this type of NMR experiment it was possible to simulate the redox conditions of a cell under stress, especially for the Endoplasmic Reticulum (ER). This is validated by other publications, where is clearly defined that the redox state of the ER in diabetes is shifted to a more reducing state and in consequence a defective protein secretion and folding of many proteins are produced[19-21]. Based on these observations, together with the results presented in this paper, it is concluded that the alteration in the ER-redox of diabetes patients plays a fundamental role for the aggregation pathway of hIAPP[34,22], because the reduced form of hIAPP aggregates nearly three times faster than the oxidized form. This process is a product of the change in the structure of the peptide and therefore of its aggregation kinetic. We discovered, that the structural properties of the hIAPP are linked with the redox environment. This observation helps to understand the pathological role of this hormone, giving the basis for future works that help to find inhibitors for this aggregation.

Results

The objectives of this study were the determination of the human IAPP structure into biological pH, prior to amyloid formation, and the characterization of its structural proprieties, linked with the redox potential of the molecule. Recombinant C-terminal amidated $hIAPP_{1-37}$ is produced using the protocol published recently[23]. First, we examined the solution properties of the peptide, the quantification of its redox potential and its structural conformation by solution NMR spectroscopy. Circular Dichroisms and Electron Microscopy are utilized to complement the NMR data, where the secondary structure propensity of the peptide is clearly observed. Finally, fluorescence spectroscopy is used to characterize the kinetics of the amyloid assembling.

Structural analysis of hIAPP

hIAPP has a strong tendency to aggregate in aqueous buffer. However, We find that at low pH (5.3), low temperature (4 deg C.), low concentration (100uM) and in a acetic acetate buffer containing no salt, fibril formation is delayed. In these conditions, the reduced form of the peptide fibrillizes faster in comparison to the oxidized peptide (Figure 1). In Electron microscopy images, we find different morphologies for fibrils of reduced and oxidized hIAPP (Figure 1). Under similar incubation conditions, $hIAPP^{oxi}$ adopts short protofilament-like aggregates, $hIAPP^{red}$ forms more mature-like fibrils.

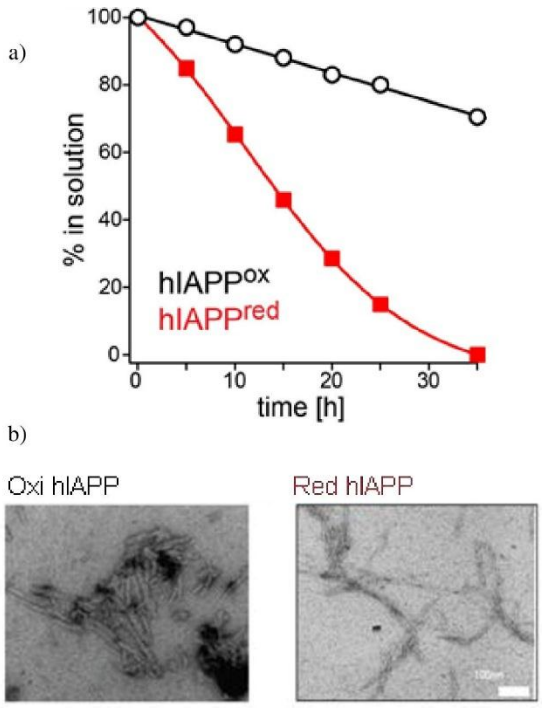

Figure 1: Aggregation kinetics measured by NMR. In the experiment 100 μM solution of hIAPP was dissolved into 30 mM d-acetic acid pH 5.3 at 5 °C. Reduce hIAPP aggregates significantly faster in comparison to the oxidize peptide a). The aggregates produced after 8 days of incubation and similar buffer conditions, was monitored by EM; images of oxidized (left) and reduced (right) hIAPP fibrils present clear difference in morphology b).

$hIAPP_{1-37}$ in aqueous buffer produces a CD spectrum which contains contributions from α-helix and random coil secondary structure. Comparison of the oxidized and reduced form of the peptide suggests that a loss of the disulphide bond induce a loss of the α-helix structure (Figure 2). Oxidation of hIAPP is in detail monitored by solution-state NMR. The $^{1}H,^{15}N$ HSQC spectra of reduced and oxidized hIAPP yield significant chemical shift differences, In particular for Cys2 and Cys7 as well as for residues in the vicinity of the disulphide bridge (Figure 2), Chemical shift assignment has been obtained from 3D HNCACB experiments, an is in agreement with previous NMR studies.

Paper in preparation for submission in 2015

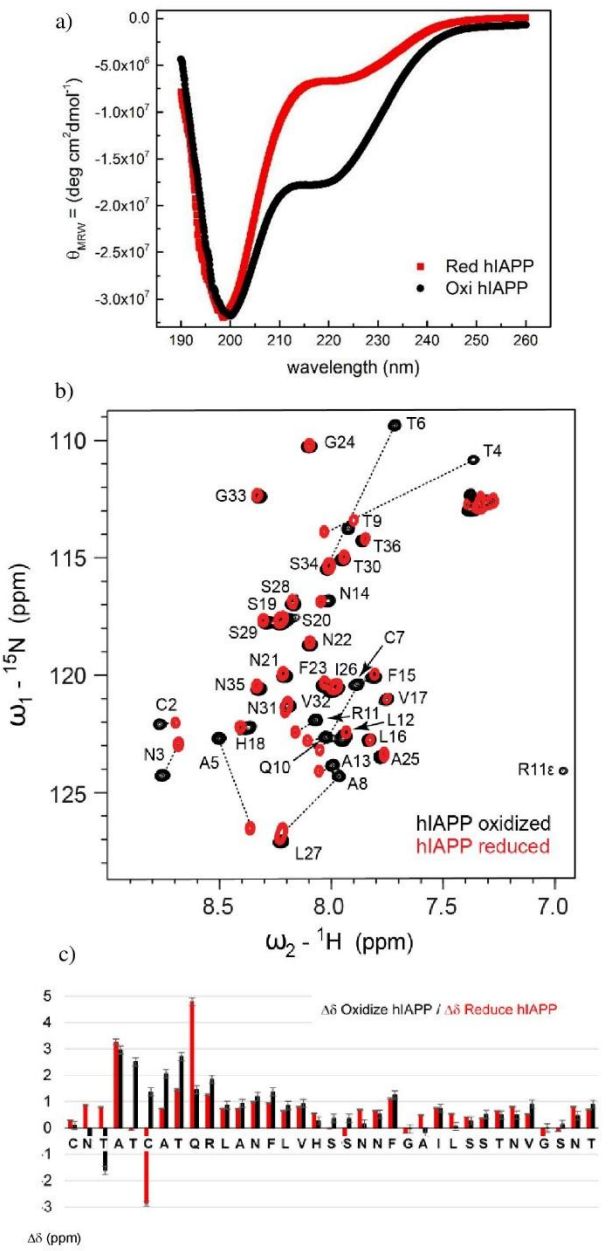

Figure 2: Circular dichroisms spectra of reduces (red) and oxidized hIAPP (black). The oxidize form shows clearly a negative band at 222 nm and 208 nm characteristic of an α-helical conformation. The reduced form shows a considerably smaller band at 222 nm indicating a larger degree of random coil conformation. The CD spectra of full-length hIAPP was recorded into acetic acid buffer pH 5.3, at 25 °C. a). ^{1}H, ^{15}N-HSQC spectra of the reduced (red) and oxidized (black) hIAPP. Amino acids are labelled according to their type and sequence number. Major chemical shift changes upon disulphide bond formation are indicated by black dashed lines. The spectra are recorded at 5 °C, pH 5.3 in 30 mM acetic acid buffer b). $13C^{\alpha/\beta}$ secondary chemical shift analysis. Differences of deviations from random coil chemical shifts for Cα and Cβ δΔ (ppm) are represented as a function of the primary sequence. The reduced conformation of hIAPP is shown in red. Reduction was induced by adding 10 mM TCEP. In turn, oxidized peptide was obtain by addition of 2 mM H_2O_2 (black) c).

The analysis of $13C^{\alpha/\beta}$ secondary chemical shifts revealed a strong helical propensity for the N-terminal half of the oxidized hIAPP peptide (residues 5-17) and random coil conformation for the C-terminal half (Figure 2). The same analysis for the reduced form of hIAPP showed a smaller helical propensity for the N-terminal half, suggesting that the N-terminal disulphide bridge stabilizes the helical conformation. The structural change between these two conformations aroused our interest to explore in more detail of the partial structure of the oxidized form of hIAPP.

For NMR structure determination we were able to collect high-quality NOESY data only for the oxidized hIAPP form. These data consisted of a ^{15}N-edited 3D NOESY and a homonuclear 2D-NOESY experiments, the latter one with improved resolution and signal-to-noise ratio that also allowed to probe the proton frequencies of the amidated C-terminus. Side chain assignments were obtained from 3D-HCCH TOCSY experiments in general. NOESY experiments allowed to assign additional proton frequencies so that an overall assignment completeness of 97% was reached. Sequential and inter-residual NOE cross-peaks that could be resolved in the 15N-edited spectrum were assigned manually for the N-terminal half and were kept fixed during structure calculations with CYANA. Peak intensities for all cross-peaks were converted to distances using the internal function of CYANA. During torsion angle dynamics CYANA assigned 93% of the input peaks including those that they were fixed. The ensemble of the 20 lowest energy structures obtained after water refinement is shown in Figure 3. A summary of the structural and restraint statistics is given in Table 1. Notice that no hydrogen bond restraints for a-helix were included in the structure calculations.

The present solution structure of native hIAPP (oxidized and amidated) shares similarities, but also has differences when compared to other structures of amylin reported under different conditions, e.g. no amidation and in presence of SDS micelles. A common theme in all structures is the N-terminal loop forced by the disulphide bridge followed by a right-handed a-helix. In our study, the oxidized state of the attached sulfur atoms is confirmed by the 13Cβ secondary chemical shifts of the two cysteines (Cys2 and Cys7). In the present structure, the α-helix spans residues 8-17 as determined by NMR experimental data, that is dihedral angles based on secondary chemical shifts and characteristic helical NOEs such as dαN(i,i+3), dαN(i,i+4), and

Paper in preparation for submission in 2015

dαβ(i,i+3), without imposing helical hydrogen bonds restraints).

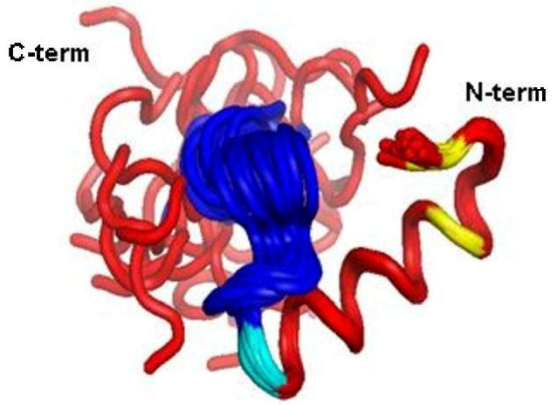

Figure 3: 20 refined structures by high-resolution NMR for residues 2-18 of amidated hIAPP1-37 at 5 °C into 30 mM d Acetic acid pH 5.3. Calculated by Solution NMR using CYANA software. The structure shows an α-helix structure until residue number 18 which correspond to the His18 (cyan), a formed disulphide bridge (yellow), a transient, helix from residue 22 (blue) and an unstructured C-terminal (red).

Table 1. Statics of structure calculation of full length hIAPP

(residues 1-37)

NMR distance and dihedral constraints	
Distance constraints	
Total NOE	515
Intra-residue	140
Inter-residue	375
Sequential ($\|i-j\|=1$)	191
Medium-range ($\|i-j\|<4$)	164
Long-range ($\|i-j\|>5$)	20
Total dihedral angle restraints	10
ϕ	5
ψ	5
Structure statistics	
Violations (mean ± s.d.)	
Distance constraints (Å)	0.023 ± 0.01
Dihedral angle constraints (°)	0.55 ± 0.18
Max. dihedral angle violation (°)	2.55
Max. distance constraint violation (Å)	0.37
Deviations from idealized geometry	
Bond lengths (Å)	0.004 ± 0.00
Bond angles (°)	0.476 ± 0.03
Impropers (°)	0.983 ± 0.11
Average pairwise r.m.s. deviation** (Å)	
Heavy	0.78 ± 0.20
Backbone	0.50 ± 020
Ramachandran plot statistics (%)	
Residues in most favoured regions	82.4
Residues in additionally allowed regions	13.9
Residues in generously allowed regions	1.2
Residues in disallowed regions	2.4

** Pairwise r.m.s. deviation was calculated among 20 refined structures for residues 2-18.

At position 18 there is a His (18His) residue that is incompatible with helical conformation and introduces a kink, in line with earlier findings. After that point the backbone follows a random-coil conformation, in contrast to previous structures determined in the presence of micelles and have reported a second, rather transient, helix from residue 22 onwards.

The NOE pattern of the ^{15}N-edited 3D NOESY experiment is dominated by strong correlations between the respective amides and (i-1) Hα atoms, which is the hallmark of disordered proteins. In addition to that, no informative NOEs are detected for the C-terminal amide suggesting that cross-talk to distant residues is unlike or faster than the chemical shift timescale.

Two distinct regions can be distinguished in the native amylin peptide: An ordered N-terminal half and a disordered C-terminal half with a kink of 3-4 residues in between. The structural model is supported by {^{1}H}-^{15}N heteronuclear NOE data that show a uniform rigidity for the N-terminal half and increasing flexibility towards the C-terminus of hIAPP.

Additionally, hetero-NOEs of the 1H-15N amide bond were measured in the oxidize conformation of hIAPP, with the objective of complementing and confirming the N terminal structure of hIAPP, calculated by solution-state NMR. The results show clearly that at the N terminus of the hIAPP in the standardized aqueous solution is a structured peptide like it is shown in the Figure 4.

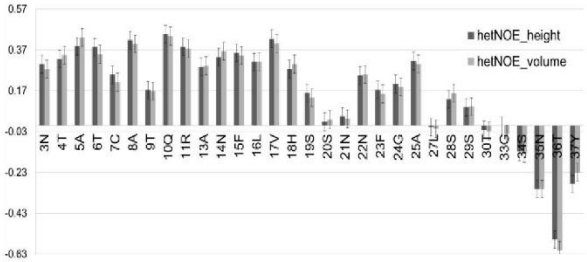

Figure 4: Heteronuclear secondary shifts for HN of 100 uM hIAPP into 30 mM d-Acetic acid pH 5.3 at 5 °C, confirming the tendency of the N-terminal part in the molecule to form an α-Helix.

Also residual dipolar couplings (DNH) for the backbone ^{15}N resonances were obtained by subtraction of the anisotropic from the isotropic JN-HN values determined from the ^{1}H-^{15}N IPAP-HSQC experiments. The data were fit to the determined solution structure described earlier by minimizing the difference between the experimental and calculated DNH values[24] of each of the lowest 10 energy models. Overlapping and non-resolved residues have been removed from the analysis. The structured part of the molecule (residue 1-20) has been analyzed separately from the flexible tail (21-37) as shown in the Figure 5.

Paper in preparation for submission in 2015

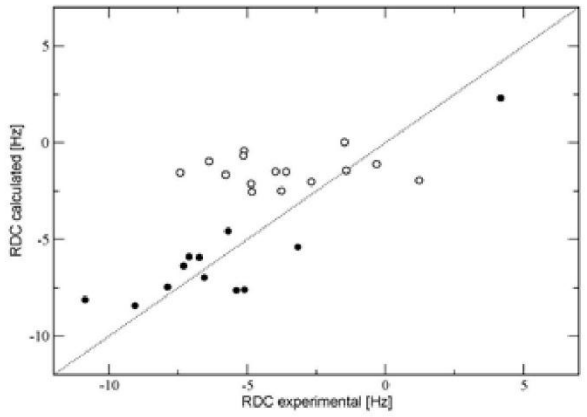

Figure 5: Correlation between experimental and calculated RDCs under partial alignment with 1.5% PEG. Full circles represent data points from the helical N-terminus and open circles are data points from the flexible C-terminus, respectively. Calculated RDC values correspond to the average of the lowest 10 energy conformations.

Assembly Kinetics analysis of hIAPP

To complement the NMR kinetic analysis, measurement of ThT assay is performed, using glutathione in the protein solution to reduce or oxidize the peptide. With this result, we are confirming that the aggregation kinetics of the hIAPP are affected by the oxidative environment.

Here is demonstrated that even in an environment in equilibrium, where the redox pair GSH/GSSG produces a ratio of 50% of reduced and 50% of oxidized hIAPP or when hIAPP is 80% reduced and 20% oxidized, the aggregation kinetic of the reduced hIAPP is similar and faster than the oxidized form. This result indicates that the aggregation of hIAPP is controlled by the reduced form and is almost three times faster than the pure oxidized form.
When the ThT results are fitting by a sigmoidal equation, it is possible to obtain the time at half-maximum intensity (T50). This value is equal to the time, where the half of the population of hIAPP is aggregated. This corresponds to the observed kinetic from each conformation. This result shows clearly that the reduced form presents a kinetic three times faster than the oxidized form.

The redox potential for the formation of the disulfide bond in the hIAPP was determined by NMR spectroscopy. ^{15}N HSQC spectra were recorded after incubating the protein with varying ratios of reduced to oxidized glutathione. A plot of average peak intensities against the $[GSH]^2/[GSSG]$ ratio converted in potential redox of the pair is shown in Figure 7. The redox potential of the hIAPP (-129 +/- 4 mV) was calculated using the Nernst equation with the respective correction for temperature and pH.

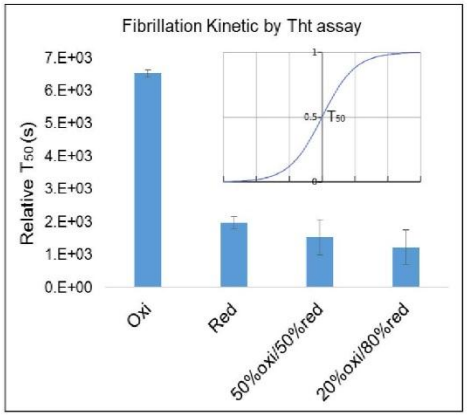

Figure 6: Thioflavin T assay was performed with a solution of 35 uM of hIAPP into acetic acid, pH 5.3 and 30 °C. The T_{50}, which correspond to the relative scales of hIAPP assembly kinetics is plotted versus different redox conditions. IAPP kinetics were monitored over the time with clear changes in the fluorescence of the exogenous ThT dye. The corresponded Kinetic profiles were fit to a sigmoid to extract the time at half-maximum intensity (T_{50}). These data show clearly that the disequilibrium in the redox environment made the peptide more fibrollogenic when the reduced peptide is present.

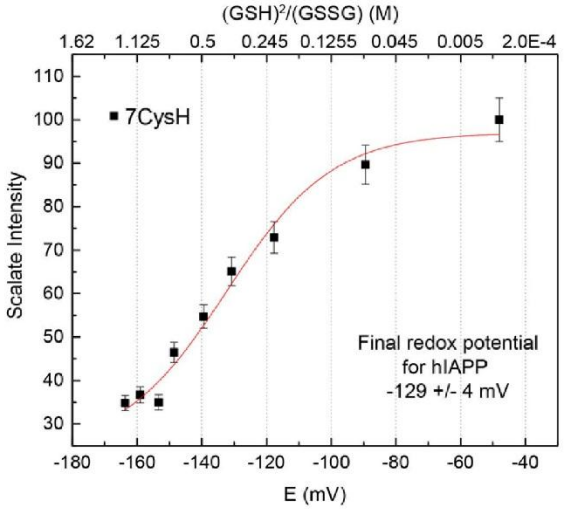

Figure 7: Determination of the redox potential by titration of the hIAPP with variating concentration of GSH/GSSG. Plotted are the normalized peak intensities of the Cys7 versus the potential of the glutathione concentration that is incremented

Paper in preparation for submission in 2015

in the NMR titration: 100 uM of complete oxidize hIAPP into 30 mM Acetic acid at pH 5.3 and 5 °C. The redox potential of hIAPP was calculated to -129 +/- 4 mV.

We demonstrate that the redox potential of the hIAPP is significant oxidative. This observation is significant because the biological status of a cell in apodosis (with changes in the redox environment)[19] could promote the production of reduced hIAPP and accelerate the aggregation of this peptide. To confirm this hypothesis, EM are performed on the aggregates, which are formed when the peptide are oxidized and reduced (Figure 8). The results show clearly that the aggregates are formed only from reduced hIAPP.

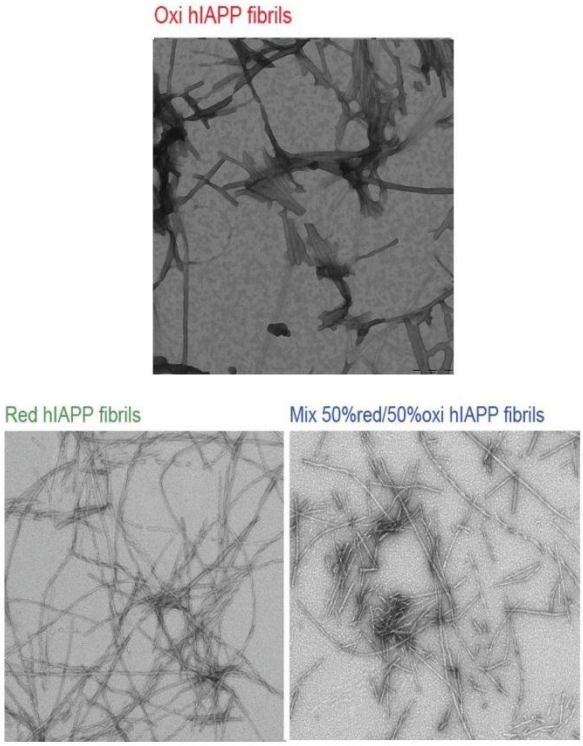

Figure 8: EM of the fibrils formed with different glutathione conditions. NMR of the dissolved fibrils into d6-Acetic acid 99.98% + 1% TFA of the total volume.

Based on these results we present a model of the possible aggregation mechanisms of the hIAPP monomer, when the redox state change in the cell (Figure 9). Here is explained how the change in the redox environment by extern factors like oxidative stress, ER stress, hyperglycemia, lipotoxity, genetic factors, etc. change dramatically the aggregation kinetic of the peptide. The reduced hIAPP is aggregating faster and the equilibrium if shifting. For this reason more oxidized hIAPP converts to a reduced one, which again is aggregating.

We explain this behavior of the reduced peptide as a result of the structural change in its conformation, where the α-helical N-terminal structure decelerates the aggregation process.

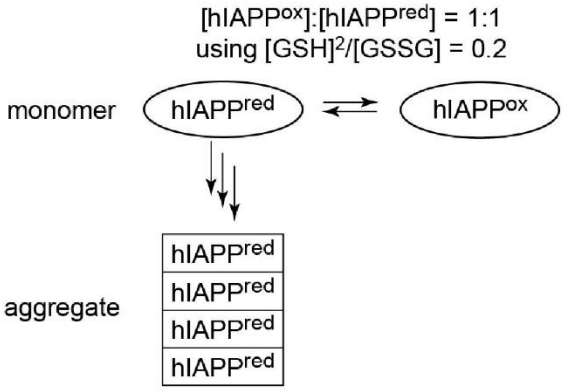

Figure 9: Model of the fibrillation mechanisms of the monomeric hIAPP correlate with the change of the redox equilibrium in the cell. If the hIAPP are present in reduced form, this aggregate and then the equilibrium is shifting to form from the oxidized peptide more reduced hIAPP, that are takeout of the solution again. We propose that this aggregation tendency are one of the pathway for the toxic aggregation of the hormone an in consequence the follow in the loss of the ß cells of the pancreas in patients of T2D.

II. Conclusion

The shoulder in the CD spectrum in the region of 222 nm in combination with a random coil conformation is indicative for a partial structure in the peptide. This structure is conserved in various buffers, even in water the spectra shows an α-helix conformation in the peptide (data not showed). This first observation together with the reported literature about the tendency of the peptide presents a structure at the N Terminus, arousing our interest to go more deep into the atomical level of the hIAPP. For this reason we performed a complete solution-NMR analysis of this monomer conformation of the hIAPP due to the strong propensity of native hIAPP to form amyloids. The sample conditions were optimized for NMR studies. We concluded that a combination of a moderate acidic pH (5.3), no salt, low temperature (278 K) and protein concentration of ≤150 mM, delayed fibril formation. However, the short lifetime of monomeric hIAPP necessitated a large number of freshly prepared, double-labeled samples to record each 3D NMR experiment, usually requiring 1 to 2 days in measurement time. A set of 3D triple-resonance experiments allowed us to assign the majority of backbone and side chain ^{1}H, ^{15}N and ^{13}C resonances for both oxidized and reduced forms of hIAPP. With

the assignments of the different nuclei, we were in the capacity of analyzing the secondary structure tendency. We found that the N terminal of the molecule presents an α-helical conformation and this decreases if the disulfide bridge in the hIAPP is reduced.

The structure part presented in the calculated structure is confirmed by the measurement of hetero-NOEs and RDCs.
Based on our experimental results obtained by NMR, CD, ThT, EM, we propose a model that shows how the reduced form of hIAPP is more amyloidogenic than the oxidized hIAPP, and it's aggregated without nucleation. With this model we can agree with the hypothesis postulated for Miranka´s group, which proposes that the reduced hIAPP does not contribute to the amyloid fiber core, but it plays a central role in the assembly mechanism. In the first moment the loss of the disulfide bridge in the molecule substantially reduces fiber formation by secondary nucleation, i.e. the ability of pre-existing fibers to participate in the formation of new fibers. In the second moment the bypass of nucleation by seed addition is a two-step process (termed activation). Loss of the disulfide bridge eliminates this two-step and accelerates the aggregation of the peptide. This hypothesis is confirmed with the analysis of the system where the population of hIAPP is 50% reduced and 50% oxidized.

We found that the reduced form aggregates approximately three times faster than the oxidized form. If the reduced form is present, the kinetic is accelerating. That means, that one time the reduced form starts to aggregate, there is no reversible process in the reaction. Furthermore the oxidized molecules that are in the solution are shifting to a reduced form and this again starts to aggregate. This observation is sustained by different publications, especially by the results presented by Nardai (2003), where was demonstrated that in the development of T2D the redox in the β-cells has changed, especially in the ER. This effect made it possible to accelerate the production of hIAPP and therefore the aggregation in the cell.

III. MATERIALS AND METHODS

Molecular biology reagents were obtained from Roche, New England Biolabs and from Sigma-Aldrich St. Louis, MO, USA. Isotopic salts and solvents were obtained from Cambridge Isotope Laboratories.

Recombinant protein

The human IAPP was expressed and purified with our published method used to produce recombinant hIAPP into E. coli culture[23]. This protocol allows the production of a full isotopic enriched peptide, ideal for NMR studies. This presents the amidation at the C-terminus and has the disulphide bridge at the N-terminus.

NMR Sample preparation

Recombinant lyophilize $hIAPP_{1-37}$ was dissolved into the termed NMR buffer, containing: 30 mM of deuterated Acetic Acid at pH 5.3 until a maximal concentration of 150 uM, supplemented with 10 % D_2O. This samples were always stored and measured at 4 °C. The formation of an intramolecular disulfide bond was determined by NMR.

NMR Experiments

All NMR experiments were performed at 5 °C on a Bruker Avance 500, 600, 750 MHz spectrometer, equipped with a cryoprobe. The proton chemical shifts were referenced to the water peak and the ^{15}N and ^{13}C shifts were referenced indirectly. Almost complete backbone and site-change assignments were obtained using Triple resonance experiments. The spectra were processed using Bruker TopSpin and NMRPIPE software and analyzed using SPARKY and ccpNMR analysis.

Structure Calculation

The NOE spectra were manually assigned. The assignments were analyzed using CYANA2.0. Restraints of the dihedral angle were derived from chemical shift using the program TALOS. Distance and angle restraints were used as input for the calculation of the structure on a linux-based cluster. All non-violated structures were recalculated using a water-refinement protocol.

Transmission electron microscopy TEM

Samples were stained with 1% uranyl acetate solution on formvar/carbon coated grids. 10 µl of the sample were placed on the grid for 1 min and the excess of the sample was dried out with paper-filter. After this process the grid was placed on a drop of uranyl solution for 30 s and again the excess of the solution was dried out with paper-filter. The measurement of the sample was performed with the microscope immediately.

RDC Calculation

Uniformly enriched ^{15}N hIAPP was freshly expressed and purified as described earlier. The lyophilized powder was dissolved in NMR buffer (30 mM Acetic acid, pH 5.3) to yield a 200 µM stock solution. The alignment medium was prepared by dissolving 15.6 µl pentaethylene glycol monooctyl ether (PEG, C8E5) in 250 µl of NMR buffer and subsequent addition of overall 8.25 µl octanol (Sigma-Aldrich), while vigorous vortexing the solution at 278 K. The medium yielded a D_2O doublet of 25.5 Hz. The hIAPP solution was combined with the dilute liquid crystalline phase and diluted using NMR buffer to yield a final concentration of 100 µM protein solution and a C8E5-to-water ratio of 1.5% (w/v). The sample was measured at 278 K on an AVIII600 Bruker NMR spectrometer equipped

with gradient coils in the z-direction operating at 600 MHz for ^{1}H.

The final sample yielded a stable D_2O doublet of 5.7 Hz after allowing a period of alignment stabilization monitored by 1-dimensional deuterium spectra. ^{1}H-^{15}N IPAP-HSQC spectra were recorded with 1024 x 64 complex data points and 64 dummy scans to ensure temperature stability. The same parameters were applied to a sample, lacking the alignment medium to obtain a reference dataset. Spectra were processed and peak picked using NMRPipe.

NMR titration Experiment for the calculation of the redox potential

For the redox titration a 100 µM sample of the oxi-hIAPP in NMR buffer (500 µl) was equilibrated with 0.2 mM reduced glutathione (GSH) and 0.2 mM oxidized glutathione (GSSG). At the beginning of the titration, the sample was clear in oxidized form. After this, the concentration of the GSH was increased step by step to 0.5, 1, 1.5, 2, 2.5,3, 5, 7.5, 10, 15 and 18 mM. A ^{15}N-HSQC spectra was recorded after each addition of GSH. For the determination of the redox potential, the intensities of Cys7 in each spectra were determined (data not shown). The highest intensity was arbitrarily scaled to 100. The intensities of the Cys7 were plotted versus $((GSH)^2/(GSSG))$ on a logarithmic scale and fitted against a sigmoidal Logistic equation. The half-point ratio of $((GSH)^2/(GSSG))$ was determinate as ca. 0.24 mM of GSH, using as reference a redox potential for the redox pair GSH/GSSG of -151 mV[17]. The Nernst equation yields a redox potential of -129 +/- 4 mV for the change between the reduced an oxidized state of hIAPP.

Circular Dichroism Spectroscopy (CD)

CD Experiments were carried out at room temperature in a JASCO spectropolarimeter. Quartz cells with a path length of 0.1 cm were used. Spectra were recorded between 260 nm and 190 nm at 0.1 nm intervals, with a response time of 1 s. For the analysis of the data the background buffer was subtracted and the data were expressed as mean residue ellipticity θ_{MRW} = (deg cm^2dmol^{-1}) x 10^{-3}.

Thioflavin-T assay

Fluorescence experiments were performed using a Bekman fluorimeter, using Quartz cells with a path length of 1 cm. The samples were freshly prepared with ThT dye and incubated in the cell with stirring at 37 °C. All solutions were prepared by adding the NMR buffer (30 mM of d-Acetic Acid at pH 5.3) into the peptide in dry on ice form immediately before the measurements. The ThT stock solution was also prepared into NMR buffer with a concentration of 25 mM. The final concentration was 30 µM of peptide and 10 µM of ThT. The Data was analyze by OriginLab. The data were fitted using a sigmoidal equation.

ACKNOWLEDGMENT

This work was performed in the framework of SFB-1035/Project-B07 (German Research Foundation, DFG). We acknowledge support by the Helmholtz-Gemeinschaft, and the Deutsche Forschungsgemeinschaft (Grants Re1435). We are also grateful to the Center for Integrated Protein Science Munich (CIPS-M) for financial support. We want to thank the HELENA and the TUM graduate school, as well as Dr. Vanessa Morris, Ashish Kawale for stimulating discussions.

REFERENCES

1 Mehnert, H. *Typ-2-Diabetes* Vol. 2., erw. Aufl. (Medikon, 2000).

2 Amos, A. F., McCarty, D. J. & Zimmet, P. The Rising Global Burden of Diabetes and its Complications: Estimates and Projections to the Year 2010. *Diabetic Medicine* **14**, S7-S85, doi:10.1002/(SICI)1096-9136(199712)14:5+<S7::AID-DIA522>3.0.CO;2-R (1997).

3 Donath, M. Y. & Shoelson, S. E. Type 2 diabetes as an inflammatory disease. *Nature reviews. Immunology* **11**, 98-107, doi:10.1038/nri2925 (2011).

4 Starke, B. M. e. A. A. R. *Diabetes mellitus*. (2000).

5 Cooper, G. *et al.* Purification and characterization of a peptide from amyloid-rich pancreases of type 2 diabetic patients. *Proceedings of the National Academy of Sciences* **84**, 8628-8632 (1987).

6 Bram, Y. *et al.* Apoptosis induced by islet amyloid polypeptide soluble oligomers is neutralized by diabetes-associated specific antibodies. *Scientific reports* **4**, 4267, doi:10.1038/srep04267 (2014).

7 Kayed, R. *et al.* Conformational transitions of islet amyloid polypeptide (IAPP) in amyloid formation in Vitro. *Journal of molecular biology* **287**, 781-796, doi:http://dx.doi.org/10.1006/jmbi.1999.2646 (1999).

8 Nanga, R. P., Brender, J. R., Vivekanandan, S. & Ramamoorthy, A. Structure and membrane orientation of IAPP in its natively amidated form at physiological pH in a membrane environment. *Biochimica et biophysica acta* **1808**, 2337-2342, doi:10.1016/j.bbamem.2011.06.012 (2011).

9 Patil, S. M., Xu, S., Sheftic, S. R. & Alexandrescu, A. T. Dynamic alpha-helix structure of micelle-bound human amylin. *The Journal of biological chemistry* **284**, 11982-11991, doi:10.1074/jbc.M809085200 (2009).

10 Williamson, J. A. & Miranker, A. D. Direct detection of transient alpha-helical states in islet amyloid polypeptide. *Protein science : a publication of the Protein Society* **16**, 110-117, doi:10.1110/ps.062486907 (2007).

11 Shen, Y., Joachimiak, A., Rosner, M. R. & Tang, W.-J. Structures of human insulin-degrading enzyme reveal a new substrate recognition mechanism. *Nature* **443**, 870-874 (2006).

12 Wiltzius, J. J., Sievers, S. A., Sawaya, M. R. & Eisenberg, D. Atomic structures of IAPP (amylin)

fusions suggest a mechanism for fibrillation and the role of insulin in the process. *Protein Science* **18**, 1521-1530 (2009).

13 Hutton, J. The insulin secretory granule. *Diabetologia* **32**, 271-281 (1989).

14 Westermark, P., Li, Z.-C., Westermark, G. T., Leckström, A. & Steiner, D. F. Effects of beta cell granule components on human islet amyloid polypeptide fibril formation. *FEBS letters* **379**, 203-206 (1996).

15 Abedini, A., Singh, G. & Raleigh, D. P. Recovery and purification of highly aggregation-prone disulfide-containing peptides: application to islet amyloid polypeptide. *Analytical biochemistry* **351**, 181-186, doi:10.1016/j.ab.2005.11.029 (2006).

16 Laghaei, R., Mousseau, N. & Wei, G. Effect of the disulfide bond on the monomeric structure of human amylin studied by combined Hamiltonian and temperature replica exchange molecular dynamics simulations. *The journal of physical chemistry B* **114**, 7071-7077 (2010).

17 Schafer FQ, B. G. Redox state of the cell as viewed through the glutathione disulfide/glutathione couple. *Free Radic Biol Med* **30**, 1191-1212 (2001).

18 Zimmermann, J., Kühne, R., Sylvester, M. & Freund, C. Redox-regulated conformational changes in an SH3 domain. *Biochemistry* **46**, 6971-6977 (2007).

19 Nardai, G., Korcsmáros, T., Papp, E. & Csermely, P. Reduction of the endoplasmic reticulum accompanies the oxidative damage of diabetes mellitus. *Biofactors* **17**, 259-267 (2003).

20 Braakman, I., Helenius, J. & Helenius, A. Manipulating disulfide bond formation and protein folding in the endoplasmic reticulum. *The EMBO Journal* **11**, 1717-1722 (1992).

21 Cuozzo, J. W. & Kaiser, C. A. Competition between glutathione and protein thiols for disulphide-bond formation. *Nature Cell Biology* **1**, 130-135 (1999).

22 Westermark, P., Andersson, A. & Westermark, G. T. Islet amyloid polypeptide, islet amyloid, and diabetes mellitus. *Physiological reviews* **91**, 795-826, doi:10.1152/physrev.00042.2009 (2011).

23 Rodriguez Camargo, D. C. *et al.* Cloning, expression and purification of the human Islet Amyloid Polypeptide (hIAPP) from Escherichia coli. *Protein expression and purification* **106**, 49-56 (2015).

24 al, d. A. e. NMR dipolar couplings for the structure determination of biopolymers in solution *Prog. NMR Spec* **40**, 175-197 (202).

25 Burton. *JACS* **129**, 1321-1326 (2006).

26 Bax, A. Weak alignment offers new NMR opportunities to study protein structure and dynamics. *Protein Science* **12**, 1-16, doi:10.1110/ps.0233303 (2003).

27 Shen, Y., Vernon, R., Baker, D. & Bax, A. De novo protein structure generation from incomplete chemical shift assignments. *Journal of biomolecular NMR* **43**, 63-78, doi:10.1007/s10858-008-9288-5 (2009).

6. Description of the third publication of FRB domain from TOR protein

The FKBP-rapamycin binding domain of human TOR undergoes strong conformational changes in the presence of membrane mimetics with and without the regulator phosphatidic acid

Biochemistry. 2012 Jun 19;51(24):4909-21. doi: 10.1021/bi3002133. Epub 2012 Jun
Diana C. Rodriguez Camargo; Nina M. Link; Sonja A. Dames

The TOR protein, also called Ser/Thr target rapamycin, plays a fundamental role in the control of the metabolism and cellular growth. For this reason when this protein presents a wrong function, the cell presents several problems in different pathways. This dysregulation is a contributing factor in human diseases, such Diabetes, obesity, depression and certain cancers. The TOR protein is a 2500 amino acid log protein, divided in two big units TORC1 and TORC2 with different function. The first one contains the domain that controls the nutrient energy redox and protein synthesis. The second one is responsible for the regulation of the cytoskeleton. The protein can be subdivided in five domains. The domain that is responsible for the interaction with the complex FKBP12-rapamycin and the membrane is the FRB domain. For this paper the FRB domain is produced in *E.coli* with isotopically enrichment media for the NMR experiment. This paper shows the interaction of this domain with different models of membrane mimetic systems such micelles, bicelles and liposomes. This work also shows the affinity and preference of this molecule for a spectrum of different lipids with neutral and negative charge. The results presented here show that the FRB domain has no preference for phosphatidic acid (PA) as was proposed before. This characteristic was attributed to the FRB because the PA is an important messenger in the membranes. The combination of NMR and CD shows that the domain presents specific interaction regions and affinity preference for different negative membrane mimetic systems. We also show that there are no changes in the alpha-helix content

in the structure of the domain in presence of membranes. However, we propose that the big changes observed in the NMR spectra are due to the dispersion of the α-helix in the lipidic environment. This paper also shows that in low concentration of these lipids the FRB domain has preference for the inhibitor complex FKBP12-rapamycin more than for the lipids.

BIOCHEMISTRY
including biophysical chemistry & molecular biology

Article

pubs.acs.org/biochemistry

The FKBP−Rapamycin Binding Domain of Human TOR Undergoes Strong Conformational Changes in the Presence of Membrane Mimetics with and without the Regulator Phosphatidic Acid

Diana C. Rodriguez Camargo,[†] Nina M. Link,[‡] and Sonja A. Dames*[,†]

[†]Biomolecular NMR Spectroscopy, Department of Chemistry, Technische Universität München, Munich, Germany
[‡]Biozentrum, University of Basel, Basel, Switzerland

Supporting Information

ABSTRACT: The Ser/Thr kinase target of rapamycin (TOR) is a central controller of cellular growth and metabolism. Misregulation of TOR signaling is involved in metabolic and neurological disorders and tumor formation. TOR can be inhibited by association of a complex of rapamycin and FKBP12 to the FKBP12−rapamycin binding (FRB) domain. This domain was further proposed to interact with phosphatidic acid (PA), a lipid second messenger present in cellular membranes. Because mammalian TOR has been localized at various cellular membranes and in the nucleus, the output of TOR signaling may depend on its localization, which is expected to be influenced by the interaction with complex partners and regulators in response to cellular signals. Here, we present a detailed characterization of the interaction of the FRB domain with PA and how it is influenced by the surrounding membrane environment. On the basis of nuclear magnetic resonance- and circular dichroism-monitored binding studies using different neutral and negatively charged lipids as well as different membrane mimetics (micelles, bicelles, and liposomes), the FRB domain may function as a conditional peripheral membrane protein. However, the data for the isolated domain just indicate an increased affinity for negatively charged lipids and membrane patches but no specific preference for PA or PA-enriched regions. The membrane-mimetic environment induces strong conformational changes that largely maintain the α-helical secondary structure content but presumably disperse the helices in the lipidic environment. Consistent with overlapping binding surfaces for different lipids and the FKBP12−rapamycin complex, binding of the inhibitor complex protects the FRB domain from interactions with membrane mimetics at lower lipid concentrations.

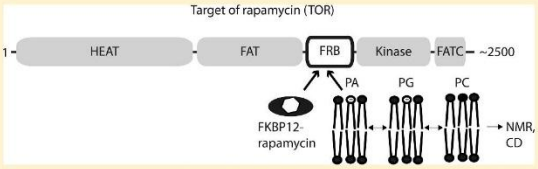

The Ser/Thr kinase target of rapamycin (TOR) is a central controller of cell growth and survival as well as cytoskeletonal reorganization processes in all eukaryotes.[1−3] TOR forms two distinct multiprotein complexes termed TORC1 and TORC2.[4] TORC1 controls the accumulation of cell mass in response to the nutrient and energy state of the cell, which is, for example, sensed through the presence of growth factors like insulin or the ATP:AMP ratio.[1,5] Processes controlled by TORC1 include protein and lipid synthesis, ribosome and mitochondrial biogenesis, and autophagy.[1,3,5] TORC2 influences cell survival and action cytoskeleton organization. Both TOR complexes intercept several signaling pathways,[6,7] and misregulation of these pathways is found in many types of metabolic and neurological disorders as well as cancer.[5,8−12] TOR has further been implicated in the immune response.[3] Whereas TORC1 is highly sensitive to the TOR-specific inhibitor complex composed of the macrolide rapamycin and the cellular protein FKPB12, TORC2 is affected by only long-term exposure to rapamycin.[4,13,14]

The highly conserved TOR proteins are ∼2500 residues long and share several functional domains (Figure 1a).[2] The N-terminal HEAT repeat-rich region[15] and the following FAT domain,[16] which presumably is also composed of an α-helical repeat motif, have been suggested to mediate protein−protein interactions.[15,16] The FKBP12−rapamycin binding (FRB) domain is ∼100 amino acids long and just N-terminal of the catalytic Ser/Thr kinase domain, which encompasses ∼250−350 residues. The C-terminal FATC domain plays an important role in the regulation of TOR function[17] and has been suggested to influence the stability of TOR through its redox state[18] as well as to contribute to TOR membrane interactions.[19]

TOR has been localized at various cellular membranes (Golgi, ER, lysosomes, mitochondria, and plasma membrane)[20−25] and in the nucleus.[26] In addition, TOR was recently found to be associated with ribosomes.[27] On the basis of these observations, the output of TOR signaling was suggested to depend on its cellular localization,[20] which itself should be regulated by pathway-specific stimuli and the composition of each TOR complex. Earlier studies indicated that protein−protein interactions mediated by the HEAT repeat region play an important role in plasma membrane localization in yeast.[21] In addition, several proposed regulators

Received: February 16, 2012
Revised: April 26, 2012

dx.doi.org/10.1021/bi3002133 | *Biochemistry* XXXX, XXX, XXX−XXX

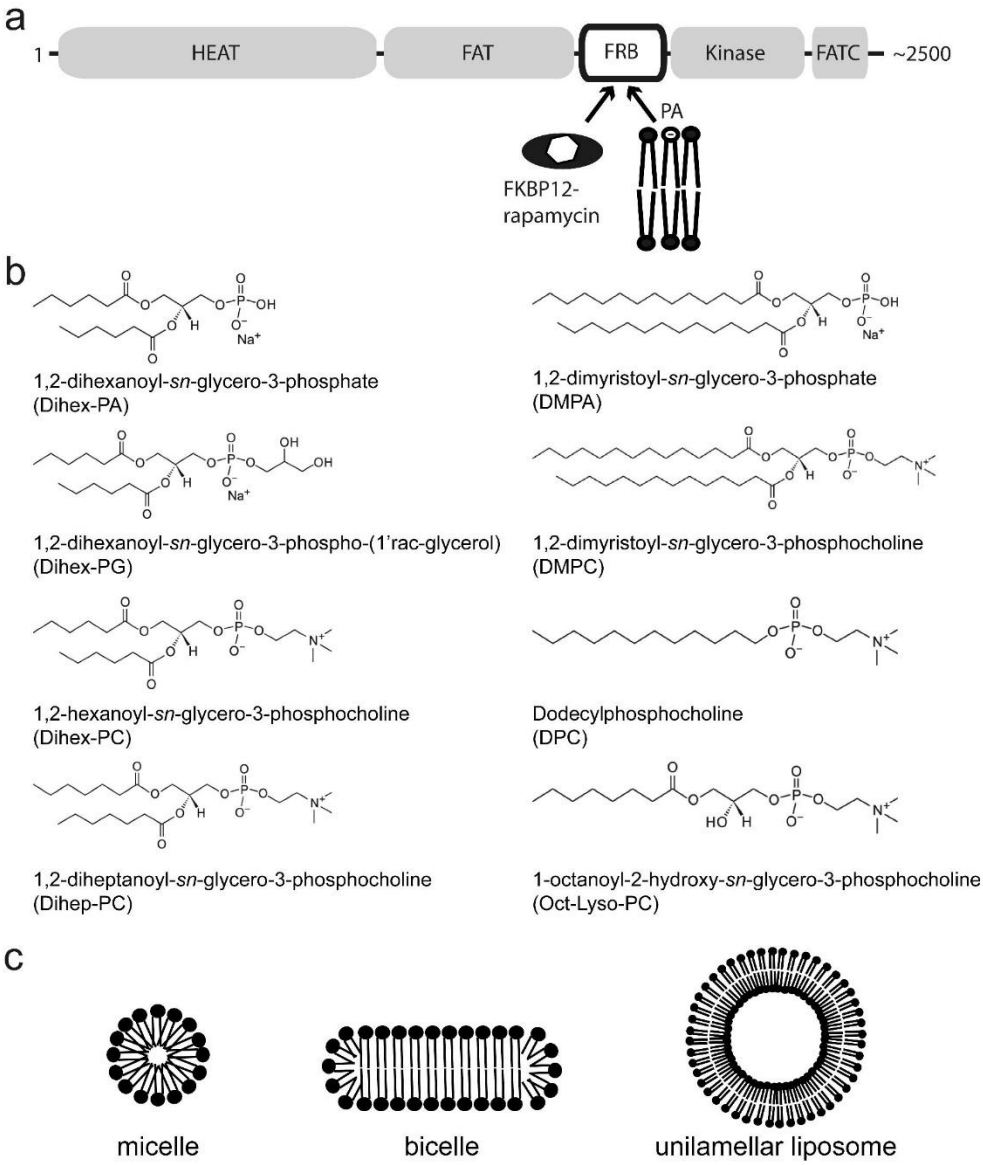

Figure 1. Domain structure of TOR proteins and schematic representations of lipids and membrane mimetics used in this study. (a) TOR proteins share several functional regions. The N-terminal ~1200-amino acid region is composed of HEAT repeats (huntingtin, elongation factor 3, regulatory subunit A of PP2A) and is followed by the ~550-residue FAT (FRAP, ATM, TTRAP) domain. The ~100-amino acid FKBP12−rapamycin binding (FRB) domain is to the N-terminal side of the ~250−350-amino acid Ser/Thr kinase domain. This domain was also suggested to interact with phosphatidic acid (PA), a phospholipid component of cellular membranes. At the C-terminus is the highly conserved, ~35-residue FATC (FAT C-terminal) domain. The FRB domain is overall also very conserved; an alignment of the amino acid sequences of this domain from different organisms is shown in Figure S2 of the Supporting Information. (b) Chemical structures of the lipids used in this study. For comparison, a PC lysolipid that is similar in length to DPC is also shown. The abbreviations used within the text are given. All lipid structure pictures were obtained from the website of Avanti Polar Lipids (http://avantilipids.com/). (c) Schematic representation of different membrane mimetics.

and interaction partners of TOR have membrane anchoring domains or fatty acid modifications, for example, the GTPases Rheb and Rac1 that are lipidated and thereby associate with endosomal membranes and the plasma membrane, respectively, or FKBP38 that has a transmembrane domain and thereby localizes to the mitochondrial membrane.[28−30] Besides this, direct TOR lipid and membrane interactions were suggested. On the basis of nuclear magnetic resonance (NMR) binding and structural studies with lipids with different headgroups and using different membrane mimetics such as micelles and

bicelles, the redox-sensitive FATC domain was suggested to contain a membrane anchor that consists of a hydrophobic bulb that has a rim of charged residues.[19] Moreover, the FRB domain has been shown to mediate interactions with the lipid second messenger phosphatidic acid (PA).[31] PA accounts for 1−4% of the total lipid content of cellular membranes.[32] Important with respect to TOR signaling is the generation of PA by phospholipases D1 and D2 (PLD1/2) and by the glycerol 3-phosphate pathway.[33−36] PLD2 is mainly localized at the plasma membrane, and its activity depends on the concentration of diacylphosphoinositol-4,5-bisphosphate (PIP45).[32,34] On the basis of later studies, PLD-generated PA is required for the association of TOR with Raptor to form TORC1 as well as with Rictor to form TORC2.[37] The effect of PA is competitive with rapamycin, with significantly higher concentrations needed to complete the interaction with TORC2 than with TORC1.[37] In contrast, PA generated by the glycerol 3-phosphate pathway was suggested to inhibit TORC2 by destabilizing the interaction with Rictor.[36] The inhibitory effect coincided thereby with increased levels of PA-containing palmitate (16:0) acyl chains.[36] NMR studies with a water-soluble PA variant with only C6 fatty acid tails (Dihex-PA) showed that PA induces specific chemical shift changes in a surface region of the FRB domain that is formed by the N-terminal half of α-helix 1 and the C-terminal half of α-helix 4.[38] Because cellular PA is embedded in a membrane environment, we present here a more detailed characterization of the interaction of the FRB domain from human TOR (hFRB) with different lipids (Figure 1b) and membrane mimetics (Figure 1c) determined by NMR and CD spectroscopy. Our studies indicate that different membranelike environments induce large conformational changes in the FRB domain that overall preserve the α-helical secondary structure content but appear to disrupt the tertiary structure. Moreover, the interaction with PA appears not to be highly specific because phosphoglycerol (PG) and phosphocholine (PC) lipids as well as dodecylphosphocholine (DPC) induce very similar chemical shift changes. However, on the basis of the decrease in the signal intensity, the affinity for negatively charged lipids appears to be higher than for neutral ones.

■ MATERIALS AND METHODS

Protein Expression and Purification. The region encoding the human TOR FRB domain (hFRB, residues 2014−2114) was expressed and purified as described previously.[39] To improve the long-term stability and solubility of the isolated FRB domain, a second construct was prepared by site-directed mutagenesis that was N-terminally truncated by five and C-terminally by two residues; this is termed hFRBs (residues 2019−2112 of human TOR). The borders for the second construct were designed on the basis of the structured region as observed in the crystal structure of the free FRB domain [Protein Data Bank (PDB) entry 1AUE]. Expression, inclusion body extraction, reversed-phase high-performance liquid chromatography purification, and refolding were conducted as described previously for hFRB.[39] The yeast FKBP12 analogue FPR1 was also expressed and purified as described previously.[39] On the basis of a comparison of the $^{1}H-^{15}N$ HSQC spectra of hFRB and hFRBs in the absence and presence of the FKBP12−rapamycin complex (Figure S1 of the Supporting Information), shortening of the construct did not significantly alter the three-dimensional structure or its ability to interact with the inhibitor complex.

Sample Preparation for NMR and CD Experiments. NMR samples contained ∼50−150 μM ^{15}N-labeled hFRB or hFRBs and where mentioned an equimolar amount of unlabeled FKBP12 and rapamycin in 20 mM Tris buffer (pH 8, 95% H_2O/5% D_2O) with 1 mM TCEP, 300 mM NaCl, and 0.02% NaN_3. CD samples contained 11−65 μM protein. Dodecylphosphocholine (DPC), 1,2-dihexanoyl-*sn*-glycero-3-phosphate (Dihex-PA), 1,2-dihexanoyl-*sn*-glycero-3-phospho-(1′-*rac*-glycerol) (Dihex-PG), and 1,2-diheptanoyl-*sn*-glycero-3-phosphocholine (Dihep-PC) were purchased from Avanti Polar Lipids. 1,2-Dihexanoyl-*sn*-glycero-3-phosphocholine (Dihex-PC) was purchased from Sigma. 1,2-Dimyristoyl-*sn*-glycero-3-phosphate (DMPA) and 1,2-dimyristoyl-*sn*-glycero-3-phosphocholine (DMPC) were obtained from Genzyme Pharmaceuticals, and deuterated DPC (d_{38}-DPC) was from Cambridge Isotopes.

In general, lipid stock solutions for the titrations were prepared as follows. A defined amount of lipid from a concentrated stock in organic solvent (mostly chloroform) was placed in a glass vial and dried under a stream of nitrogen gas. The dried lipid was then dissolved in buffer or a protein sample. Only Dihep-PC was weighed and directly dissolved in buffer. The concentration of the used lipid stocks ranged from 5 mM to 1 M. For protein samples with a defined lipid concentration, an appropriate amount of the respective lipid in organic solvent was placed in a glass vial and dried under nitrogen gas before the protein solution was added. The acquisition of one-dimensional (1D) ^{1}H NMR spectra for each titration point allowed us to follow the increase in the lipid concentration as well as the shift of the equilibrium from free to micellar lipid, because micelle formation results in a shift of several lipid signals. In the samples with high DPC concentrations, the presence of micelles was further confirmed by NMR diffusion measurements.

Bicelles were prepared by first drying an appropriate amount of the long chain phospholipids in organic solvent (DMPC or DMPA) under a stream of nitrogen gas in a glass vial. The dried lipid was first resuspended in a small amount of buffer (20 μL), followed by the addition of the short chain lipid (DihepPC) in buffer. After the bicelle mixture had been thoroughly vortexed, the protein solution was added.

Liposomes were prepared by drying an appropriate amount of DMPC in chloroform under a stream of nitrogen gas, followed by incubation under vacuum overnight to remove remaining traces of the organic solvent. The resulting pellet was dissolved in buffer to obtain a 100 mM solution. To resuspend the pellet, it was exposed to seven cycles of freezing in liquid nitrogen followed by incubation in a water bath at 40 °C and vortexing. To induce the formation of small unilamellar vesicles from large uni- and multilamellar vesicles, the DMPC suspension was incubated in a sonication bath for ∼0.5 h; during this time, the temperature increased from ∼20 to ∼50 °C. To remove the remaining large vesicles, the milky suspension was centrifuged in a tabletop centrifuge for 5 min at 14.8K rpm. This resulted in a clear supernatant and a rather big fluffy white precipitate. For the preparation of a sample of hFRBs in the presence of liposomes, we initially used only the supernatant that should contain small unilamellar vesicles (SUVs). Because the precipitate after centrifugation of the liposomes was very large and the lipid signal in the 1D ^{1}H spectrum of the respective sample was very small compared to the ones we usually observe for micelles and bicelles, we resuspended the liposome precipitate and added 50 μL of this

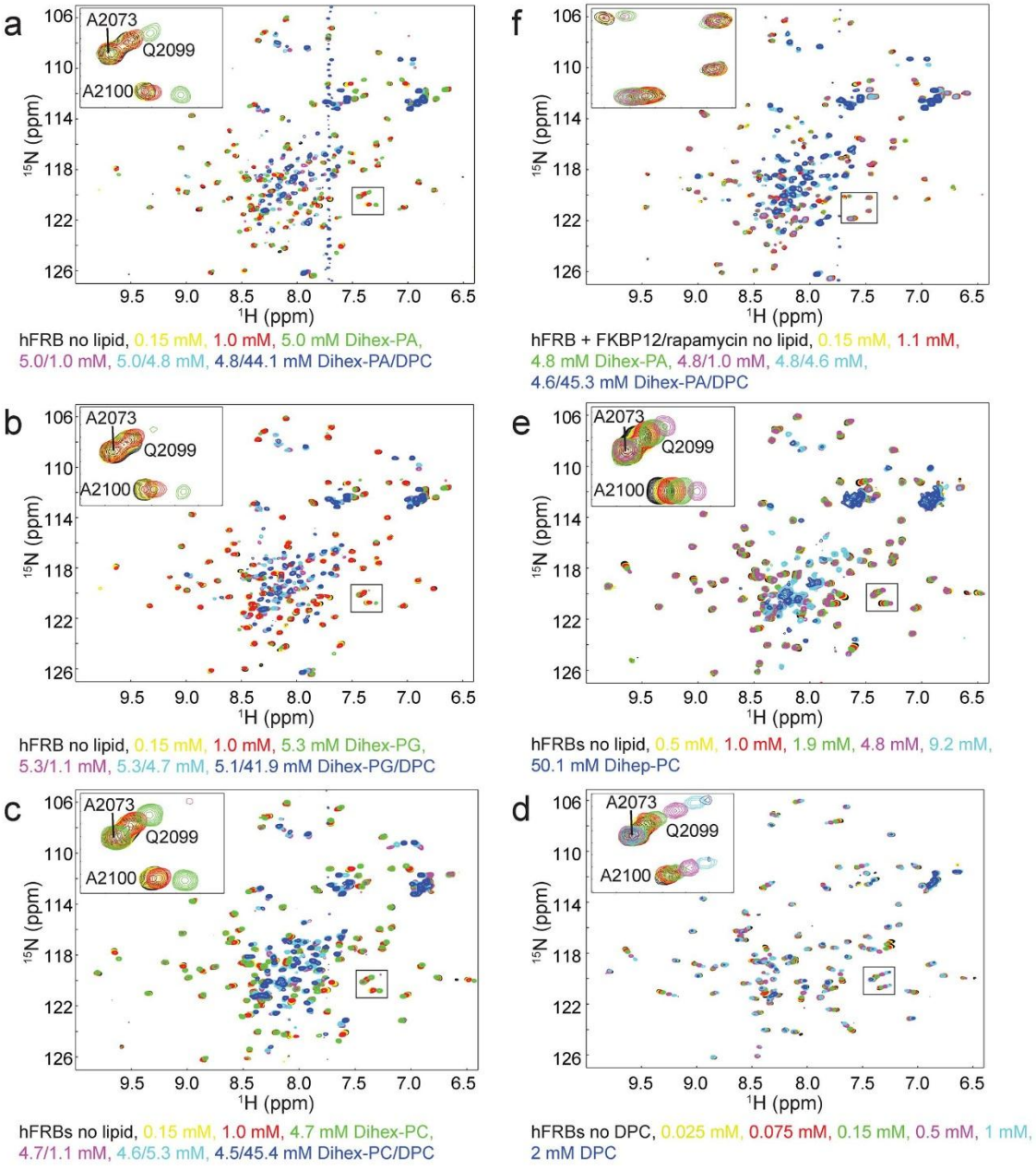

Figure 2. Interactions of the human TOR FRB domain with lipids and membrane mimetics as monitored by NMR spectroscopy. (a–f) ^{1}H–^{15}N HSQC spectra of [^{15}N]hFRB or [^{15}N]hFRBs in the presence of increasing amounts of lipids. The color coding of the spectra and the respective lipid concentrations are given below each plot. An enlarged view of the region highlighted with a black square is given in the top left corner of each spectrum.

more concentrated DMPC suspension to the 200 μL protein sample that had been prepared using 100 μL of the centrifuged liposome supernatant. However, the lipid signal remained rather small, presumably because of line broadening because of the huge size of the liposome particles.

NMR Spectroscopy. NMR spectra were recorded at 298 K on Bruker DRX600, DRX750, and DRX800 spectrometers. Titrations with different lipids were followed by recording regular or SOFAST[40] ^{1}H–^{15}N HSQC spectra. Data were processed with NMRPipe[41] and analyzed using NMRView.[42] The average chemical shift changes for the backbone amide

dx.doi.org/10.1021/bi3002133 | *Biochemistry* XXXX, XXX, XXX–XXX

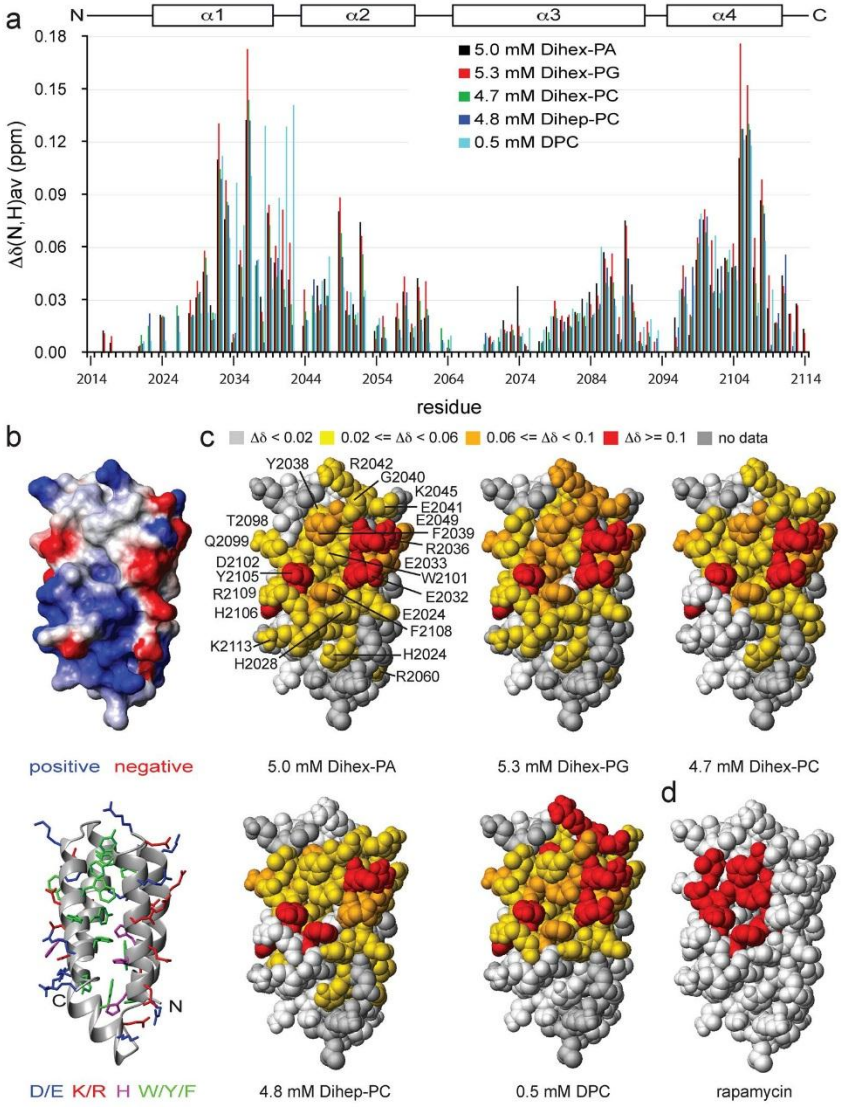

Figure 3. Analysis of the chemical shift changes observed for the human FRB domain at a concentration of ~5 mM for the indicated lipids and for 0.5 mM DPC. (a) Plot of the average chemical shift change for the backbone amide nitrogen and proton [$\Delta\delta$(N,H)av = $\Delta\delta$] as a function of the sequence position. The secondary structure elements are indicated at the top.[52] (b) The top picture shows a surface charge representation of the human FRB domain and the bottom picture a ribbon representation of the same structure. Positively charged surface areas or residues are colored blue and negatively charged ones red. For the bottom representation, the side chains of histidines were additionally colored magenta and those of tryptophans, tyrosines, and phenylalanines green. (c) For this representation, the chemical shift changes observed at a lipid concentration of ~5 mM for the indicated lipids and for 0.5 mM DPC (Figure 2a–e and panel a) have been mapped onto a space-filled model of the structure of the human FRB domain. Weak shifts are highlighted in yellow, medium shifts in orange, and strong shifts in red. For residues colored darker gray, no information could be obtained because of spectral overlap, missing signals, or unclear assignments. (d) For this surface representation of the FRB domain, the residues interacting with rapamycin in the crystal structure of a complex between the FRB domain and the FKBP12–rapamycin complex are colored red.[53] Representations of the structures in panels b–d corresponding to 180° rotations around the vertical axis are given in Figure S3 of the Supporting Information. All structures were made with MolMol[68] and POV-Ray (http://www.povray.org) using the crystal structure of the free FRB domain of human TOR (PDBentry 1AUE).[52]

nitrogen and proton [$\Delta\delta$(N,H)av] were calculated as $[(\Delta\delta_{HN})^2 + (\Delta\delta_N/5)^2]^{1/2}$. Chemical shift assignments for hFRB and hFRBs were adapted from the published values (BMRB entry 6760).[43] The lipid concentration during titration experiments varied in general from 0.05 to 50 mM; only in the titration with DPC alone did it range from 0.025 to 2 mM. NMR samples in the presence of micelles contained either 150 or 135 mM DPC and 15 mM DMPA. The lipid concentrations in the bicelle

dx.doi.org/10.1021/bi3002133 | Biochemistry XXXX, XXX, XXX–XXX

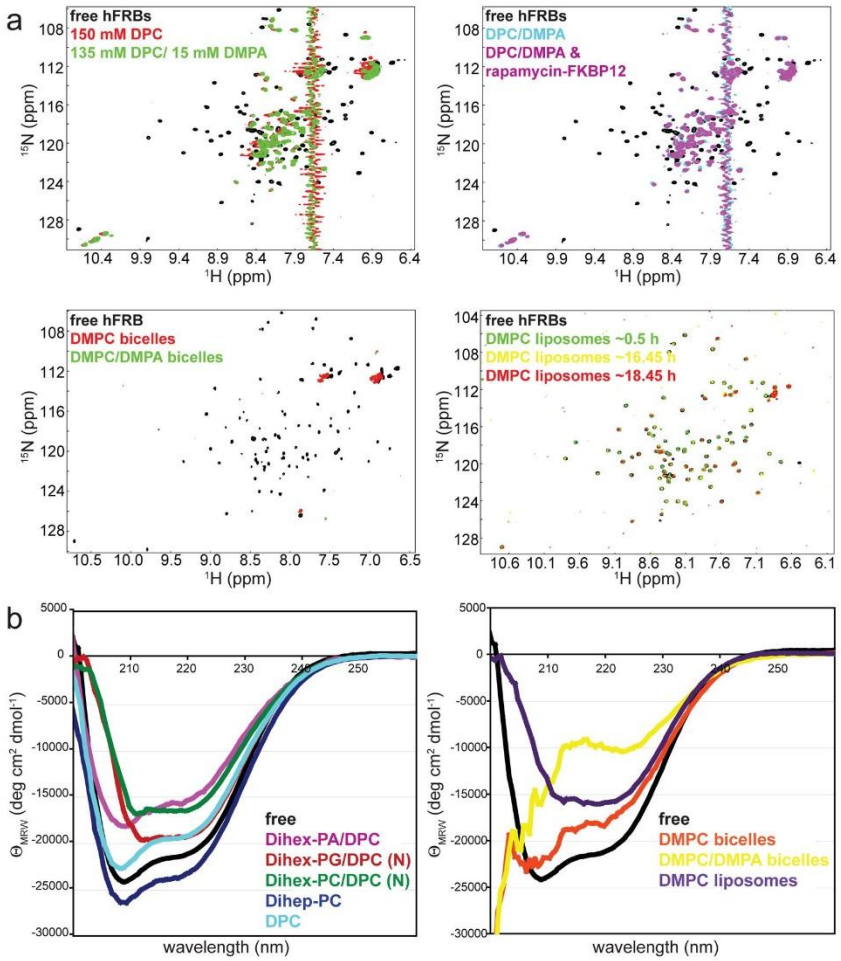

Figure 4. Influence of various membrane mimetics on the NMR spectra and secondary structure of the FRB domain of human TOR. (a) ^{1}H−^{15}N HSQC spectra of the free FRB domain in the presence of high concentrations of DPC or DPC/PA micelles (top left) and after addition of the unlabeled FKBP12−rapamycin complex at a 1:1 ratio with respect to the micelle-immersed FRB domain (top right). The bottom left representation shows ^{1}H−^{15}N HSQC spectra of the human FRB domain in the presence of DMPC or DMPC/DMPA bicelles (total lipid concentration of ∼300 mM, 4:1 DMPC:DMPA ratio) and the bottom right picture spectra in the presence of DMPC liposomes (total lipid concentration of <60 mM) at different time steps. (b) The left plot shows CD spectra of the human FRB domain alone and in the presence of pure DPC micelles or such containing additionally the indicated diacyl lipid. (N) means that the spectrum was recorded using the more concentrated sample from the NMR titration. The DPC concentration was ∼42−45 mM in the mixed micelles and 50 mM if DPC alone was used. The concentration of the diacyl lipid was ∼5 mM. The right plot shows a superposition of the CD spectra of the free FRB domain and those in the presence of DMPC or DMPC/DMPA bicelles, or DMPC liposomes. Note that in the samples containing high protein concentrations and/or PC-based membrane mimetics the spectrum is distorted below ∼220 nm because of an overly high voltage at the detector. See also Figure S4 of the Supporting Information and the text.

samples were 72 mM DMPC or 15 mM DMPA with 57 mM DMPC and 239 mM Dihep-PC, corresponding to a q of 0.3 and a c_L of 15%.

CD Spectroscopy. All CD spectra were recorded at room temperature on a Jasco J715 spectropolarimeter using a cuvette with a path length of 0.1 cm. All spectra were recorded with an acquisition time of 50 nm per minute (8 s response time) and five scans if not otherwise mentioned. The CD samples in the presence of micelles contained all ∼50 mM lipid, either 50 mM DPC or ∼5 mM Dihex-PA, Dihex-PG, or Dihex-PC, and ∼45 mM DPC or 50 mM Dihep-PC. The lipid concentrations in the bicelle samples were 44.8 mM DMPC or 9.4 mM DMPA with 35.3 mM DMPC and 147.9 mM Dihep-PC, corresponding to a q of 0.3 and a c_L of 9.3%.

RESULTS

Different Lipids Induce Similar Spectral Changes in the TOR FRB Domain. Ververka et al. have shown that Dihex-PA, which because of its short acyl chains is well water-soluble, induces specific spectral changes in the FRB domain of TOR.[38] Because they had used a slightly different construct, which had an additional non-native N-terminal extension, we first tried to reproduce their observations with our nontagged construct. Increasing the Dihex-PA concentration from ∼0 to 5 mM

dx.doi.org/10.1021/bi3002133 | Biochemistry XXXX, XXX, XXX−XXX

induces specific chemical shift changes (Figure 2a). At ∼0.15 mM Dihex-PA (Figure 2a, yellow spectrum), there are no significant spectral changes. From 1 to 5 mM (Figure 2a, red and green spectra), many peaks shift gradually, which is accompanied by a decrease in intensity. The strength of the observed chemical shift changes at 5 mM Dihex-PA as a function of the sequence (Figure 3a) reproduces very well the data published by Ververka et al.[38] Also, in our case, the strongest chemical shift changes localize to residues on the surfaces of α-helices 1 and 4 (Figure 3c).

PA is a component of cellular membranes; therefore, the surrounding membrane environment is expected to influence the interaction with PA. Because Dihex-PA has a very high CMC (>10 mM) and negatively charged PA contributes only a fraction of the membrane lipids, a neutral membrane mimetic was added in increasing amounts to induce micelle formation. We used DPC, because it has a rather low CMC (1.1 mM)[44] and is a well-established membrane mimetic for solution NMR studies.[19,45−48] The presence of 1 mM DPC in addition to 5 mM Dihex-PA (Figure 2a, magenta spectrum), which is expected to induce the formation of micelles, results in a complete change in the spectrum. The resonances for the free form that had shifted only upon addition of 5 mM Dihex-PA disappear, and new resonances appear. Increasing the DPC concentration to 5 mM and subsequently to 44 mM (Figure 2a, cyan and blue spectra) increases the concentration of micelles and shifts the equilibrium to the micelle-immersed state. This results in an overall increase in the peak intensities of the bound form that is accompanied by additional small chemical shift changes. Using even higher concentrations of PA and DPC [15 mM DMPA and 135 mM DPC (Figure 4a, green spectrum)] shifts the equilibrium further to the micelle-immersed state, resulting in a further increase in the respective peak intensities. The spectrum of the micelle-immersed state is characterized by a narrow chemical shift dispersion. This indicates that the chemical environment of the residues became overall more uniform. Approximately 70 peaks can be counted for the backbone amide groups of the micelle-immersed state (Figure 4a, green spectrum). On the basis of the shape and intensity, several of them must correspond to more than one peak. The number of peaks in the region where the glycine backbone amide groups are typically visible (∼105−110 ppm) indicates that the spectrum of the micelle-associated form shows presumably most to all of the expected resonances (≲91 for hFRBs; 94 minus 2 Pro residues minus the N-terminal residue).

The specificity of the interaction of the FRB domain with PA was first evaluated from a titration of [^{15}N]hFRB with Dihex-PG that has as PA a negatively charged headgroup (Figure 1b). The titration was done exactly as with Dihex-PA. At first, the concentration of Dihex-PG was increased in small steps from 0 to ∼5 mM, and then DPC was added from a concentration of 1 to 42 mM to induce the formation of micelles (Figure 2b). The observed spectral changes with 5 mM Dihex-PG are highly similar to those with Dihex-PA, only that the chemical shift differences and the decrease in the peak intensities are slightly larger (Figures 2a,b and 3a). The NMR spectra in the additional presence of DPC are also highly similar for PA and PG (Figure 2a,b, dark blue spectra).

Because both lipids with negatively charged headgroups resulted in overall comparable chemical shift changes, we also titrated the FRB domain with the neutral lipid Dihex-PC (Figure 1b). Again, Dihex-PC was first added in small steps, from 0 to ∼5 mM, followed by addition of DPC from a concentration of 1 to 45 mM to induce the formation of micelles (Figure 2c). At ∼5 mM Dihex-PC, the pattern of chemical shift changes is overall similar to those observed for the two negatively charged lipids (Figure 3a); however, the signal intensity of the peaks is still considerably higher, indicating a lower affinity for the neutral phospholipid (Figure 2c, green spectrum). The formation of micelles due to addition of DPC results as for Dihex-PA and Dihex-PG in a complete change in the appearance of the spectra (Figure 2c, magenta, cyan, and blue spectra).

The influence of DPC in the absence of PA, PG, or PC at concentrations below or slightly above its CMC (1.1 mM)[44] was determined from a titration of hFRBs with 0−2 mM DPC (Figure 2d). Unexpectedly, the pattern of chemical shift changes in the presence of only 0.5 mM DPC is very similar to that for ∼5 mM Dihex-PA, Dihex-PG, or Dihex-PC (Figure 3a). Only several residues in the first α-helix show slightly stronger and some in the fourth α-helix slightly smaller chemical shift changes. DPC has as Dihex-PC a neutral phosphocholine headgroup (Figure 1b). This further indicates that the FRB domain appears not to interact only with lipids with a headgroup with a net negative charge. Compared to Dihex-PA, -PG, and -PC, DPC has only a single but longer fatty acid chain and thus more resembles a lysolipid (Figure 1b). This may at least in part explain why only 0.5 mM DPC induces chemical shift changes similar to those induced by the tested dihexanoyl phospholipids at ∼5 mM. The spectrum of the micelle-immersed state at high concentrations of pure DPC [150 mM (Figure 4a, red spectrum)] looks very similar to that obtained with DPC micelles containing additionally ∼10% Dihex-PA [15 mM Dihex-PA and 135 mM DPC (Figure 4a, green spectrum)].

The influence of the headgroup charge and the length and number of fatty acid chains was further derived from a titration of hFRBs with 0−50 mM Dihep-PC (Figure 2e). The pattern of the induced chemical shift changes at ∼4.8 mM is overall similar to those obtained for ∼5 mM Dihex-PA, Dihex-PG, or Dihex-PC as well as for 0.5 mM DPC (Figure 3a). However, the decrease in signal intensity at ∼5 mM (Figure 2e, magenta spectrum) is as for Dihex-PC (Figure 2c, green spectrum) lower than for the negatively charged lipids Dihex-PA and Dihex-PG (Figure 2a,b, green spectra). The CMC for Dihep-PC from the literature is ∼1.4−1.8 mM[49,50] and thereby only somewhat higher than that for DPC (1.1 mM).[44] Therefore, the difference in the length and/or number of fatty acid chains as well as the presence of the glycerol backbone between the phosphate group and the fatty acid chain in Dihep-PC (Figure 1b) may be responsible for the fact that lower concentrations of DPC versus those of Dihep-PC are necessary to achieve chemical shift changes similar in strength. At the next titration point (9.2 mM) at which the majority of Dihep-PC molecules are expected to be present in micelles, the appearance of the spectra changes completely (Figure 2e, cyan spectrum). The resulting spectrum looks overall similar to those obtained with 5 mM Dihex-PA, -PG, and -PC or 1−5 mM DPC (Figure 2a−c, magenta and cyan spectra). However, increasing the Dihep-PC concentration further to 50 mM appears to broaden the peaks of the micelle-immersed state (Figure 2e, dark blue spectrum). This observation can be explained by the fact that Dihep-PC micelles are very polydisperse and show a significant increase in micellar weight as the lipid concentration increases.[51] In summary, the titrations with different lipids indicate that the FRB domain shows a similar pattern of chemical shift changes

for all tested lipids (Figure 3a). However, the data indicate an increased affinity for negatively charged lipids and membrane regions compared to neutral ones. Besides the charge of the lipid headgroups, differences in the shape and packing of the respective formed micelles appear to influence the affinity for a specific membrane-mimetic structure.

Because DPC may just unspecifically destabilize the tertiary structure, we further analyzed the influence of DPC on a protein that was not suggested to interact with membranes. For this, we titrated the B1 domain of streptococcal protein G (GB1) with 0−50 mM DPC (Figure S5 of the Supporting Information). The respective $^{1}H-^{15}N$ HSQC spectra indeed show no significant spectral changes.

α-Helices 1 and 4 of the Four-Helix Bundle Exhibit the Strongest Lipid-Induced Chemical Shift Changes. A plot of the observed chemical shift changes for ∼5 mM Dihex-PA, Dihex-PG, Dihex-PC, or Dihep-PC or 0.5 mM DPC (Figure 3a) illustrates that the strongest chemical shift changes at lower lipid concentrations are observed in α-helices 1 and 4, which pack antiparallel with respect to each other in the four-helix bundle (Figure 3b). For Figure 3c, the chemical shift changes have been classified and mapped onto a surface representation of the crystal structure of the FRB domain (PDB entry 1AUE).[52] The residues showing medium to strong changes cluster to a hydrophobic surface region that is surrounded by several positively charged and some negatively charged residues. The two α-helices 1 and 4 forming this surface region contain several highly or completely conserved aromatic and aliphatic as well as charged residues (Figure S2 of the Supporting Information). Among these, E2032, E2033, R2036, A2100, Y2105, H2106, and F2108 show medium to strong backbone chemical shift changes in all five titrations using the free FRB domain (Figures 2a−e and 3a). E2032 and E2033 are in very few sequences replaced with aspartate. R2036, A2100, and F2108 are replaced with another residue in only one of the sequences from organisms having two TOR proteins such as yeast or silk moth. Position 2106 is in the sequences of higher eukaryotes always occupied by histidine; only some lower eukaryotes like yeast or *Dictyostelium* have asparagine or glutamate at this position or in the case of brown alga an aspartate. The sequence of TOR from brown alga is the least conserved compared to the other TOR sequences (Figure S2 of the Supporting Information). For Figure 3d, the residues that make interactions with rapamycin in the crystal structure of the ternary complex of the FRB domain with rapamycin and FKBP12 (PDB entry 1FAP)[53] are colored red. A comparison of the binding region for rapamycin (Figure 3d) with those for the tested lipids (Figure 3c) indicates that they strongly overlap.

Bicelles and Liposomes Also Induce Changes in the NMR Spectra of the FRB Domain. The membrane association of conditional peripheral membrane proteins depends not only on the surface charge but also on other factors such as curvature or lipid packing.[54] Because micelles are rather small spherical particles with a high curvature (Figure 1c, left), the interaction with more planar bicelles (Figure 1c, middle) was also tested. Figure 4a shows a superposition of the spectra of the FRB domain in the free form and in the presence of neutral DMPC and negatively charged DMPC/DMPA bicelles. The rim was always formed by Dihep-PC. In both cases, the interaction with the large bicelles (>250 kDa) resulted in the disappearance of nearly all backbone resonances, presumably because of broadening of the respective NMR signals beyond detection. On the basis of these data, the interaction of the FRB domain with membrane mimetics appears not to be very sensitive to the different surface properties of bicelles versus micelles.

Fang et al. suggested that the FRB domain mediates the regulation of TOR by PA because the isolated FRB domain bound strongly to liposomes containing a significant amount of PA (from 50 to 10%) but apparently not to neutral liposomes consisting of only PC.[31] Fang et al. incubated ∼18 μM purified FRB domain with ∼5 mM lipid, forming the respective liposome, and then applied the mixture to a gel filtration column to separate free protein from liposome-bound and free liposomes, the latter two both eluting in the void volume. The amount of protein in each fraction was determined by sodium dodecyl sulfate−polyacrylamide gel electrophoresis analysis.[31] Because we observed small chemical shift changes already with 5 mM Dihex-PC indicating a weak interaction as well as a complete spectral rearrangement in the presence of neutral micelles and bicelles, we wondered if the interaction of the FRB domain with neutral liposomes (Figure 1c, right) may have been too weak to be detected by the experimental setup used by Fang et al.[31] The $^{1}H-^{15}N$ HSQC spectrum of the FRB domain recorded shortly after it had been mixed with an aqueous suspension of liposomes shows no strong chemical shift changes of single peaks (Figure 4a, bottom right). However, in the spectrum recorded after incubation overnight, several peaks are weaker or had disappeared, which was even more pronounced in the spectrum recorded 2 h later. After the sample had been ejected from the NMR machine, it exhibited a fluffy precipitate. On the basis of the UV-determined protein concentration and CD spectra of the supernatant (see below) and the resuspended pellet, the precipitate consisted mostly of lipid, presumably large uni- and multilamellar lipid vesicles that had been present in the liposome preparation. It should be noted that because of the used preparation procedure and the properties of the resulting liposomes (size and formation of vesicles consisting of single as well as multiple bilayers) the amount of solvent accessible membrane surface using, for example, 100 mM lipid is much smaller compared to that of micelles and bicelles prepared using the same amount of lipid. This and the fact that the lipid concentration in the liposome sample was less than 60 mM may at least in part explain why the observed spectral changes occurred more slowly and less drastically than for bicelles and why Fang et al. did not observe an interaction with ∼5 mM neutral PC liposomes.[31] It should also be noted that in our bicelle NMR samples the total lipid concentration was ∼300 mM and therefore presumably sufficiently high to drive the equilibrium to the bicelle-associated state.

Membrane Mimetics Can Disrupt the Interaction with the FKPB12−Rapamycin Inhibitor Complex. Because the FKPB12−rapamycin inhibitor complex has been suggested to compete with PA for binding to the FRB domain and because the binding regions for both overlap (Figure 3c,d), we further analyzed how formation of a complex with the FKBP12−rapamycin species influences the interaction with PA and DPC. First, $[^{15}N]$hFRB in a complex with the unlabeled FKPB12−rapamycin species was titrated with Dihex-PA and DPC (Figure 2f) exactly as the free FRB domain (Figure 2a). As in the titration of the free FRB domain, up to ∼5 mM PA several peaks shift. However, the decrease in signal intensity is generally lower than for the free form. Moreover, the additional presence of 1 mM DPC only further weakens or shifts several peaks but does not yet induce a complete change in the

spectrum as observed for the free FRB domain. The latter is observed only at the next titration point (~5 mM Dihex-PA and ~5 mM DPC). This suggests that binding of the inhibitor complex (K_d = 12 nM)[55] can, at least in part, protect the FRB domain from lipid/membrane-induced conformational changes at lower lipid concentrations (lower than ~10 mM). The shift of peaks up to 5 mM indicates that PA can already interact with FKBP12−rapamycin complex-associated hFRB below the CMC. The final spectrum of the micelle-immersed form at higher lipid concentrations (4.6 mM Dihex-PA and 45.3 mM DPC) looks overall like that obtained for the free FRB domain (Figure 2a,f, dark blue spectra). Second, a mixture of FKBP12 and rapamycin was added in a 1:1 ratio to [^{15}N]hFRBs that had been immersed in a large amount of micelles composed of DPC and DMPA (Figure 4a, top right). However, the spectrum did not significantly change, suggesting that in the presence of 135 mM DPC and 15 mM DMPA the inhibitor complex cannot recognize the micelle-immersed state and/or induce conformational changes that allow an interaction.

The Micelle-Immersed State Shows an α-Helical Secondary Structure Content Similar to That of the Free Form. The ^{1}H−^{15}N HSQC spectra of the TOR FRB domain in the presence of high concentrations of membrane mimetics (Figure 2, blue spectra, and Figure 4a, top) show a narrow chemical shift dispersion. A very similar spectral appearance is usually observed for unstructured proteins, because unfolding of the protein chain results in a similar chemical environment for most residues and thereby in similar chemical shifts. To obtain information about the structure of the FRB domain in the presence of different membrane mimetics, CD spectra were recorded. For all membrane mimetics, a reference spectrum was recorded in buffer (Figure S4b of the Supporting Information) and used to correct the protein spectrum recorded in the presence of the respective membrane mimetic. This was particularly important for Dihep-PC/DMPC/DMPA bicelles, for DMPC liposomes, and for Dihep-PC micelles because all give a large to very large positive CD signal (Figure S4b of the Supporting Information). Therefore, CD spectroscopy may also be used to check and compare preparations of PC-based micelles, bicelles, or liposomes.

The CD spectrum of the free FRB domain (Figure 4b, black curve) is characteristic of a fully α-helical protein, in this case a four-helix bundle (Figure 3b). The CD spectra with neutral or negatively charged membrane-mimetic DPC-based micelles (Figure 4b, left plot) look very similar with respect to their shape. The shapes of the CD spectra in the presence Dihex-PG and DPC or Dihex-PC and DPC look different only below ~215 nm because for these measurements the significantly more concentrated NMR samples were used. The CD-monitored titration of hFRBs with DPC (Figure S4a of the Supporting Information) shows that the shape of the CD spectrum also does not change significantly if the DPC concentration is increased stepwise as during the NMR titration. The CD spectra in the presence of DMPC liposomes as well as DMPC- or DMPC/DMPA-based bicelles show a shape typical for an α-helical protein (Figure 4b, right plot). However, although the protein concentration was low, the spectra are significantly distorted below ~220 nm. This is because the respective membrane mimetics produce themselves a strong CD signal (Figure S4b of the Supporting Information), which together with the protein signal results in an overly high voltage of the detector. Altogether, the CD data indicate that the FRB domain in the presence of membrane mimetics maintains an overall content of α-helical secondary structure similar to that of the free form and that the interaction with membrane mimetics may only disrupt the tertiary structure and disperse the α-helices in the interior or on the surface of the micelle, bicelle, or liposome.

■ DISCUSSION

PA is the phospholipid component of cellular membranes with the smallest headgroup [-H (Figure 1b)]. Therefore, its headgroup is not expected to be as accessible on the membrane surface as, for example, the large headgroups of phosphoglycerol (Figure 1b) or phosphoinositides. Consistent with this, our studies with different membrane mimetics indicate that the surrounding membrane environment has a strong influence on the interaction of the FRB domain with PA. Moreover, higher concentrations of neutral membrane mimetics such as Dihep-PC (Figure 2e) or DPC micelles or Dihep-PC/DMPC bicelles (Figure 4a, left two plots) induced a complete change in the NMR spectrum even in the absence of PA. Such strong spectral changes in the presence of membrane mimetics were also observed for other known or putative conditional peripheral membrane proteins. A similar abrupt change in the ^{1}H−^{15}N HSQC spectrum that is characterized by a significant reduction in the extent of peak dispersion was, for example, observed for the anti-apoptotic protein Bcl-x_L[47,56] and for the putative GTPase-binding domain of *Dictyostelium* Formin C.[48] On the basis of additional CD and NMR data, Bcl-x_L maintains as the FRB domain a largely α-helical structure in the micelle-dissolved state,[47] whereas induction of additional α-helical secondary structure was proposed for Formin C.[48] Further studies revealed that key regulatory interactions of Bcl-2 family members occur at and in intracellular membranes (reviewed in ref 57), and the actin-binding protein Formin C was suggested to play a role in phagocytosis, which is regulated by GTPases and phosphoinositides.[58] Transformation of a β-strand into an α-helix and additional changes in the secondary and tertiary structure in the presence of micelles containing phosphoinositol 4,5-phosphate have further been reported for another actin-binding protein, gelsolin.[59]

Whereas the NMR titration data (Figure 2) indicate that the interaction with membrane-mimetic structures induces a rearrangement of the tertiary structure, it also shows that the FRB domain can interact with lipids below the CMC and therefore at concentrations at which no membrane-mimetic structures should be present. On the basis of the analysis of the observed chemical shift changes with Dihex-PA, -PG, and -PC up to ~5 mM (Figure 3a), thus ~5 mM below the CMC, the lipids can bind to a hydrophobic surface patch that overlaps with the binding region for the FKBP12−rapamycin complex (Figure 3c,d). In contrast to membrane mimetics, the interaction with single lipid molecules results in only small spectral and therefore conformational changes that overall maintain the fold. Thus, with the shift from low to high lipid concentrations, several association reactions occur: the interaction of the FRB domain with free lipids at low lipid concentrations and the association of lipid and DPC molecules to form micelles as well as the association of the FRB domain with micelles at lipid concentrations above the CMC.

Because neutral liposomes corresponding to a DMPC concentration of <60 mM resulted in NMR spectral changes significantly weaker than those seen with Dihep-PC/DMPC bicelles at a total lipid concentration of ~300 mM or Dihep-PC

dx.doi.org/10.1021/bi3002133 | *Biochemistry* XXXX, XXX, XXX−XXX

micelles at a concentration of ≥10 mM, a strong interaction with a neutral membrane surface appears to happen in the presence of only a certain amount of solvent accessible membrane surface area. Because the FRB domain can also interact with single lipid molecules, the equilibrium between the free and the membrane-mimetic state in a micelle, bicelle, or liposome preparation may further play a role. In addition to the presence of negatively charged lipids, the membrane curvature, fluidity, and acyl chain accessibility may influence the affinity for membrane structures and thereby membrane-induced conformational changes.

Dihex-PA and the other tested lipids target a surface region on the FRB domain that overlaps with the binding region for rapamycin. In agreement with this, binding of the FKPB12−rapamycin complex protects the FRB domain at lower lipid concentrations from interacting with membrane mimetics. The fact that the binding sites for the FKPB12−rapamycin complex, PA, and other lipids overlap might in part explain why some mutations of the FRB domain affect the phosphorylation of target proteins in the absence of rapamycin or if they have no effect on the inhibition by rapamycin.[60] Some of these mutations may affect the interaction of either TOR complex with specific membrane patches and thereby influence substrate recognition. However, some mutations, especially of residues in the hydrophobic core, may also just destabilize the fold of the FRB (e.g., W2027F) and thereby hamper TOR function.

Fang et al.[31] described that mutating R2109 to alanine decreased the affinity for PA. Like Ververka et al.,[38] we observed only weak chemical shift changes for the backbone amide of R2109. However, Ververka et al. mentioned that they had observed significant shifts for the side chain amide of R2109.[38] Because the side chain of R2109 is located between two strongly shifting residues (Y2105 and H2106) (Figure 3c), it makes sense that it is affected by the interaction with PA and other lipids. The position corresponding to R2109 is in most TOR sequences (Figure S2 of the Supporting Information) occupied by an arginine; some have a lysine, and only one (fruit fly) has a glutamine. However, all sequences have additionally a positively charged residue at the neighboring position, R2110 in human TOR (Figure S2 of the Supporting Information), which may also participate in electrostatic interactions with negatively charged areas of lipid headgroups. In the titrations with PA and PG but also PC, the backbone amide of this residue shows a weak shift (Figure 3a). To the best of our knowledge, the effect of mutating R2110 on TOR signaling has not yet been studied.

The chemical shift changes for the two negatively charged lipids Dihex-PA and Dihex-PG at a concentration of ∼5 mM are nearly identical (Figures 2a,b and 3a). Initial studies using the isolated purified FRB domain and liposomes composed of PC alone or a mixture of 50% PC and 50% PA, PE, PI, or PS indicated that the FRB domain interacts strongly only with liposomes containing PA. On the basis of the small strip of the SDS gel documenting the amount of liposome-associated FRB, at least a small fraction appears to have bound to liposomes containing PS and, as far as what is visible, also to liposomes containing PI. Binding to liposomes containing PG was not tested. This raises the question of whether the FRB domain alone can be responsible for the specific effect of PA on TOR signaling or if other components of the TOR complex are involved. In addition, other negatively charged lipids or membrane-localized proteins could contribute to this effect. Whereas PLD-generated PA is needed for the interaction of TOR with Raptor in TORC1 and Rictor in TORC2,[37] PA generated in the glycerol 3-phosphate pathway inhibits TORC2 by destabilizing the TOR−Rictor interaction.[36] This discrepancy was explained by structural differences between the PA species generated in both pathways, with the inhibitory effect on TORC2 being specifically achieved by PA species containing palmitate (16:0) acyl chains.[36] Because TORC2 complexes can be further distinguished on the basis of the association with different isoforms of Sin1,[61] this may additionally influence the interaction with PA. Therefore, Raptor in TORC1 and Rictor/Sin1 in TORC2 may further influence or mediate the interaction with PA-containing membrane patches. This would also be consistent with the idea that TORC2 containing Rictor is sensitive to only a long-term exposure with rapamycin, because TORC2 has a higher affinity for PLD-generated PA than TORC1.[34]

As mentioned in the preceding paragraph, the inhibitory effect of PA on TORC2 was suggested to depend on its acyl chains.[36] In addition, DPC that resembles more a lysolipid (Figure 1b) induced below the CMC chemical shift changes in the FRB domain comparable to those induced by Dihex-PA. Therefore, the interaction of either TOR complex with PA-containing membrane patches may also depend on the local membrane composition and structure and the resulting accessibility of specific lipid acyl chains. Lysolipids are known to strongly influence the local membrane structure.[62] Thus, it may be possible that LPA influences TOR signaling not only indirectly by being the precursor for the synthesis of PA in the glycerol 3-phosphate pathway[36] or by stimulating PLD1 to produce PA[63] but also by directly influencing TOR−membrane association. Alternatively, another lysolipid could influence the local membrane structure and thereby increase the membrane affinity of the TOR FRB domain. Moreover, the interaction with PA-containing membrane patches may additionally depend on the interaction with membrane-associated regulators of PA-influenced TOR signaling such as phospholipase D2 (PLD2) that produces PA and has been shown to form a complex with TOR and Raptor[33] or the GTPases RalA and Arf6.[64]

Recently, it was shown that glucose starvation decreases the intracellular pH in yeast from ∼7−7.5 to ∼6.[65,66] This influences the interaction of the transcription factor Opi1 with PA, because it has a lower affinity for the protonated phosphate headgroup.[65] Because starvation also influences TOR signaling, its interaction with PA-containing membrane patches may also be pH-sensitive. In this respect, it is interesting to note that the determined lipid-binding surface of the FRB domain contains three histidines, H2024 and H2028 on α-helix 1 and H2106 on α-helix 4 (Figure 3b,c). The three histidines are conserved in all higher eukaryotes, whereas some lower eukaryotes have only one or two of them; only *Dictyostelium* has none. Using the crystal structure of the FRB domain of human TOR (PDB entry 1AUE) as input for PROPKA version 3.1,[67] the pK_a values for these three histidines were predicted to be in the range from ∼5.7 to ∼7 (5.98 and 6.92 for H2024, 6.06 and 6.69 for H2028, and 5.65 and 6.02 for H2106 for monomers A and B, respectively, of the crystal structure). Thus, lowering the pH below 6−7 could change the protonation state and thereby the affinity for negatively charged membrane patches. In mammalian cells, efficient glycolysis was thought to promote high cytosolic pH values; thus, glucose starvation may as in yeast result in a decrease in the cytosolic pH.[66]

dx.doi.org/10.1021/bi3002133 | *Biochemistry* XXXX, XXX, XXX−XXX

In summary, our studies with different lipids and membrane mimetics suggest that the TOR FRB domain may function as a conditional peripheral membrane protein. However, the data for the isolated domain indicate not a strict specificity for PA or PA-containing membranes but simply an increased affinity for negatively charged lipids and surface patches. Specific differences of the membrane-immersed states in the presence or absence of PA or another negatively charged lipid have to be derived on the basis of the structure determination of the FRB domain in suitable membrane mimetics. Because the specific output of TOR signaling was suggested to depend on its subcellular localization, the latter is presumably regulated by a tight network of different interactions with complex partners and regulators as well as specific membrane regions. Future studies must therefore also target the structural and biophysical characterization of the interaction of TOR with other membrane components and membrane-associated regulatory proteins.

■ ASSOCIATED CONTENT

Supporting Information

Superpositions of the $^{1}H-^{15}N$ HSQC spectra of the used constructs of the FRB domain of human TOR in the presence and absence of the FKPB12−rapamycin inhibitor complex (Figure S1), an alignment of the amino acid sequences of the TOR FRB domain from different organisms (Figure S2), complementary views of the surface representations in Figure 3b−d (Figure S3), CD spectra of the titration of the TOR FRB domain with DPC and of the buffers and membrane mimetics (Figure S4), and a superposition of the $^{1}H-^{15}N$ HSQC spectra of the B1 domain of protein G in the presence of increasing amounts of DPC (Figure S5). This material is available free of charge via the Internet at http://pubs.acs.org.

■ AUTHOR INFORMATION

Corresponding Author

*Technische Universität München, Department of Chemistry, Biomolecular NMR Spectroscopy, Lichtenbergstr. 4, 85747 Garching, Germany. Phone: +49-(0)89-28913292. Fax: +49-(0)89-28913869. E-mail: sonja.dames@tum.de.

Funding

This work was supported from the German Research Foundation (DFG Grant DA1195/3-1) to S.A.D. N.L.M. was supported by a stipend from the Novartis foundation (Basel, Switzerland) and funding from the Freie Akademische Gesellschaft Basel (Basel, Switzerland).

Notes

The authors declare no competing financial interest.

■ ACKNOWLEDGMENTS

We thank Andrea Löschmann-Hage in Prof. Michael Hall's group at the Biozentrum of the University of Basel for help with the cloning and Prof. Hall for providing a template plasmid encoding full-length human TOR as well as an expression plasmid for yeast FKBP12. We acknowledge Klara Rathgeb-Szabo in Prof. Stephan Grzesiek's group for help during the purification of hFRB. We thank Prof. Stephan Grzesiek from the Biozentrum of the University of Basel for providing measurement time at his 800 MHz spectrometer for the acquisition of spectra in the presence of bicelles.

■ ABBREVIATIONS

Dihex-PA, 1,2-dihexanoyl-*sn*-glycero-3-phosphate; Dihep-PC, 1,2-diheptanoyl-*sn*-glycero-3-phosphocholine; Dihex-PC, 1,2-hexanoyl-*sn*-glycero-3-phosphocholine; Dihex-PG, 1,2-dihexanoyl-*sn*-glycero-3-phospho-(1′-*rac*-glycerol); DMPA, 1,2-dimyristoyl-*sn*-glycero-3-phosphate; DMPC, 1,2-dimyristoyl-*sn*-glycero-3-phosphocholine; DPC, dodecylphosphocholine; FKBP12, FK506 binding protein of 12 kDa, here equivalent to *Saccharomyces cerevisiae* FPR1; FRB, FKBP12−rapamycin binding; hFRB, residues 2014−2114 of human TOR; hFRBs, residues 2019−2112 of human TOR; (m)TOR, (mammalian) target or rapamycin.

■ REFERENCES

(1) Wullschleger, S., Loewith, R., and Hall, M. N. (2006) TOR signaling in growth and metabolism. *Cell 124*, 471−484.

(2) Jacinto, E., and Hall, M. N. (2003) Tor signalling in bugs, brain and brawn. *Nat. Rev. Mol. Cell Biol. 4*, 117−126.

(3) Araki, K., Ellebedy, A. H., and Ahmed, R. (2011) TOR in the immune system. *Curr. Opin. Cell Biol. 23*, 707−715.

(4) Loewith, R., Jacinto, E., Wullschleger, S., Lorberg, A., Crespo, J. L., Bonenfant, D., Oppliger, W., Jenoe, P., and Hall, M. N. (2002) Two TOR complexes, only one of which is rapamycin sensitive, have distinct roles in cell growth control. *Mol. Cell 10*, 457−468.

(5) Dazert, E., and Hall, M. N. (2011) mTOR signaling in disease. *Curr. Opin. Cell Biol. 23*, 744−755.

(6) De Virgilio, C., and Loewith, R. (2006) Cell growth control: Little eukaryotes make big contributions. *Oncogene 25*, 6392−6415.

(7) Corradetti, M. N., and Guan, K. L. (2006) Upstream of the mammalian target of rapamycin: Do all roads pass through mTOR? *Oncogene 25*, 6347−6360.

(8) Guertin, D. A., and Sabatini, D. M. (2007) Defining the role of mTOR in cancer. *Cancer Cell 12*, 9−22.

(9) Guertin, D. A., and Sabatini, D. M. (2005) An expanding role for mTOR in cancer. *Trends Mol. Med. 11*, 353−361.

(10) Tee, A. R., and Blenis, J. (2005) mTOR, translational control and human disease. *Semin. Cell Dev. Biol. 16*, 29−37.

(11) Choo, A. Y., and Blenis, J. (2006) TORgeting oncogene addiction for cancer therapy. *Cancer Cell 9*, 77−79.

(12) Bjornsti, M. A., and Houghton, P. J. (2004) The TOR pathway: A target for cancer therapy. *Nat. Rev. Cancer 4*, 335−348.

(13) Jacinto, E., Loewith, R., Schmidt, A., Lin, S., Ruegg, M. A., Hall, A., and Hall, M. N. (2004) Mammalian TOR complex 2 controls the actin cytoskeleton and is rapamycin insensitive. *Nat. Cell Biol. 6*, 1122−1128.

(14) Sarbassov, D. D., Ali, S. M., Sengupta, S., Sheen, J. H., Hsu, P. P., Bagley, A. F., Markhard, A. L., and Sabatini, D. M. (2006) Prolonged rapamycin treatment inhibits mTORC2 assembly and Akt/PKB. *Mol. Cell 22*, 159−168.

(15) Andrade, M. A., and Bork, P. (1995) HEAT repeats in the Huntington's disease protein. *Nat. Genet. 11*, 115−116.

(16) Bosotti, R., Isacchi, A., and Sonnhammer, E. L. (2000) FAT: A novel domain in PIK-related kinases. *Trends Biochem. Sci. 25*, 225−227.

(17) Takahashi, T., Hara, K., Inoue, H., Kawa, Y., Tokunaga, C., Hidayat, S., Yoshino, K., Kuroda, Y., and Yonezawa, K. (2000) Carboxyl-terminal region conserved among phosphoinositide-kinase-related kinases is indispensable for mTOR function in vivo and in vitro. *Genes Cells 5*, 765−775.

(18) Dames, S. A., Mulet, J. M., Rathgeb-Szabo, K., Hall, M. N., and Grzesiek, S. (2005) The solution structure of the FATC domain of the protein kinase target of rapamycin suggests a role for redox-dependent structural and cellular stability. *J. Biol. Chem. 280*, 20558−20564.

(19) Dames, S. A. (2010) Structural basis for the association of the redox-sensitive target of rapamycin FATC domain with membrane-mimetic micelles. *J. Biol. Chem. 285*, 7766−7775.

(20) Drenan, R. M., Liu, X., Bertram, P. G., and Zheng, X. F. (2004) FKBP12-rapamycin-associated protein or mammalian target of

rapamycin (FRAP/mTOR) localization in the endoplasmic reticulum and the Golgi apparatus. *J. Biol. Chem. 279*, 772−778.
(21) Kunz, J., Schneider, U., Howald, I., Schmidt, A., and Hall, M. N. (2000) HEAT repeats mediate plasma membrane localization of Tor2p in yeast. *J. Biol. Chem. 275*, 37011−37020.
(22) Wedaman, K. P., Reinke, A., Anderson, S., Yates, J., III, McCaffery, J. M., and Powers, T. (2003) Tor kinases are in distinct membrane-associated protein complexes in *Saccharomyces cerevisiae*. *Mol. Biol. Cell 14*, 1204−1220.
(23) Berchtold, D., and Walther, T. C. (2009) TORC2 plasma membrane localization is essential for cell viability and restricted to a distinct domain. *Mol. Biol. Cell 20*, 1565−1575.
(24) Withers, D. J., Ouwens, D. M., Nave, B. T., van der Zon, G. C., Alarcon, C. M., Cardenas, M. E., Heitman, J., Maassen, J. A., and Shepherd, P. R. (1997) Expression, enzyme activity, and subcellular localization of mammalian target of rapamycin in insulin-responsive cells. *Biochem. Biophys. Res. Commun. 241*, 704−709.
(25) Sancak, Y., Bar-Peled, L., Zoncu, R., Markhard, A. L., Nada, S., and Sabatini, D. M. (2010) Ragulator-Rag complex targets mTORC1 to the lysosomal surface and is necessary for its activation by amino acids. *Cell 141*, 290−303.
(26) Zhang, X., Shu, L., Hosoi, H., Murti, K. G., and Houghton, P. J. (2002) Predominant nuclear localization of mammalian target of rapamycin in normal and malignant cells in culture. *J. Biol. Chem. 277*, 28127−28134.
(27) Zinzalla, V., Stracka, D., Oppliger, W., and Hall, M. N. (2011) Activation of mTORC2 by association with the ribosome. *Cell 144*, 757−768.
(28) Saci, A., Cantley, L. C., and Carpenter, C. L. (2011) Rac1 regulates the activity of mTORC1 and mTORC2 and controls cellular size. *Mol. Cell 42*, 50−61.
(29) Buerger, C., DeVries, B., and Stambolic, V. (2006) Localization of Rheb to the endomembrane is critical for its signaling function. *Biochem. Biophys. Res. Commun. 344*, 869−880.
(30) Bai, X., Ma, D., Liu, A., Shen, X., Wang, Q. J., Liu, Y., and Jiang, Y. (2007) Rheb activates mTOR by antagonizing its endogenous inhibitor, FKBP38. *Science 318*, 977−980.
(31) Fang, Y., Vilella-Bach, M., Bachmann, R., Flanigan, A., and Chen, J. (2001) Phosphatidic acid-mediated mitogenic activation of mTOR signaling. *Science 294*, 1942−1945.
(32) Selvy, P. E., Lavieri, R. R., Lindsley, C. W., and Brown, H. A. (2011) Phospholipase D: Enzymology, functionality, and chemical modulation. *Chem. Rev. 111*, 6064−6119.
(33) Ha, S. H., Kim, D. H., Kim, I. S., Kim, J. H., Lee, M. N., Lee, H. J., Kim, J. H., Jang, S. K., Suh, P. G., and Ryu, S. H. (2006) PLD2 forms a functional complex with mTOR/raptor to transduce mitogenic signals. *Cell. Signalling 18*, 2283−2291.
(34) Foster, D. A. (2009) Phosphatidic acid signaling to mTOR: Signals for the survival of human cancer cells. *Biochim. Biophys. Acta 1791*, 949−955.
(35) Sun, Y., Fang, Y., Yoon, M. S., Zhang, C., Roccio, M., Zwartkruis, F. J., Armstrong, M., Brown, H. A., and Chen, J. (2008) Phospholipase D1 is an effector of Rheb in the mTOR pathway. *Proc. Natl. Acad. Sci. U.S.A. 105*, 8286−8291.
(36) Zhang, C., Wendel, A. A., Keogh, M. R., Harris, T. E., Chen, J., and Coleman, R. A. (2012) Glycerolipid signals alter mTOR complex 2 (mTORC2) to diminish insulin signaling. *Proc. Natl. Acad. Sci. U.S.A. 109*, 1667−1672.
(37) Toschi, A., Lee, E., Xu, L., Garcia, A., Gadir, N., and Foster, D. A. (2009) Regulation of mTORC1 and mTORC2 complex assembly by phosphatidic acid: Competition with rapamycin. *Mol. Cell. Biol. 29*, 1411−1420.
(38) Veverka, V., Crabbe, T., Bird, I., Lennie, G., Muskett, F. W., Taylor, R. J., and Carr, M. D. (2007) Structural characterization of the interaction of mTOR with phosphatidic acid and a novel class of inhibitor: Compelling evidence for a central role of the FRB domain in small molecule-mediated regulation of mTOR. *Oncogene 27*, 585−595.
(39) Dames, S. A. (2008) A fast and simple method to prepare the FKBP-rapamycin binding domain of human target of rapamycin for NMR binding assays. *Protein Expression Purif. 59*, 31−37.
(40) Schanda, P., Kupce, E., and Brutscher, B. (2005) SOFAST-HMQC experiments for recording two-dimensional heteronuclear correlation spectra of proteins within a few seconds. *J. Biomol. NMR 33*, 199−211.
(41) Delaglio, F., Grzesiek, S., Vuister, G. W., Zhu, G., Pfeifer, J., and Bax, A. (1995) NMRPipe: A multidimensional spectral processing system based on UNIX pipes. *J. Biomol. NMR 6*, 277−293.
(42) Johnson, B. A. (2004) Using NMRView to visualize and analyze the NMR spectra of macromolecules. *Methods Mol. Biol. 278*, 313−352.
(43) Veverka, V., Lennie, G., Crabbe, T., Bird, I., Taylor, R. J., and Carr, M. D. (2006) NMR assignment of the mTOR domain responsible for rapamycin binding. *J. Biomol. NMR 36* (Suppl. 1), 3.
(44) Stafford, R. E., Fanni, T., and Dennis, E. A. (1989) Interfacial properties and critical micelle concentration of lysophospholipids. *Biochemistry 28*, 5113−5120.
(45) Kutateladze, T. G., Capelluto, D. G., Ferguson, C. G., Cheever, M. L., Kutateladze, A. G., Prestwich, G. D., and Overduin, M. (2004) Multivalent mechanism of membrane insertion by the FYVE domain. *J. Biol. Chem. 279*, 3050−3057.
(46) Ahn, H. C., Juranic, N., Macura, S., and Markley, J. L. (2006) Three-dimensional structure of the water-insoluble protein crambin in dodecylphosphocholine micelles and its minimal solvent-exposed surface. *J. Am. Chem. Soc. 128*, 4398−4404.
(47) Losonczi, J. A., Olejniczak, E. T., Betz, S. F., Harlan, J. E., Mack, J., and Fesik, S. W. (2000) NMR studies of the anti-apoptotic protein Bcl-xL in micelles. *Biochemistry 39*, 11024−11033.
(48) Dames, S. A., Junemann, A., Sass, H. J., Schonichen, A., Stopschinski, B. E., Grzesiek, S., Faix, J., and Geyer, M. (2011) Structure, dynamics, lipid binding, and physiological relevance of the putative GTPase-binding domain of *Dictyostelium* formin C. *J. Biol. Chem. 286*, 36907−36920.
(49) Weschayanwiwat, P., Scamehorn, J., and Reilly, P. (2005) Surfactant properties of low molecular weight phospholipids. *J. Surfactants Deterg. 8*, 65−72.
(50) Tausk, R. J., Karmiggelt, J., Oudshoorn, C., and Overbeek, J. T. (1974) Physical chemical studies of short-chain lecithin homologues. I. Influence of the chain length of the fatty acid ester and of electrolytes on the critical micelle concentration. *Biophys. Chem. 1*, 175−183.
(51) Hauser, H. (2000) Short-chain phospholipids as detergents. *Biochim. Biophys. Acta 1508*, 164−181.
(52) Odagaki, Y., and Clardy, J. (1997) Structural basis for peptidomimicry by the effector element of rapamycin. *J. Am. Chem. Soc. 119*, 10253−10254.
(53) Choi, J., Chen, J., Schreiber, S. L., and Clardy, J. (1996) Structure of the FKBP12-rapamycin complex interacting with the binding domain of human FRAP. *Science 273*, 239−242.
(54) Moravcevic, K., Oxley, C. L., and Lemmon, M. A. (2012) Conditional Peripheral Membrane Proteins: Facing up to Limited Specificity. *Structure 20*, 15−27.
(55) Banaszynski, L. A., Liu, C. W., and Wandless, T. J. (2005) Characterization of the FKBP·rapamycin·FRB ternary complex. *J. Am. Chem. Soc. 127*, 4715−4721.
(56) Bhat, V., McDonald, C. B., Mikles, D. C., Deegan, B. J., Seldeen, K. L., Bates, M. L., and Farooq, A. (2012) Ligand Binding and Membrane Insertion Compete with Oligomerization of the BclXL Apoptotic Repressor. *J. Mol. Biol. 416*, 57−77.
(57) Bogner, C., Leber, B., and Andrews, D. W. (2010) Apoptosis: Embedded in membranes. *Curr. Opin. Cell Biol. 22*, 845−851.
(58) Yeung, T., Ozdamar, B., Paroutis, P., and Grinstein, S. (2006) Lipid metabolism and dynamics during phagocytosis. *Curr. Opin. Cell Biol. 18*, 429−437.
(59) Xian, W., and Janmey, P. A. (2002) Dissecting the gelsolin-polyphosphoinositide interaction and engineering of a polyphosphoinositide-sensitive gelsolin C-terminal half protein. *J. Mol. Biol. 322*, 755−771.

(60) McMahon, L. P., Choi, K. M., Lin, T. A., Abraham, R. T., and Lawrence, J. C., Jr. (2002) The rapamycin-binding domain governs substrate selectivity by the mammalian target of rapamycin. *Mol. Cell. Biol. 22*, 7428−7438.
(61) Frias, M. A., Thoreen, C. C., Jaffe, J. D., Schroder, W., Sculley, T., Carr, S. A., and Sabatini, D. M. (2006) mSin1 is necessary for Akt/PKB phosphorylation, and its isoforms define three distinct mTORC2s. *Curr. Biol. 16*, 1865−1870.
(62) Zimmerberg, J., and Kozlov, M. M. (2006) How proteins produce cellular membrane curvature. *Nat. Rev. Mol. Cell Biol. 7*, 9−19.
(63) Kam, Y., and Exton, J. H. (2004) Role of phospholipase D1 in the regulation of mTOR activity by lysophosphatidic acid. *FASEB J. 18*, 311−319.
(64) Xu, L., Salloum, D., Medlin, P. S., Saqcena, M., Yellen, P., Perrella, B., and Foster, D. A. (2011) Phospholipase D mediates nutrient input to mammalian target of rapamycin complex 1 (mTORC1). *J. Biol. Chem. 286*, 25477−25486.
(65) Young, B. P., Shin, J. J., Orij, R., Chao, J. T., Li, S. C., Guan, X. L., Khong, A., Jan, E., Wenk, M. R., Prinz, W. A., Smits, G. J., and Loewen, C. J. (2010) Phosphatidic acid is a pH biosensor that links membrane biogenesis to metabolism. *Science 329*, 1085−1088.
(66) Dechant, R., Binda, M., Lee, S. S., Pelet, S., Winderickx, J., and Peter, M. (2010) Cytosolic pH is a second messenger for glucose and regulates the PKA pathway through V-ATPase. *EMBO J. 29*, 2515−2526.
(67) Olsson, M. H. M., Søndergaard, C. R., Rostkowski, M., and Jensen, J. H. (2011) PROPKA3: Consistent Treatment of Internal and Surface Residues in Empirical pKa Predictions. *J. Chem. Theory Comput. 7*, 525−537.
(68) Koradi, R., Billeter, M., and Wuthrich, K. (1996) MOLMOL: A program for display and analysis of macromolecular structures. *J. Mol. Graphics 14*, 29−32 , 51−55.

7. References

1 Becker, E. D. *High Resolution NMR: Theory and Chemical Applications*. (Elsevier Science, 1999).

2 Cavanagh, J., Fairbrother, W. J., Palmer, A. G., Skelton, N. J. & Rance, M. *Protein NMR Spectroscopy: Principles and Practice*. (Elsevier Science, 2010).

3 Keeler, J. *Understanding NMR Spectroscopy*. (Wiley, 2011).

4 Levitt, M. H. *Spin Dynamics: Basics of Nuclear Magnetic Resonance*. (Wiley, 2013).

5 Jeener, J., Meier, B., Bachmann, P. & Ernst, R. Investigation of exchange processes by two-dimensional NMR spectroscopy. *The Journal of chemical physics* **71**, 4546-4553 (1979).

6 Macura, S., Huang, Y., Suter, D. & Ernst, R. Two-dimensional chemical exchange and cross-relaxation spectroscopy of coupled nuclear spins. *Journal of Magnetic Resonance (1969)* **43**, 259-281 (1981).

7 Aue, W., Bartholdi, E. & Ernst, R. R. Two-dimensional spectroscopy. Application to nuclear magnetic resonance. *The Journal of Chemical Physics* **64**, 2229-2246 (1976).

8 Grzesiek, S. & Bax, A. An efficient experiment for sequential backbone assignment of medium-sized isotopically enriched proteins. *Journal of Magnetic Resonance (1969)* **99**, 201-207, doi:http://dx.doi.org/10.1016/0022-2364(92)90169-8 (1992).

9 Kay, L. E., Ikura, M., Tschudin, R. & Bax, A. Three-dimensional triple-resonance NMR spectroscopy of isotopically enriched proteins. *Journal of Magnetic Resonance (1969)* **89**, 496-514, doi:http://dx.doi.org/10.1016/0022-2364(90)90333-5 (1990).

10 Bax, A. & Ikura, M. An efficient 3D NMR technique for correlating the proton and15N backbone amide resonances with the α-carbon of the preceding residue in uniformly15N/13C enriched proteins. *Journal of biomolecular NMR* **1**, 99-104, doi:10.1007/BF01874573 (1991).

11 Muhandiram, D. R. & Kay, L. E. Gradient-Enhanced Triple-Resonance Three-Dimensional NMR Experiments with Improved Sensitivity. *Journal of Magnetic Resonance, Series B* **103**, 203-216, doi:http://dx.doi.org/10.1006/jmrb.1994.1032 (1994).

12 Clubb, R. T., Thanabal, V. & Wagner, G. A constant-time three-dimensional triple-resonance pulse scheme to correlate intraresidue 1HN, 15N, and 13C′ chemical shifts in 15N□13C-labelled proteins. *Journal of Magnetic Resonance (1969)* **97**, 213-217, doi:http://dx.doi.org/10.1016/0022-2364(92)90252-3 (1992).

13 Pervushin, K., Riek, R., Wider, G. & Wüthrich, K. Attenuated T(2) relaxation by mutual cancellation of dipole–dipole coupling and chemical shift anisotropy indicates an avenue to NMR structures of very large biological macromolecules in solution. *Proceedings of the National Academy of Sciences of the United States of America* **94**, 12366-12371 (1997).

14 Salzmann, M., Pervushin, K., Wider, G., Senn, H. & Wüthrich, K. NMR assignment and secondary structure determination of an octameric 110 kDa protein using TROSY in triple resonance experiments. *Journal of the American Chemical Society* **122**, 7543-7548 (2000).

15 Tian, C. *et al.* in *Methods in Enzymology* Vol. Volume 394 321-334 (Academic Press, 2005).

16 Dias, D. M. & Ciulli, A. NMR approaches in structure-based lead discovery: Recent developments and new frontiers for targeting multi-protein complexes. *Progress in*

Biophysics and Molecular Biology **116**, 101-112, doi:10.1016/j.pbiomolbio.2014.08.012 (2014).
17 Pervushin, K. *et al.* NMR scalar couplings across Watson–Crick base pair hydrogen bonds in DNA observed by transverse relaxation-optimized spectroscopy. *Proceedings of the National Academy of Sciences of the United States of America* **95**, 14147-14151 (1998).
18 al, d. A. e. NMR dipolar couplings for the structure determination of biopolymers in solution *Prog. NMR Spec* **40**, 175-197 (202).
19 Rückert, M. & Otting, G. Alignment of biological macromolecules in novel nonionic liquid crystalline media for NMR experiments. *Journal of the American Chemical Society* **122**, 7793-7797 (2000).
20 Andrew, E., Bradbury, A. & Eades, R. Nuclear magnetic resonance spectra from a crystal rotated at high speed. (1958).
21 Andrew, E., Bradbury, A. & Eades, R. Removal of dipolar broadening of nuclear magnetic resonance spectra of solids by specimen rotation. (1959).
22 Andrew, E. & Eades, R. Possibilities for high-resolution nuclear magnetic resonance spectra of crystals. *Discussions of the Faraday Society* **34**, 38-42 (1962).
23 Pines, A., Chang, J. & Griffin, R. Carbon-13 nuclear magnetic resonance in solid ammonium tartrate. *The Journal of Chemical Physics* **61**, 1021-1030 (1974).
24 Schaefer, J. & Stejskal, E. Carbon-13 nuclear magnetic resonance of polymers spinning at the magic angle. *Journal of the American Chemical Society* **98**, 1031-1032 (1976).
25 Vinod Chandran, C., Madhu, P. K., Kurur, N. D. & Bräuniger, T. Swept-frequency two-pulse phase modulation (SWf-TPPM) sequences with linear sweep profile for heteronuclear decoupling in solid-state NMR. *Magnetic Resonance in Chemistry* **46**, 943-947, doi:10.1002/mrc.2285 (2008).
26 Comellas, G., Lopez, J. J., Nieuwkoop, A. J., Lemkau, L. R. & Rienstra, C. M. Straightforward, effective calibration of SPINAL-64 decoupling results in the enhancement of sensitivity and resolution of biomolecular solid-state NMR. *Journal of magnetic resonance (San Diego, Calif. : 1997)* **209**, 131-135, doi:10.1016/j.jmr.2010.12.011 (2011).
27 Duer, M. J. *Introduction to Solid-State NMR Spectroscopy*. (Wiley, 2005).
28 Chan, J. C. C. *Solid State NMR*. (Springer Berlin Heidelberg, 2011).
29 Klinowski, J. *New Techniques in Solid-State NMR*. (Springer, 2005).
30 Opella, S. Solid state NMR of biological systems. *Annual Review of Physical Chemistry* **33**, 533-562 (1982).
31 Brenner, B. M. *et al.* Effects of losartan on renal and cardiovascular outcomes in patients with type 2 diabetes and nephropathy. *New England Journal of Medicine* **345**, 861-869 (2001).
32 Petkova, A. T. *et al.* A structural model for Alzheimer's β-amyloid fibrils based on experimental constraints from solid state NMR. *Proceedings of the National Academy of Sciences* **99**, 16742-16747 (2002).
33 Heise, H. *et al.* Molecular-level secondary structure, polymorphism, and dynamics of full-length α-synuclein fibrils studied by solid-state NMR. *Proceedings of the National Academy of Sciences of the United States of America* **102**, 15871-15876 (2005).
34 Tycko, R. Solid State NMR Studies of Amyloid Fibril Structure. *Annual review of physical chemistry* **62**, 279-299, doi:10.1146/annurev-physchem-032210-103539 (2011).

35 Cross, T. & Opella, S. Solid-state NMR structural studies of peptides and proteins in membranes. *Current opinion in structural biology* **4**, 574-581 (1994).
36 Mack, J. W., Torchia, D. A. & Steinert, P. M. Solid-state NMR studies of the dynamics and structure of mouse keratin intermediate filaments. *Biochemistry* **27**, 5418-5426 (1988).
37 Sun, S., Siglin, A., Williams, J. C. & Polenova, T. Solid-state and solution NMR studies of the CAP-Gly domain of mammalian dynactin and its interaction with microtubules. *Journal of the American Chemical Society* **131**, 10113-10126 (2009).
38 Renault, M., Cukkemane, A. & Baldus, M. Solid-State NMR Spectroscopy on Complex Biomolecules. *Angewandte Chemie International Edition* **49**, 8346-8357 (2010).
39 Castellani, F. *et al.* Structure of a protein determined by solid-state magic-angle-spinning NMR spectroscopy. *Nature* **420**, 98-102 (2002).
40 Grey, C. P., Dobson, C. M., Cheetham, A. K. & Jakeman, R. J. Studies of rare-earth stannates by trin-119 MAS NMR. The use of paramagnetic shift probes in the solid state. *Journal of the American Chemical Society* **111**, 505-511 (1989).
41 Brown, S. P. & Spiess, H. W. Advanced solid-state NMR methods for the elucidation of structure and dynamics of molecular, macromolecular, and supramolecular systems. *Chemical reviews* **101**, 4125-4156 (2001).
42 Braun, J. *et al.* NMR study of the tautomerism of porphyrin including the kinetic HH/HD/DD isotope effects in the liquid and the solid state. *Journal of the American Chemical Society* **116**, 6593-6604 (1994).
43 Levitt, M., Suter, D. & Ernst, R. Spin dynamics and thermodynamics in solid-state NMR cross polarization. *The Journal of chemical physics* **84**, 4243-4255 (1986).
44 Mehnert, H. *Typ-2-Diabetes* Vol. 2., erw. Aufl. (Medikon, 2000).
45 Amos, A. F., McCarty, D. J. & Zimmet, P. The Rising Global Burden of Diabetes and its Complications: Estimates and Projections to the Year 2010. *Diabetic Medicine* **14**, S7-S85, doi:10.1002/(SICI)1096-9136(199712)14:5+<S7::AID-DIA522>3.0.CO;2-R (1997).
46 Hutton, J., Penn, E. & Peshavaria, M. Isolation and characterisation of insulin secretory granules from a rat islet cell tumour. *Diabetologia* **23**, 365-373 (1982).
47 Knight, J. D., Hebda, J. A. & Miranker, A. D. Conserved and cooperative assembly of membrane-bound α-helical states of islet amyloid polypeptide. *Biochemistry* **45**, 9496-9508 (2006).
48 Vaiana, S. M., Best, R. B., Yau, W.-M., Eaton, W. A. & Hofrichter, J. Evidence for a partially structured state of the amylin monomer. *Biophysical journal* **97**, 2948-2957 (2009).
49 Field, A. E., Coakley, E. H., Must, A. & et al. IMpact of overweight on the risk of developing common chronic diseases during a 10-year period. *Archives of Internal Medicine* **161**, 1581-1586, doi:10.1001/archinte.161.13.1581 (2001).
50 Mokdad, A. H. *et al.* Prevalence of obesity, diabetes, and obesity-related health risk factors, 2001. *Jama* **289**, 76-79 (2003).
51 Willett, W. C., Dietz, W. H. & Colditz, G. A. Guidelines for healthy weight. *New England Journal of Medicine* **341**, 427-434 (1999).
52 Grant, R. W., Moore, A. F. & Florez, J. C. Genetic architecture of type 2 diabetes: recent progress and clinical implications. *Diabetes care* **32**, 1107-1114 (2009).
53 Seino, S. & Mellitus, S. G. o. C. A. o. G. F. i. D. S20G mutation of the amylin gene is associated with Type II diabetes in Japanese. *Diabetologia* **44**, 906-909 (2001).

54 Pérez-Escamilla, R. & Putnik, P. The role of acculturation in nutrition, lifestyle, and incidence of type 2 diabetes among Latinos. *The Journal of nutrition* **137**, 860-870 (2007).

55 Haan, M. N. *et al.* Prevalence of dementia in older Latinos: the influence of type 2 diabetes mellitus, stroke and genetic factors. *Journal of the American Geriatrics Society* **51**, 169-177 (2003).

56 Brancati, F. L., Kao, W. L., Folsom, A. R., Watson, R. L. & Szklo, M. Incident type 2 diabetes mellitus in African American and white adults: the Atherosclerosis Risk in Communities Study. *Jama* **283**, 2253-2259 (2000).

57 O'Rahilly, S. & Farooqi, I. S. Genetics of obesity. *Philosophical Transactions of the Royal Society B: Biological Sciences* **361**, 1095-1105 (2006).

58 Barroso, I. Genetics of type 2 diabetes. *Diabetic Medicine* **22**, 517-535 (2005).

59 Andrulionyte, L., Zacharova, J., Chiasson, J.-L., Laakso, M. & Group, S.-N. S. Common polymorphisms of the PPAR-γ2 (Pro12Ala) and PGC-1α (Gly482Ser) genes are associated with the conversion from impaired glucose tolerance to type 2 diabetes in the STOP-NIDDM trial. *Diabetologia* **47**, 2176-2184 (2004).

60 Ali, O. Genetics of type 2 diabetes. *World Journal of Diabetes* **4**, 114-123, doi:10.4239/wjd.v4.i4.114 (2013).

61 Furuta, H. *et al.* Nonsense and Missense Mutations in the Human Hepatocyte Nuclear Factor-1β Gene (TCF2) and Their Relation to Type 2 Diabetes in Japanese. *The Journal of Clinical Endocrinology & Metabolism* **87**, 3859-3863, doi:doi:10.1210/jcem.87.8.8776 (2002).

62 Reaven, G. M., Hollenbeck, C., Jeng, C.-Y., Wu, M. S. & Chen, Y.-D. I. Measurement of plasma glucose, free fatty acid, lactate, and insulin for 24 h in patients with NIDDM. *Diabetes* **37**, 1020-1024 (1988).

63 Walker, K. Z. *et al.* Body fat distribution and non-insulin-dependent diabetes: comparison of a fiber-rich, high-carbohydrate, low-fat (23%) diet and a 35% fat diet high in monounsaturated fat. *The American journal of clinical nutrition* **63**, 254-260 (1996).

64 Maedler, K. *et al.* Distinct effects of saturated and monounsaturated fatty acids on β-cell turnover and function. *Diabetes* **50**, 69-76 (2001).

65 Unger, R. H. Lipotoxicity in the pathogenesis of obesity-dependent NIDDM: genetic and clinical implications. *Diabetes* **44**, 863-870 (1995).

66 Prentki, M. & Corkey, B. E. Are the β-cell signaling molecules malonyl-CoA and cystolic long-chain acyl-CoA implicated in multiple tissue defects of obesity and NIDDM? *Diabetes* **45**, 273-283 (1996).

67 Carpentier, A. C. Postprandial fatty acid metabolism in the development of lipotoxicity and type 2 diabetes. *Diabetes & metabolism* **34**, 97-107 (2008).

68 Yki-Järvinen, H., Helve, E. & Koivisto, V. A. Hyperglycemia decreases glucose uptake in type I diabetes. *Diabetes* **36**, 892-896 (1987).

69 Weir, G. C. & Bonner-Weir, S. Five stages of evolving beta-cell dysfunction during progression to diabetes. *Diabetes* **53**, S16-S21 (2004).

70 Donath, M. Y., Gross, D. J., Cerasi, E. & Kaiser, N. Hyperglycemia-induced beta-cell apoptosis in pancreatic islets of Psammomys obesus during development of diabetes. *Diabetes* **48**, 738-744 (1999).

71 Bonner-Weir, S., Trent, D. & Weir, G. Partial pancreatectomy in the rat and subsequent defect in glucose-induced insulin release. *Journal of Clinical Investigation* **71**, 1544 (1983).

72 Leahy, J., Cooper, H., Deal, D. & Weir, G. Chronic hyperglycemia is associated with impaired glucose influence on insulin secretion. A study in normal rats using chronic in vivo glucose infusions. *Journal of Clinical Investigation* **77**, 908 (1986).

73 Poitout, V. & Robertson, R. P. Glucolipotoxicity: fuel excess and β-cell dysfunction. *Endocrine reviews* **29**, 351-366 (2008).

74 Evans, J. L., Goldfine, I. D., Maddux, B. A. & Grodsky, G. M. Oxidative stress and stress-activated signaling pathways: a unifying hypothesis of type 2 diabetes. *Endocrine reviews* **23**, 599-622 (2002).

75 Evans, J. L., Goldfine, I. D., Maddux, B. A. & Grodsky, G. M. Are Oxidative Stress−Activated Signaling Pathways Mediators of Insulin Resistance and β-Cell Dysfunction? *Diabetes* **52**, 1-8 (2003).

76 Ceriello, A. & Motz, E. Is oxidative stress the pathogenic mechanism underlying insulin resistance, diabetes, and cardiovascular disease? The common soil hypothesis revisited. *Arteriosclerosis, thrombosis, and vascular biology* **24**, 816-823 (2004).

77 Harding, H. P. & Ron, D. Endoplasmic reticulum stress and the development of diabetes a review. *Diabetes* **51**, S455-S461 (2002).

78 Araki, E., Oyadomari, S. & Mori, M. Endoplasmic reticulum stress and diabetes mellitus. *INTERNAL MEDICINE-TOKYO-JAPANESE SOCIETY OF INTERNAL MEDICINE-* **42**, 7-14 (2003).

79 Araki, E., Oyadomari, S. & Mori, M. Impact of endoplasmic reticulum stress pathway on pancreatic β-cells and diabetes mellitus. *Experimental Biology and Medicine* **228**, 1213-1217 (2003).

80 Izumi, T. *et al.* Dominant negative pathogenesis by mutant proinsulin in the Akita diabetic mouse. *Diabetes* **52**, 409-416 (2003).

81 Hummasti, S. & Hotamisligil, G. S. Endoplasmic reticulum stress and inflammation in obesity and diabetes. *Circulation research* **107**, 579-591 (2010).

82 Cooper, G. *et al.* Purification and characterization of a peptide from amyloid-rich pancreases of type 2 diabetic patients. *Proceedings of the National Academy of Sciences* **84**, 8628-8632 (1987).

83 Westermark, P. *et al.* Amyloid fibrils in human insulinoma and islets of Langerhans of the diabetic cat are derived from a neuropeptide-like protein also present in normal islet cells. *Proceedings of the National Academy of Sciences* **84**, 3881-3885 (1987).

84 Westermark, P., Johnson, K., O'Brien, T. & Betsholtz, C. Islet amyloid polypeptide—a novel controversy in diabetes research. *Diabetologia* **35**, 297-303 (1992).

85 Westermark, P., Li, Z.-C., Westermark, G. T., Leckström, A. & Steiner, D. F. Effects of beta cell granule components on human islet amyloid polypeptide fibril formation. *FEBS letters* **379**, 203-206 (1996).

86 Westermark, P., Andersson, A. & Westermark, G. T. Is aggregated IAPP a cause of beta-cell failure in transplanted human pancreatic islets? *Current diabetes reports* **5**, 184-188 (2005).

87 Westermark, P., Andersson, A. & Westermark, G. T. Islet amyloid polypeptide, islet amyloid, and diabetes mellitus. *Physiological reviews* **91**, 795-826, doi:10.1152/physrev.00042.2009 (2011).

88 Zraika, S. *et al.* Toxic oligomers and islet beta cell death: guilty by association or convicted by circumstantial evidence? *Diabetologia* **53**, 1046-1056 (2010).

89 Cooper, G. J. Amylin compared with calcitonin gene-related peptide: structure, biology, and relevance to metabolic disease. *Endocrine reviews* **15**, 163-201 (1994).

90 Abedini, A. *Protein Misfolding Diseases*. (WILEY, 2010).
91 Davidson, H. W. & Hutton, J. C. The insulin-secretory-granule carboxypeptidase H. Purification and demonstration of involvement in proinsulin processing. *Biochemical Journal* **245**, 575-582 (1987).
92 Hutton, J. The insulin secretory granule. *Diabetologia* **32**, 271-281 (1989).
93 Betsholtz, C. *et al.* Islet amyloid polypeptide (IAPP): cDNA cloning and identification of an amyloidogenic region associated with the species-specific occurrence of age-related diabetes mellitus. *Experimental cell research* **183**, 484-493 (1989).
94 Mosselman, S., Höppener, J., Lips, C. & Jansz, H. The complete islet amyloid polypeptide precursor is encoded by two exons. *FEBS letters* **247**, 154-158 (1989).
95 Nishi, M., Chan, S. J., Nagamatsu, S., Bell, G. I. & Steiner, D. F. Conservation of the sequence of islet amyloid polypeptide in five mammals is consistent with its putative role as an islet hormone. *Proceedings of the National Academy of Sciences* **86**, 5738-5742 (1989).
96 Sanke, T., Bell, G., Sample, C., Rubenstein, A. & Steiner, D. An islet amyloid peptide is derived from an 89-amino acid precursor by proteolytic processing. *Journal of Biological Chemistry* **263**, 17243-17246 (1988).
97 Wang, J. *et al.* The prohormone convertase enzyme 2 (PC2) is essential for processing pro-islet amyloid polypeptide at the NH2-terminal cleavage site. *Diabetes* **50**, 534-539 (2001).
98 Mulder, H., Ekelund, M., Ekblad, E. & Sundler, F. Islet amyloid polypeptide in the gut and pancreas: localization, ontogeny and gut motility effects. *Peptides* **18**, 771-783 (1997).
99 Gebre-Medhin, S., Mulder, H., Zhang, Y., Sundler, F. & Betsholtz, C. Reduced nociceptive behavior in islet amyloid polypeptide (amylin) knockout mice. *Molecular brain research* **63**, 180-183 (1998).
100 Mulder, H. *et al.* Islet amyloid polypeptide (amylin) is expressed in sensory neurons. *The Journal of neuroscience* **15**, 7625-7632 (1995).
101 Ferrier, G. *et al.* Expression of the rat amylin (IAPP/DAP) gene. *Journal of molecular endocrinology* **3**, R1-R4 (1989).
102 Wiltzius, J. J., Sievers, S. A., Sawaya, M. R. & Eisenberg, D. Atomic structures of IAPP (amylin) fusions suggest a mechanism for fibrillation and the role of insulin in the process. *Protein Science* **18**, 1521-1530 (2009).
103 Abedini, A., Meng, F. & Raleigh, D. P. A single-point mutation converts the highly amyloidogenic human islet amyloid polypeptide into a potent fibrillization inhibitor. *Journal of the American Chemical Society* **129**, 11300-11301 (2007).
104 Dodson, G. & Steiner, D. The role of assembly in insulin's biosynthesis. *Current opinion in structural biology* **8**, 189-194 (1998).
105 Hutton, J. C. The internal pH and membrane potential of the insulin-secretory granule. *Biochem. J* **204**, 171-178 (1982).
106 Wullschleger, S., Loewith, R. & Hall, M. N. TOR signaling in growth and metabolism. *Cell* **124**, 471-484 (2006).
107 Oshiro, N. *et al.* Dissociation of raptor from mTOR is a mechanism of rapamycin-induced inhibition of mTOR function. *Genes to Cells* **9**, 359-366 (2004).
108 Jacinto, E. & Hall, M. N. Tor signalling in bugs, brain and brawn. *Nature reviews Molecular cell biology* **4**, 117-126 (2003).

109 Loewith, R. *et al.* Two TOR complexes, only one of which is rapamycin sensitive, have distinct roles in cell growth control. *Molecular cell* **10**, 457-468 (2002).
110 Jacinto, E. *et al.* Mammalian TOR complex 2 controls the actin cytoskeleton and is rapamycin insensitive. *Nature cell biology* **6**, 1122-1128 (2004).
111 Verardi, R., Traaseth, N. J., Masterson, L. R., Vostrikov, V. V. & Veglia, G. in *Isotope labeling in Biomolecular NMR* 35-62 (Springer, 2012).
112 Greenfield, N. J. Using circular dichroism spectra to estimate protein secondary structure. *Nature protocols* **1**, 2876-2890 (2006).
113 Wall, J., Murphy, C. L. & Solomon, A. [14] In vitro immunoglobulin light chain fibrillogenesis. *Methods in enzymology* **309**, 204-217 (1999).
114 Lottspeich, F., Solodkoff, Z. L. & Engels, J. W. *Bioanalytik*. (Spektrum Akademischer Verlag, 2008).